Technische Universität München

Fakultät für Medizin

Understanding the function of NF-κB transcription factor c-Rel in pancreatic cancer

Derya Kabacaoğlu

Vollständiger Abdruck der von der Fakultät für Medizin der Technischen Universität München zur Erlangung des akademischen Grades einer Doktorin der Naturwissenschaften genehmigten Dissertation.

Vorsitz: Prof. Dr. Roland Rad

Prüfende/-r der Dissertation:

1. Prof. Dr. Hana Algül
2. Prof. Dr. Martin Klingenspor
3. Prof. Dr. Florian Bassermann

Die Dissertation wurde am 16.02.21 bei der Technischen Universität München eingereicht und durch die Fakultät für Medizin am 10.08.2021 angenommen.

1 ZUSAMMENFASSUNG

In der vorliegenden Studie wollten wir die Funktion des NF-κB-Transkriptionsfaktors c-Rel im Pankreaskarzinom untersuchen. Zunächst wurde analysiert, ob c-Rel in Proben humaner Pankreaskarzinome exprimiert wird. Die Ergebnisse zeigten keinen Zusammenhang zwischen den *REL* mRNA/ CNV Level und dem Überleben der Patienten. Jedoch fand sich mehr *REL* mRNA Expression in Tumorproben als in gesundem Pankreasgewebe. Am wichtigsten hierbei ist, dass Tumore im Spätstadium (lokal fortgeschritten und invasiv) mehr *REL* mRNA exprimieren als in früheren Stadien. Außerdem konnten wir eine ubiquitäre Produktion von c-Rel sowohl in humanen als auch in murinen Pankreaskrebsproben feststellen.

Ermutigt durch diese Ergebnisse und um die Funktion von c-Rel in Pankreaskrebs zu entschlüsseln, nutzten wir ein CKP-Mausmodel mit pankreas-spezifischer Expression von $Kras^{G12D}$ und Knockout von p53. Durch genetische Manipulation von *Rel* überexprimierten sowie deletierten wir c-Rel in CKP-Mäusen. In diesem autochthonen Model reduzierte eine Überexpression von c-Rel (GCKP) das Überleben, wohingegen der Knockout (CCKP) dieses verlängerte. Histopathologische Analysen zeigten, dass von CCKP über CKP zu GCKP-Mäusen die Inzidenz undifferenzierter Tumore zunahm. In Übereinstimmung damit wurde beobachtet, dass das *REL*-Level verstärkt in Bailey's molekularem Plattenepithelsubtyp exprimiert wird.

Außerdem konnten wir sowohl in Tumorgewebe als auch in isolierten Krebszellen zeigen, dass steigende c-Rel Level mit einer Verschiebung der zellulären Plastizität zu einem mesenchymalen Phänotyp einhergehen.

Basierend auf unseren vorherigen Ergebnissen, dass die *REL* mRNA-Expression in Krebs-Stammzellen (CSC)-angereicherten humanen Zelllinien erhöht ist, analysierten wir CSC-bezogene Eigenschaften in isolierten murinen Pankreaskrebszellen. GCKP-Zellen bildeten im Vergleich zu CKP-Kontrollzellen größere Sphäroide, während CCKP-Zellen eine höhere Anzahl von Sphäroiden hervorbrachten. Außerdem erhöhte sich die Oberflächenexpression von CSC-Markern von GCKP über CKP zu CCKP-Zellen. Im Gegensatz dazu waren bei GCKP-Zellen mehr Zellen einer zuvor identifizierten Subpopulation (CD44+; Sca1-; CD133-) mit hoher Tumorinitiationskapazität zu beobachten. Des Weiteren zeigten GCKP-Tumoren eine erhöhte Fibronektin-Integrin-Signalübertragung. Diese ist bekannt dafür, dass sie unter verschiedenen Bedingungen Stammzellen induziert.

Für eine weitere Charakterisierung der Konsequenzen einer c-Rel-Manipulation in EMT-und CSC-assoziierten Metastasen *in vivo* wurden Zellen intravenös transplantiert. Sowohl CCKP- als auch GKCP-Zellen zeigten ein höheres metastatisches Potential als die CKP-Kontrollen. RNAseq-Analysen ergaben, dass CCKP- und GCKP-Zellen eine Anreicherung von Transkription in entsprechenden Sets zeigten, welche mit ihren hier dargestellten Phänotypen assoziiert sind. Wie experimentell mittels RNAseq und Zytokin-Array gezeigt, ist die Expression von pro-inflammatorischen Zytokinen in CCKP- und GCKP-Zellen erhöht. Abschließend liefern wir Beweise dafür, dass die Funktion von c-Rel durch das Vorhandenseins eines einzelnen *Tp53*-Allels umgekehrt werden kann.

Alles in allem deuten die gesammelten Ergebnisse darauf hin, dass die c-Rel-Expression als Biomarker für die Klassifizierung des Tumortyps verwendet werden kann. Die pharmakologische Hemmung von c-Rel ist möglich, der Kontext in welchem eine therapeutische Intervention stattfinden kann, muss jedoch noch geklärt werden.

- Part of this thesis was submitted for publication and the final accepted publication is:

  1. Kabacaoğlu D, Ruess DA, Görgülü K, et al. A Pancreas-Specific Ptf1a-Driven Cre Mouse Line Causes Paternally Transmitted Germline Recombination. Gastroenterology (2021).

  Additional publications not related to this thesis include:

  1. Kabacaoglu, D., Ciecielski, K. J., Ruess, D. A. & Algül, H. Immune checkpoint inhibition for pancreatic ductal adenocarcinoma: current limitations and future options. *Front. Immunol.* **9,** 1878 (2018).
  2. Kabacaoglu, D., Ruess, D. A., Ai, J. & Algül, H. NF-κB/Rel Transcription Factors in Pancreatic Cancer: Focusing on RelA, c-Rel, and RelB. *Cancers (Basel)* **11,** (2019).
  3. Kabacaoglu, D., Ruess, D. A. & Algül, H. in *Translational pancreatic cancer research: from understanding of mechanisms to novel clinical trials* (eds. Michalski, C. W., Rosendahl, J., Michl, P. & Kleeff, J.) 203–218 (Springer International Publishing, 2020). doi:10.1007/978-3-030-49476-6_14
  4. Görgülü, K. *et al.* Levels of the Autophagy-Related 5 Protein Affect Progression and Metastasis of Pancreatic Tumors in Mice. *Gastroenterology* **156,** 203–217.e20 (2019).
  5. Ruess, D. A. *et al.* Mutant KRAS-driven cancers depend on PTPN11/SHP2 phosphatase. *Nat. Med.* **24,** 954–960 (2018).
  6. Jochheim, L. S. *et al.* The neuropeptide receptor subunit RAMP1 constrains the innate immune response during acute pancreatitis in mice. *Pancreatology* **19,** 541–547 (2019).
  7. Ai J, Wörmann SM, Görgülü K, et al. Bcl3 couples cancer stem cell enrichment with pancreatic cancer molecular subtypes. Gastroenterology (2021).

2 TABLE OF CONTENTS

3 INTRODUCTION

3.1 Pancreatic Cancer

The pancreas is a part of the gastrointestinal system with both endocrine and exocrine functions [1]. It is responsible for the secretion of digestive enzymes into the intestines within its exocrine function. On the other hand, within the endocrine function, it can release hormones to regulate blood sugar levels. In parallel to its relevant operations, the pancreas is histologically divided into two compartments; exocrine and endocrine. Up to 95% of the pancreatic mass is the exocrine pancreas composed of acinar and ductal cells and associated nerves, vessels, and connective tissues. The endocrine pancreas holding 1-2% of the pancreatic mass, comprises islet cells secreting hormones insulin, glucagon, somatostatin, and pancreatic polypeptides.

The 5-year survival rate for pancreatic cancer (the lowest among many other cancer types) accounts for only 9% within the United States [2]. In the United States, within 2020, 57.600 new pancreatic cancer cases are diagnosed, of which 47.050 died [2] as the fourth leading cause of cancer-related deaths. Global Cancer Observatory-Cancer Tomorrow projections predict a two-fold increase in pancreatic cancer incidence by 2040 (https://gco.iarc.fr/tomorrow/home).

The poor prognosis can be attributed to several characteristics of pancreatic cancer [3]. The diagnosed tumors are mostly at a late stage, of which only 10% is locally resectable, 29% already developed into a locally advanced tumor with 52% metastatic incidence while the remainder couldn't be staged [4]. The lack of pancreatic cancer-specific markers makes it hard to diagnose the disease in the early stages. Due to its aggressiveness, the metastatic and invasive tumor becomes hard to resect. Pancreatic cancer is resistant to most conventional therapeutic options like chemotherapy, radiotherapy, targeted therapy, and immunotherapy. The dense desmoplastic stroma with a highly immunosuppressive tumor microenvironment and the genetic and epigenetic alterations in cancer cells are attributed to therapy resistance in pancreatic cancer. Although remarkable progress has been achieved to understand the disease pathophysiology, the prognostic impact of developed therapeutic strategies remained marginal. For example, small drug inhibitors developed against prominent oncogenic signaling pathways showed either none (i.e., MEK and PI3K) or mild benefits (e.g., EGFR) in the overall survival of pancreatic cancer patients [5–10]. Recent advances in combinatorial chemotherapeutics may

provide an advantage for survival; yet, it will not be enough to reduce mortality rates [11–13]. The revolution of immunotherapy led to considerable advantage for many solid and hematological malignancies [14]. However, the impact is minor for pancreatic cancer, which highlights the requirement of a deeper understanding of molecular pathophysiology of therapy resistance in pancreatic cancer [14]

Risk factors for pancreatic cancer involve age since the incidence rate increases from 1.5 to 55 cases in 100.000/year for patients 15-44 to >65 years old, respectively [15]. The second is tobacco smoking, which increases the incidence at least two-fold although it is preventable [16]. And thirdly, obesity [17] and dietary factors [18–20] are also associated risk factors for higher pancreatic cancer formation. Other chronic diseases like chronic pancreatitis [21] and diabetes mellitus [22] are also associated with a higher risk. Family history is an important factor in the likelihood of pancreatic cancer development. For example, oncogenic mutations in *BRCA1, BRCA2,* or *PALB2* genes are also associated with increased risk [23–25]. And finally, mutations in DNA mismatch repair genes *MLH1*, *MSH2*, *MSH6,* and *PMS2* are identified as hereditary factors increasing microsatellite instability (MSI high) [26].

On the other hand, hereditary factors may also provide a vulnerability for therapeutics. For example, olaparib (Poly-ADP Ribose Polymerase-PARP inhibitor) treatment for *BRCA1-2* mutant familial pancreatic cancer patients almost doubled progression-free survival in a phase-3 clinical trial [27]. Additionally, pembrolizumab (PD-1 inhibitor) is approved for MSI high tumors, including pancreatic cancer, due to tumors' high potential to express neoantigens to evoke an antitumor immune response [14,28].

The malignant transformation of the pancreas in the majority of cases forms adenocarcinomas (~85%) [29]. Neuroendocrine tumors, acinar carcinomas, colloid carcinomas, pancreatoblastomas, and solid-pseudopapillary neoplasms are other histological types with less incidence. Pancreatic ductal adenocarcinoma (PDAC) is the most common pancreatic cancer type with a dismal prognosis. Histopathological classification of pancreatic cancer based on microscopic observation may provide benefit for prognosis determination. However, this has not been adequate for the selection of treatment regimen [30]. Therefore, an extensive understanding of the molecular drivers for the disease pathology may provide better classification and associated treatment options in the era of personalized medicine.

It is widely accepted that PDAC formation follows a stepwise carcinogenic process involving metaplastic ductal cell formation to neoplastic transformation. In the

conventional model, oncogenic driver mutations on *KRAS, CDKN2A, TP53,* and *SMAD4* in parallel with a highly inflammatory microenvironment supports carcinogenic transformation. At least 50% of the patients possess separate but mostly overlapping mutations on these genes [31–35]. With bigger patient cohorts, additional mutations on *KDM6A, BCORL1, RBM10, KMT2C, ARID1A,* and *TGFBR2* with lower prevalence have also been identified [36].

KRAS encodes a RAS family member protein activating multiple cellular pathways influencing proliferation, survival, cytoskeletal remodeling, and inflammation among many [37]. Most of the *KRAS* mutations (more than 95% of the patients have somatic mutation [34,38]) are gain of function mutations through which KRAS becomes constitutively active. Recent data suggest that mutant *KRAS* gene dosage is also increased from carcinogenic progression to metastasis in two-thirds of the tumors. Interestingly, in cases without *KRAS* gene amplification, alternative oncogenes (*Myc, Yap1, Nfkb2*) are amplified [39].

CDKN2A is a tumor suppressor gene encoding two different mRNAs (not isoforms) as products of alternative splicing, namely $p16^{INK4A}$ and $p19^{ARF}$. Their first exons are encoded from different sequences, while they share the location of encoded exon-2 and 3. Interestingly though, the preference of open reading frames in exon-2 are different, creating distinct products [40]. In pancreatic cancer, their loss of function mutations (alone or together, more than 90% of the patients have somatic mutation [41]) are associated with abnormal cell cycle control, genomic instability, and apoptosis [42].

TP53 is a tumor suppressor gene encoding a transcription factor getting activated upon DNA damage or cellular stress [43]. Its activity regulates cell cycle, DNA repair, metabolism, and apoptosis. Its mutations (85% of patients have somatic mutation [38]) cause loss of tumor suppressor function or oncogenic gain of function. Of note, it is noted that in late-stage pancreatic tumors, up to 50% of the *TP53* mutations create *null* alleles (highlighting the clinical significance of both mutant and knockout *TP53* disease models [38].

SMAD4 is a downstream mediator of canonical TGFβ signaling, and its loss of function mutations are existent in 55% of the tumors [44]. TGFβ signaling acts as a tumor suppressor in the early carcinogenesis, unlike its oncogenic function in late-neoplastic and invasive cancer stages when *SMAD4* is mutated [45,46]. Interestingly, 10% of the

tumors without *SMAD4* inactivation bypass canonical TGFβ signaling via mutations on other protein components (*TGFBR1/2*, *ACVR1B, SMAD3*) [34,35].

There are multiple levels in which these mutations can interact with each other. SMAD4 inactivation with p53 gain-of-function or intact SMAD4 with p53 loss-of-function mutations has more likelihood to co-exist [38]. A gain-of-function mutation of KRAS can suppress TGFβ signaling either through inhibition of SMADs [47,48]; or by p53 activation, which is important for downstream TGFβ signaling transcriptional activation [49,50]. Identification of such interactions at the functional level may provide information about in-depth tumor vulnerabilities and therapeutic opportunities.

Pancreatic intraepithelial neoplasia (PanIN) is considered as the precursor form of carcinogenic cells in the progressive model [51]. Throughout the spectrum of progressive PanIN grades, the morphological alterations along with higher cellular proliferation reflect the severity of the lesions [52]. Studies indicate that these neoplastic lesions already possess specific genetic mutations (e.g., mutations on *CDKN2A, TP53, SMAD4,* and *KRAS*) before carcinogenic transformation [53–56]. Interestingly, from lower PanIN stages to higher, the frequency of cells with mutant Kras increases, reflecting the clonal expansion of the advantageous cells [54].

Based on these results, it has been generally accepted that PDAC arises from ductal cells and their lesions. However, the development of various mouse models suggested that metaplastic conversion of acinar cells can also give rise to PanIN lesions [57]. The presence of ADM structures in human samples also supports this theory [58], although in vitro studies indicate the requirement of alternative pathways in human vs. mouse ADM formation [59].

Recent advances in sequencing technologies with bioinformatics revealed an alternative model in which instantaneous genomic rearrangements can circumvent the need for stepwise accumulation of carcinogenic mutations [60]. In this model, a general punctuated equilibrium of evolution is reflected into pancreatic carcinogenesis. Accordingly, instant bottleneck events lead to sudden divergences in the evolutionary trajectories [61]. In the renewed carcinogenesis model, break-fusion-bridge (BFB) or chromothripsis genomic rearrangements act as the bottlenecks for the cellular adaptation. Unlike the progressive model of mutation accumulation, a single mitotic crisis with BFB and chromothripsis can delete *CDKN2A*, *TP53*, and *SMAD4* alleles concurrently. Another study performed with samples from a cohort of 100 patients

show traces of BFB for nine or chromothripsis for fifteen patients [25]. Overall, it is predicted that although the punctuated evolution of cancer may contribute, it may not be the dominating magic shortcut for transformation, unlike the progressive model [42].

3.1.1 Molecular subtypes of pancreatic cancer

Multiple studies identified some-what overlapping subtypes of pancreatic cancer with the transcriptomics analysis of pancreatic tumors dissected from patients [36]. Collisson et al. micro-dissected epithelial tissue (separately from tumor stroma) from 27 untreated-resected primary pancreatic tumors and performed a hybridization-based microarray analysis [62]. They identified three subtypes of pancreatic cancer, which are: 1) Classical (KRAS-dependent, high GATA6 expression); 2) Quasi-mesenchymal (high tumor grade, short survival, QM-PDA); and 3) Exocrine-like (signature overlaps with terminally differentiated pancreas).

Moffitt et al. [63] performed microarray analysis on bulk resected tumors from both primary (n=145) and metastatic sites (n=61) along with healthy tissues from the pancreas (n=46) and adjacent-metastatic area (n=88). In parallel, additional primary tumors, patient-derived xenografts (PDX), cancer cell lines, and cancer-associated fibroblasts (CAF) are used for RNAseq to be compared with microarray results. They excluded the transcripts, which are considered to be part of TME and healthy tissue. Eventually, they identified two subtypes: 1) Classical; and 2) Basal-like, along with a stromal characterization: normal and activated stroma.

Bailey et al. [64] performed RNAseq analysis on 96 bulk tumor samples, which possess high epithelial cellularity (>40%), and identified four subtypes based on unsupervised clustering. The subtypes are also validated with a bigger patient cohort (n=232) microarray transcriptome, which has a broader cellularity interval. Accordingly, they identified: 1) squamous; 2) pancreatic progenitor; 3) immunogenic; and 4) aberrantly differentiated endocrine exocrine (ADEX) subtypes. The subtypes were highly superimposing with previously defined subtypes of Collisson et al. except immunogenic subtype, likely because Collisson et al. used micro-dissected epithelial cells without stroma. The squamous subtype is parallel to QM-PDA and basal-like subtypes of the pancreas and other squamous tumors of various organs with an increased ΔNp63 transcription factor expression. ADEX subtype reflects the exocrine-like class of Collisson classification with terminal differentiation. Nevertheless, another

analysis proposed that the subtypes of immunogenic and ADEX are actually a byproduct of the cellularity problem from surrounding healthy tissue and TME [65]

The potential benefits of patient stratification based on molecular characteristics are shown by a COMPASS trial [66]. They performed RNAseq and Whole-genome-seq to the biopsy samples followed by various chemotherapy regimens for 50~ patients. Accordingly, classical subtype treated with modified FOLFIRINOX had more likelihood to have more prolonged survival and tumor shrinkage. Although not significant, basal-subtype had a trend to have more prolonged survival to Gemcitabine/nab-Paclitaxel treatment. Additionally, in their samples, GATA6 *in-situ* hybridization correlates with transcriptomics subtyping, which might be a pathologic tool to stratify patients before treatment.

These results suggest the urgent necessity for the identification of molecular subtypes in intra and inter-heterogenous pancreatic tumors. Not only the identification of specific markers but their feasibility of use in hospitals in a cost-effective manner are significant bottlenecks for bench-to-bedside scientific translation. Subtyping is especially important for clinical trial settings, as, without stratification, statistics can be blunted. Not only marker identification but mechanistic details making types different may also pave the way for the re-purposing and identification of novel therapeutics.

3.1.2 Mouse models of pancreatic cancer

In order to study pancreatic cancer pathophysiology, genetically engineered mouse models (GEMMs) are highly utilized. Instead predicted to follow the conventional progressive model, pancreas-specific gain-of-function $Kras^{G12D}$ expression can mimic the sequential formation of ADM-PanIN-cancer (Figure 1) [67,68]. Reflecting human disease, the model possesses a very dense desmoplastic stroma along with an immunosuppressive tumor microenvironment starting from pre-neoplastic stages to cancer, and also form metastasis [69,70].

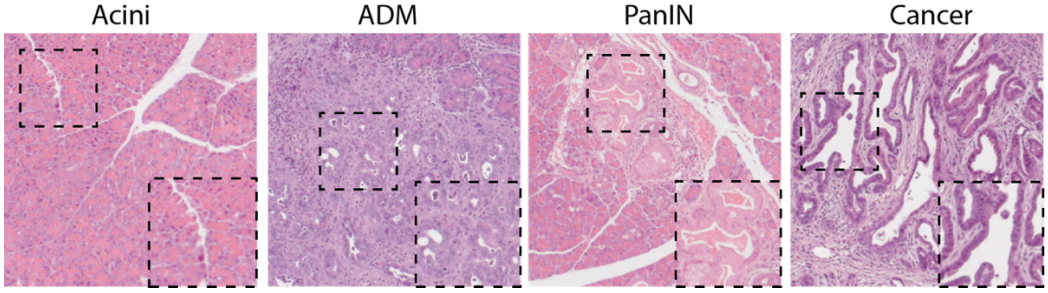

Figure 1: Stages of pancreatic cancer formation in mice from intact acini to acinar-to-ductal metaplasia (ADM), Pancreatic Intraepithelial neoplasia (PanIN) and Cancer.

Pancreas specific expression of $Kras^{G12D}$ is achieved by the spatiotemporal control of Cre expression. *Pdx1-Cre* [67] and *Ptf1a-Cre* [71] are the most used models since both transcription factors are important for embryonic pancreatic development. Pdx1 is important for pancreatic epithelium and endocrine cell differentiation [72,73]. Whereas Ptf1a is important for exocrine cell formation, and the absence of Ptf1a causes duodenal differentiation of pancreatic progenitors [71,74,75]. A vector harboring a mutation for the 12th amino acid of Kras converting G to D, under the control of a *lox-stop-lox* (LSL) cassette is introduced into the endogenous *Kras* locus [76]. Upon Cre expression, the *stop* cassette gets floxed, allowing the expression of $Kras^{G12D}$ [67].

Our group highly utilizes another *Ptf1a-Cre* model ($Ptf1a^{tm1(cre)Hnak}$) in which exon-1 of *Ptf1a* locus is replaced with Cre coding sequence, allowing regulation by endogenous transcription regulatory elements [77]. $Kras^{G12D}$ expression under the control of $Ptf1a^{tm1(cre)Hnak}$ can recapitulate the disease progression from ADM-PanIN to cancer, along with invasive tumor formation and metastasis [68]. The median survival of this model is at least one year, while tumor initiation takes ~8 months with low frequency. Therefore, the CK model is preferably used to study carcinogenesis since it allows a broad spectrum of neoplastic lesion formation from low-grade to high-grade PanINs.

In order to study tumors, CK is crossed with a conditional p53 knockout model ($Trp53^{tm1Br}$) [78]. Homozygous deletion of *Trp53* permits accelerated tumor formation with median survival age of ~60 days. Although this model is perfect for studying tumors with 100% penetrance, it has no autochthonous metastasis formation.

3.1.3 Tumor microenvironment in pancreatic cancer

In parallel to carcinogenesis, pancreatic tissue stroma undergoes alterations involving a response resembling wound healing: desmoplasia formation, vasculature remodeling, or immune cell recruitment associated with inflammation. Cancer acquires an ability to hijack such responses for its own benefit, forming a favorable tumor microenvironment (TME).

The desmoplastic reaction is a hallmark of pancreatic cancer, forming in both primary tumors and metastatic sites [79]. Fibroblast like pancreatic stellate cells (PSCs) gets activated by cancer cells to produce fibrotic extracellular matrix [80]. The desmoplastic reaction is considered a mechanical barrier of drug delivery since it limits vascularization around the tumor cells [81]. Initially, the desmoplastic reaction is described as being fully tumor-promoting. However, accumulating evidence suggests

that such a simplistic view is flawed. Therefore, elucidation of the molecular properties of stroma down to its particular components are essential.

ECM is a complex of proteins, e.g., collagen, fibronectin, hyaluronic acid. Hyaluronan is a glycosainoglycan, and its expression negatively correlates with patient survival [79,82]. A recombinant human hyaluronidase was shown to increase vascular permeability and associated chemotherapy drug delivery in a preclinical mouse model [82]. However, these results were not replicated in human clinical trials in which the drug is used together with standard care chemotherapy on patients [83–85]. Collagen has multiple subtypes, but I, II, and IV are the main ones constituting ECM [86]. Type IV levels in serum correlated negatively with survival for patients after surgery [87]. Fibronectin is a glycoprotein binding to the membrane-spanning cellular integrins. Bulk fibronectin expression is shown not to be correlated with overall survival [88,89], but its expression together with specific integrins is prognostically unfavorable [90] for pancreatic cancer patients.

While direct targeting of ECM components is conceivable, an approach instead targeting their source has been employed more. Fibroblasts are bystanders in every organ for supportive purposes, including homeostatic expression of soluble factors and ECM components [91]. Pancreatic stellate cells (PSCs) are pancreatic fibroblasts located in the peri-acinar/ductal and vascular area in healthy organs [92]. Within the disease context, PSCs form cancer-associated fibroblasts (CAFs), which are initially considered solely as tumorigenic [93]. However, subsequent research outdated the view describing CAFs pure evil [94,95]. Additionally, therapeutic targeting of cancer cell-CAF paracrine signaling is a double-edged sword, as shown by the SHH-inhibition studies. Initially, drug or antibody-mediated SHH inhibition was shown to reduce desmoplasia while increasing survival [96,97], but clinical trials with PDAC patients were terminated early since the chemo-combination accelerated disease progression [98].

Recently, multiple studies confirmed the expected heterogeneity of CAFs. Once PSCs are co-cultured with mouse pancreatic cancer organoids in vitro, they induce a myofibroblast gene expression signature along with the production of α-smooth muscle actin (αSMA- a marker for CAF staining) [99]. On the other hand, when a physical barrier is put between co-cultured cells allowing diffusion of soluble factors, PSCs rather upregulated some inflammatory cytokines, including IL-6 but not αSMA. The groups of CAFs are named as myCAFs and iCAFs, respectively. Supporting these

findings, αSMA+ fibroblasts were positioned in the perimeter of cancer cells, whereas IL-6+ fibroblasts were positioned in the distant peri-tumoral area. These results are also validated by single-cell RNA sequencing (scRNAseq) experiments [100–102].

Inflammation with its many immune cell players constitutes a significant portion of the TME pie. Starting from the pre-neoplastic cells, inflammatory immune cell deposition in the microenvironment with its complex interaction networks still holds a puzzle to solve. Inflammation is a natural response to wound healing, but during carcinogenesis, the process is exploited for the benefit of carcinogenic transformation. According to the Triple E hypothesis, three steps of carcinogenesis occur 1) elimination, 2) equilibrium, and 3) escape [103,104]. During the elimination phase, the immune system surveys the body for any unnatural transformation to terminate them (immunosurveillance). With the pressure of immunosurveillance, some transforming clones manage to escape immunosurveillance through a Darwinian-like selection. And finally, in the escape phase surviving clones expand to form tumor mass. Next to intrinsic factors, cancer cells also employ specific characteristics to modify their inflammatory microenvironment for their benefit during this micro-evolutionary process.

GEMMs are perfect tools to analyze the steps of inflammation during carcinogenesis. CD45+ leukocytes already start to accumulate around neoplastic regions in young age CK model [69]. Around the PanIN lesions, a significant portion of CD4+ T cells is Foxp3+ Treg (regulatory T cell marker with immunosuppressive functions), while cytotoxic CD8+ T cells were scarce. The myeloid compartment is composed of plenty of tumor-associated macrophages (TAMs) and myeloid-derived suppressor cells (MDSCs).

Physiologically, macrophages can be activated either classically (M1) by IFNγ and bacteria associated products or alternatively (M2) by IL-4, IL-10, IL-13, and glucocorticoids [105]. M1 activation acts antitumorigenic with high IL-12 and low IL-10 expression, whereas M2 activation is tumorigenic due to elevated IL-10 and low IL-12 expression. TAMs in TME instead act like M2 macrophages mediating angiogenesis, tumor cell invasion, and metastasis [106,107]. Additionally, IL-10 production skews helper T cell (Th) differentiation to type 2 (Th2), blocking cytotoxic T cell (CTL) activity [108]. IL-4 production by Th2 further increases M2 differentiation in a positive feedback loop. TAMs can also secrete PD-L1, which is a direct inhibitor of immune checkpoint proteins on active T cells [109]. Metabolically, the production of arginase by TAMs breaks

down available L-arginine stocks, which is required for tumoricidal T cell activity [110]. IL-10 and CCL22 produced by TAMs can enhance immunosuppressive Treg activity [111,112].

Neutrophils are the most abundant granulocytes in the body. Both anti- and pro-tumorigenic properties of neutrophils are reported as in macrophages [113]. Accordingly, TGFβ mediated recruitment of N2 neutrophil (high arginase expression with low CCL3, TNF and ICAM1) is pro-tumorigenic since it blocks CTL activity, while TGF-β inhibition increases antitumor N1 subtype occupancy [114]. In PDAC, tumor-associated neutrophils (TANs) are also reported in the PanIN stage, with negative prognostic impact [115,116].

Carcinogenesis also involves a macroenvironment in which soluble factors released can influence distant organs, which in turn can create a feedback response to the primary site. Among many, immature myeloid cells localized in bone-marrow can form immunosuppressive cells, namely myeloid-derived suppressor cells (MDSCs). Under normal conditions, immature myeloid cells in bone marrow differentiate their terminal types, e.g., dendritic cells, macrophages, neutrophils [105]. However, in cancer, they divert this differentiation, eventually forming CD11b+, GR1+ MDSCs [117]. Broadly, MDSCs are divided into two: monocytic (M-MDSCs) and granulocytic (polymorphonuclear, PMN-MDSCs). M-MDSCs block CTL function via arginase [118] and iNOS production, which increases reactive nitrogen species (RNS) [119]. PMN-MDSCs block CTL function mainly by ROS production of myeloperoxidase [120]. MDSCs can also block antitumor lymphocyte recruitment and survival while increasing Treg expansion [105]

Interestingly, in the absence of tumor-derived conditioning, MDSCs can terminally differentiate into mature cells, while tumor cell conditioning increases their immunosuppressive character [121,122]. These results imply extensive crosstalk between tumor cells and immature myeloid cells. GM-CSF, G-CSF, M-CSF are some growth factors regulating myelopoiesis of immature myeloid cells in the bone marrow. In cancer, inflammation associated production of such factors provides a suitable environment to keep myeloid cells immature. Additionally, pro-inflammatory factors like IL-1β, IL-6, S100A8, S100A9, CCL2, CCL12, TGFβ and CXCL5 secreted from tumor cells and, IFNγ, IL-4, IL-10 and IL-13 from T cells form a complex network, which is increasing inflammation associated recruitment and maintenance of MDSC cells [123].

T cells are lymphocytes, which possess the ability to recognize specific antigens to create an immune response [124]. The antigens are presented to them via specialized myeloid antigen-presenting cells (APCs), e.g., dendritic cells (DC). DC antigen presentation happens through major histocompatibility complexes (MHCs), which starts the process called “T cell priming” [125]. MHC-class determines the type of naïve T cell differentiation. While MHC-II priming of CD4+ T cell differentiation into helper T cell subtypes (Th1, Th2) and Tregs, MHC-I priming of CD8+ T cell differentiation into CTL with direct cytotoxic ability. Broadly speaking, Th1 and CTL differentiation are antitumorigenic, whereas the Th2 and Treg are pro-tumorigenic. Th1 cells are characterized by IFNγ production, which increases APC-MHC expression [126] and antitumor T cell and myeloid cell activity [127]. Th2 cells produce IL-4 and IL-13, which causes T cell exhaustion, a process in which previously activated T cells become resistant to continual activation [128]. Tregs produce TGFβ and IL-10, which can block T cell effector function [129].

T cell activation by MHC engagement is under the tight control of co-regulatory checkpoint proteins. Under physiological conditions, there is a balance between activatory and inhibitory regulation of checkpoint proteins to create an immune response to eliminate foreign substances but not to harm self. However, tumor cells bypass this regulation by somewhat shifting the balance to inhibitory checkpoints leading to T cell anergy and exhaustion. CTLA-4 and PD-1 are the most famous of these checkpoint inhibitors [14].

All of these results brought up a rather preferable therapeutic approach in which TME is not depleted but remodeled. Elucidation of critical components of the TME is the goal for the development of precision medicine. Identification of serum markers to classify tumor stroma and associated high response drugs will hold promise for strategic therapy selection. NF-κB signaling at the crossroads of inflammation and cancer is “not” a novel signaling pathway. However, even with the contribution of 35 years’ significant work, there are a plethora of mysteries to be revealed about how it works and how it can be targeted therapeutically.

3.2 NF-κB signaling and c-Rel

The κB-DNA binding sequence was discovered by Ranjan Sen and David Baltimore in 1986 [130]. NF-κB pathway activates transcription factors, which bind to various κB-

DNA binding sequences to regulate target transcription. NF-κB is predicted to evolve as a stress response pathway, with high conservation within eukaryotic species [131].

There are 5 NF-κB transcription factors: RelA (p65), RelB, c-Rel, p105-50 (NFKB1), and p100-52 (NFKB2). All of these transcription factors possess an RHD domain (Rel homology domain), which is important for their homo/hetero-dimerization, inhibitory κB protein (IκB) binding, and binding to κB DNA sequences [132]. The five proteins are divided into two groups. p50 and p52 proteins are products of p105 and p100 proteolytic cleavage, respectively [133–140]. With their cleavable C-terminal ankyrin repeats p105 and p100 act as IκB proteins. RelA, RelB, and c-Rel additionally contain transcriptional transactivation domain (TAD). In resting conditions, they are held in the cytoplasm by IκB proteins [141–144]. IκBs contain ankyrin repeats, which bind to TADs of transcription factors, thereby blocking their DNA binding activity and masking nuclear localization signals (NLS), which is important for transcription factors' nuclear translocation [145]. Of note, p105 and p100 proteins cleave their ankyrin repeats to become p50 and p52, respectively. Homo-heterodimers of p50 and p52 are transcription repressors since they do not possess TAD [146]. However, if they dimerize with other NF-κB transcription factors harboring TAD, they become transcriptional activators. Bcl-3 is an atypical member of the IκB family, containing both ankyrin repeats and TAD [147,148]. It can be both activator and inhibitor by its regulation on p50 and p52 dimers [148–154].

Broadly, NF-κB signaling is divided into two: canonical and non-canonical pathways (Figure 2). Canonical pathway gets activated by cytokine (TNFα, IL-1) receptors, pattern recognition receptors, T-cell receptor or B-cell receptor [155]. Downstream, ligand binding to the receptor initiates a signaling cascade involving multiple phosphorylation/ubiquitination modifications. Although first downstream effectors of the aforementioned receptors are different, they converge at activation of a complex of IκB kinases (IKKs). The IKK complex has three subunits: IKKα (IKK1, CHUK) and IKKβ (IKK2) with kinase activity, and IKKγ (NEMO) with regulatory function [156–162]. IKK complex phosphorylates IκB proteins to be ubiquitinated and degraded by proteasomes. This releases dimers of NF-κB transcription factors,e.g., RelA:p50, c-Rel:p50, to translocate into the nucleus and regulate transcriptional activation. Of note, other than external ligand stimulation, internal cell stress associated products like ROS or damaged DNA can also activate NF-κB [155].

The non-canonical NF-κB pathway is different from the canonical pathway due to the difference in the processing of p105 and p100 proteins. While canonical p105 protein is truncated into p50 in a translation coupled manner [163], p100 requires pathway activation [164]. This difference also reflects the reasons why canonical pathway response is robust and quick, while non-canonical pathway is generally late-trailing and persistent. BAFF, CD40, lymphotoxinβ and RANK are some of the ligands inducing the non-canonical signaling [165–168]. Subsequently, NF-κB inducing kinase (NIK) together with IKKα phosphorylate p100 to be ubiquitinated on C' terminus and truncated by βTrCP [164,169,170]. Free p52:RelB dimers then can translocate to the nucleus to initiate transcriptional regulation [167,171].

IKK proteins hold a pivotal position since a variety of NF-κB inducers converge on them. Still, the responses to stimuli diverge a lot at the downstream [155]. The output of NF-κB activity can vary based on the type of transcription factor dimer-pairs and their post-translational modifications, the crosstalk with parallel signaling pathways, epigenetic status of the target gene, and the binding partners of NF-κB dimers.

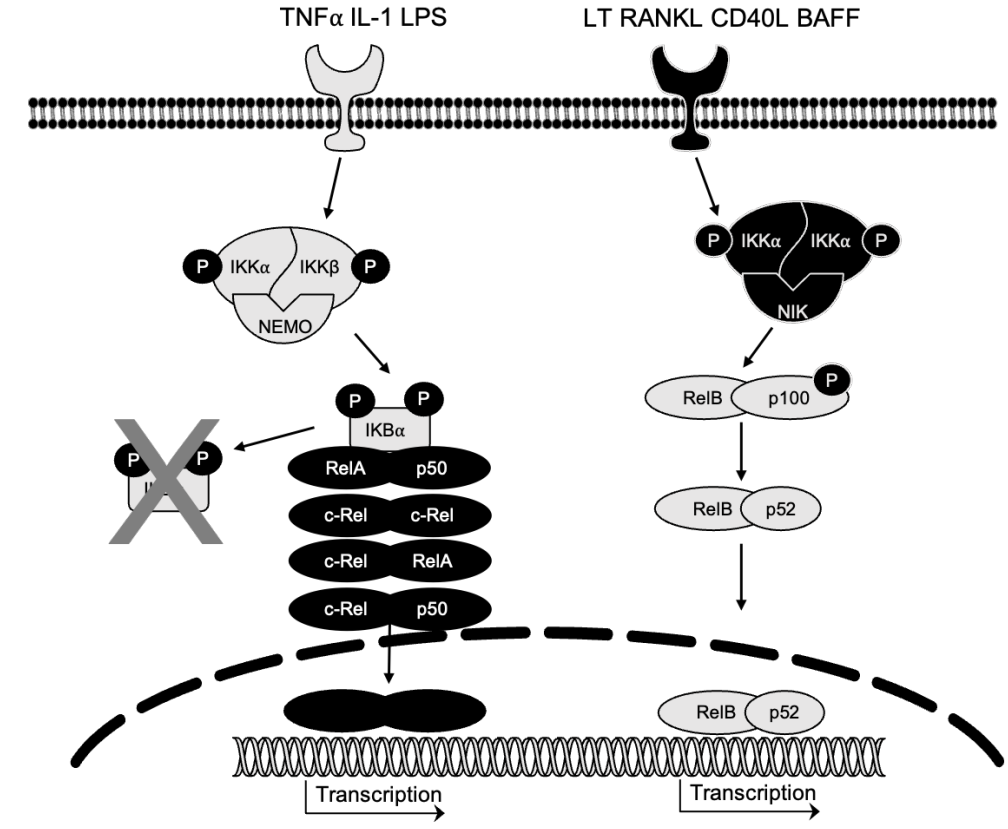

Figure 2: Schematic overview of NF-κB signaling, with canonical and noncanonical pathway components. c-Rel dimers act at the downstream of the canonical pathway.

NF-κB as the matchmaker of inflammation and cancer holds a unique position for therapeutics [172]. Cumulative evidence supports that it would be a mistake to classify NF-κB as per se oncogenic or tumor suppressor. Rather an imbalance in the cumulative output of the signaling pathway along with a crosstalk with the others defines its cancer association, highlighting the importance of "properness" of the pathway. Unlike hematological malignancies, mutations in NF-κB proteins are not observed in pancreatic cancer. However, there is still an NF-κB addiction in pancreatic tumors, likely due to its highly inflammatory nature [172].

Up to date, most of the research of NF-κB in solid tumors relied on the GEMMs of IKK proteins. While some studies classified NF-κB signaling as an oncogene, others did as a tumor suppressor, again reflecting the importance of the pathway balance [173–180]. Of note, a hepatocarcinogenesis model revealed that triple *Rela;Relb;Rel* knockout model couldn't phenocopy *Ikbkg* knockout (NEMO) phenotype, while overexpression of constitutively active kinase mutant *Ikbkb* (IKKβ) can rescue it [180]. The result is actually expected considering the NF-κB independent functions of IKK proteins [181]. Therefore, studies instead focusing on the very downstream transcription factors of NF-κB signaling can provide a relatively clear understanding.

Previously, research from our group and others revealed the role of RelA and RelB in pancreatic carcinogenesis [182,183]. However, c-Rel in pancreatic cancer GEMMs are not studied.

3.2.1 RelA and RelB

Oncogenic Ras is accepted to induce NF-κB signaling, while its necessity for Ras-mediated carcinogenic transformation is disputed [184–187]. In pancreatic cancer, NF-κB signaling is assumed to be active constitutively based on high RelA nuclear localization and DNA binding in both isolated cancer cells and patient histology specimens [175,188]. An of note study identified IL-1α as a mutant Kras induced cytokine, which activates constitutive NF-κB signaling in a feed-forward positive feedback loop in PDAC GEMMs [175]. The same study also showed a correlation between IL-1α expression and RelA nuclear localization in human patient samples. In parallel, inflammation generated by mutant Kras is also shown to constitutively activate NF-κB, further sustaining pathologic Ras-GTP levels again in a positive feedback loop [189]. Kras effector signaling pathways involving PI3K and GSK-3 kinases are also shown to be in positive feedback loops with canonical NF-κB pathway involving RelA [190–192].

A study from our group [182] revealed the dual nature of RelA function in pancreatic cancer in which RelA acts as a tumor suppressor during carcinogenesis. Once the senescence barrier is bypassed by mutations on *Trp53* or *Cdkn2a*, the oncogenicity of RelA overcomes tumor suppressor function. Constitutive activation of the non-canonical NF-κB pathway in pancreatic cancer has been reported based on NIK and phosphorylated p100 levels [193]. In a pancreatic carcinogenesis GEMM, RelB is identified as an oncogene during carcinogenesis since its knockout reduces PanIN formation and increases survival [183].

The relevance of RelA and RelB in pancreatic cancer and other solid tumors are, of course, not only limited to these results. Additional associated remarks were already compiled in a review article we wrote [194]. Canonical NF-κB signaling, in general, focused on RelA in cancer studies, which is evident by simple literature research. It may create a bias towards the function of c-Rel in solid tumors, disregarding its potential relevance in the disease. Therefore, further studies revealing c-Rel function in pancreatic cancer are required.

3.2.2 c-Rel

c-Rel is a homolog of avian reticuloendotheliosis virus strain T protein (v-Rel) [195,196]. v-Rel is identified as a retroviral protein, which can cause the oncogenic transformation of avian lymphoid cells [197,198]. Interestingly, compared to other NF-κB transcription factors RelA, RelB, p50, and p52, v-Rel and c-Rel have better ability to cause carcinogenic transformation in chicken splenocytes [199]. Although alone not enough, along with additional driver events, c-Rel overexpression in mouse mammary can cause spontaneous carcinogenesis [200,201]. c-Rel is mostly studied in hematological malignancies. However, recent research highlights its importance in solid tumors.

Table 1: List of literature delineating c-Rel function in various solid tumors

Tumor	Pancreas	Ovarian	Colorectal	Liver	Lung	Squamous	Breast
Reference	202–204	205,206	207,208	180,209	186,204,210,211	212–219	200,204

Ras-induced carcinogenic transformation of MEF cells doesn't necessarily require c-Rel, but it is enhanced by it. In parallel, in a Ras-induced lung cancer mouse model, c-Rel nuclear localization is increased in transformed cells compared to healthy cells [186]. Another study revealed Tank binding kinase-1 (TBK1):c-Rel axis as a synthetic lethality partner for mutant Kras in multiple cancer cell lines (no pancreatic cancer cell included) [220]. In their screen, they tested multiple mutant Kras downstream pathways,

including PI3K, Raf, and RalGEFs. While RNAi knockdown of PI3K and Raf didn't show synthetic lethality with mutant Kras, RalB did. Previously, it is already established that RalB complexes are critical components of Kras induced TBK1 activation [221]. Interestingly, TBK1-IKKε induces c-Rel nuclear localization by increasing its phosphorylation [222]. In their RNAi screen, both TBK1 and c-Rel knockdown are identified as synthetic lethality partners of mutant Kras next to RalB. c-Rel can activate both pro-survival and antiapoptotic genes [223]. Antiapoptotic Bcl-xL production could rescue the synthetic lethality upon TBK1 knockdown.

Another work identified c-Rel as a critical component for resistance to EGFR inhibition on multiple cancer cell lines, this time including pancreatic cancer [204]. Stemness of cancer cells is a proposed mechanism for therapy resistance. αVβ3 integrin induced Kras-RalB signaling increases c-Rel activation, which is associated with stemness involved in erlotinib resistance. However, further studies put the controversy to the importance of TBK1 function in Kras mutant cancer [224,225]. In pancreatic cancer cells, for TBK1 activity readout, researchers used IRF3, not c-Rel [224]. Therefore, more research is required to delineate possible therapeutic implications for Kras-TBK synthetic lethality.

c-Rel is also identified as a checkpoint for immunotherapy by multiple groups because of its importance in Treg and MDSC function [226,227]. Both studies used melanoma cell lines and their transplantation models to elaborate c-Rel function in tumor-associated inflammation. Genetic and pharmacological c-Rel inhibition synergized with immune checkpoint inhibitors (anti-PD-1), reducing tumor growth with higher CTL function. Another recent study classified c-Rel as a positive regulator of fibrogenesis by mediating paracrine crosstalk between epithelial, mesenchymal, and myeloid cells [228]. With the use of genetic and pharmacologic tools, c-Rel inhibition was shown to have a therapeutic benefit to reduce fibrosis.

These studies highlight a potential benefit of targeting c-Rel in solid tumors, matchmaking not only inflammation and cancer but also fibrosis. In simple words, by targeting c-Rel, one can kill "multiple birds with one stone". Additionally, unlike RelA, the c-Rel knockout mouse is not embryonically lethal but has functional defects later in humoral immune response [229,230]. Therefore, c-Rel is a preferable therapeutic target for the canonical NF-κB signaling pathway.

3.3 Epithelial to Mesenchymal Transition (EMT) and Metastasis

EMT is a reversible cellular process in which epithelial characteristics involving basal-apical cell polarity, high cell-cell adhesion, and cell-basal membrane interaction and associated cytoskeletal architecture are reduced to achieve a more invasive phenotype associated with mesenchymal characteristics [231].

Cell-cell adhesion is achieved by tight junctions, adherens junctions, desmosomes, and gap junctions. Tight junctions are formed of membrane-spanning occludins, claudins, and junction adhesion molecules [232]. These molecules are connected to actin filaments in cells, thereby connecting cytoskeletons of neighbor cells. Tight junctions are important for epithelial cell polarity maintenance and paracellular barrier function. Adherens junctions are composed of cadherin and catenin proteins interacting with actin filaments forming adhesion plaques [233]. Adhesion plaques are like continuous cellular belts maintaining polarity across tough epithelia. Desmosomes are composed of membrane-spanning desmosomal cadherins, desmoglein, and desmocollin proteins connecting cell-cell adhesion to intermediate filaments such as keratins [234]. Gap junctions are cellular gates allowing passage of ions and molecules between contacting cells [235]. Epithelial cells are attached to the basal membrane via hemidesmosomes, which are composed of α6β4 integrin complexes connecting cytokeratin intermediate filaments to the basal membrane.

Within the EMT process, epithelial products are transcriptionally or post-transcriptionally repressed. Mesenchymal phenotype is reflected in fibroblast-like cells in which cell-cell junctions are not functional, while cellular polarity is instead seen as front-rear with actin stress fibers. Vimentins compose intermediate filaments forming invasion-migration associated focal adhesions attaching to ECM [231]. Integrin-β1, integrin-β3, N-cadherin, and fibronectin are some mesenchymal cell-associated proteins, which are expressed more in EMT cells [236].Three types of EMTs are defined, which are happening in 1) embryonic development, 2) wound healing and tissue fibrosis and 3) cancer pathogenesis [237].

Multiple transcription factors (EMT-TFs) are identified, enhancing EMT in cancer. Among these factors are Snail [238,239], Slug [240], Zeb1 [241], Zeb2 [242] and Twist [243]. In cancer, primarily E-cadherin expression is tightly regulated by EMT-TFs. EMT-TFs'

activation can be achieved by their transcriptional activation or post-translational modifications, increasing their stability [244].

The complete EMT is a rare event in vivo, as observed in human tumor samples with the exception of carcinosarcomas [244]. Nonetheless, recent evidence suggests instead an intermediate EMT phenotype in which cancer cells adopt “epithelial-mesenchymal plasticity (EMP)” [231]. EMP favors cells to gain mixed epithelial (E) and mesenchymal (M) properties allowing rapid transition between E/M states. EMP is considered to provide an advantage to fulfill the requirements of the multistep metastasis cascade.

The metastatic cascade in cancer is broadly divided into five steps: 1) invasion, 2) intravasation, 3) survival in circulation, 4) extravasation, and 5) colonization in secondary organs [245]. Initially, cells detach from the basal membrane, break cell-cell junctions to increase motility, and remodel ECM to physical breakdown barriers, which block their entry into circulation. These processes are highly associated with EMT. During intravasation, cells penetrate leaky endothelial cells to translocate into vascular or lymphatic lamina, joining systemic circulation. Not all cells, but some survive the mechanical shears of circulation, anoikis, and immune surveillance. These cells are called circulating tumor cells (CTCs). CTCs then extravasate into secondary organs where again, a limited number of cells can establish micro-metastasis and colonize. Interestingly, EMT and metastatic dissemination start before bulk tumor formation in pancreatic cancer during premalignant stage [246].

E-cadherin loss (in parallel to EMT) has been considered as an important step for the initial invasion of cancer cells preceding metastasis. However, E-cadherin expression is shown to be retained in invasive primary tumors and metastatic colonies [247]. An of note study revealed that E-cadherin loss, in fact, increased invasion but reduced their proliferation, survival, dissemination to circulation, and forming metastatic colonies in distant organs [248].

Two independent groups challenged the requirement of EMT with the use of *in vivo* mouse models. Fischer et al. used a linage tracing breast cancer model in which cells were expressing EMT associated S100A4 (Fsp1), and vimentin were marked [249]. Most of the cells in metastatic lung colonies were composed of unmarked cells indicating they have not passed through EMT. Zheng et al. proposed that EMT is important for chemoresistance but not required for metastasis by using Snail and Twist knockout PDAC model [250]. Firstly, since EMP cells might not pass through a mesenchymal stage where vimentin or S100A4 are robustly expressed, metastatic cells might be activating

EMT partially but not entirely during metastasis. Secondly, many EMT-TFs have highly overlapping functions. Hence, the absence of one TF might be compensated by the other [244]. Krebs et al. demonstrated Zeb1 is a key protein for invasion and metastasis in PDAC. Accordingly, evaluating "a whole EMT process as dispensable" based on the phenotype of two transcription factors (Snail and Twist) should be taken with caution.

Overall, these results highlight the importance of evaluating EMT based not on the expression of single transcription factors. In a recent EMT consensus statement, it is highly recommended for a researcher to assess EMT in many aspects, not only by checking few EMT protein markers at the molecular level but also their broad functional/characteristic evaluation at the cellular level [231].

Mesenchymal to epithelial transformation (MET) is the reverse process of EMT. However, the exact mechanisms for this transition remain unknown [251]. Currently, simplistic models suggest that the repression of EMT-TFs' activity causes a reverse EMT program: MET. Until now, it is widely accepted that MET is important, especially for the final step of metastatic cascade, colonization. Interestingly though, E-cadherin expression has been shown to important also for CTCs and extravasation for breast cancer [248]. A combination of cellular genetic/epigenetic alterations along with the absence of primary TME might contribute to the reversal of EMT in the metastatic sites. Of note, EMT mostly is not a cell-autonomous process but instead in crosstalk with TME [251].

3.4 Cancer Stem Cells

Cancer is initially proposed to form from stochastic genetic/epigenetic alterations of neoplastic cells, and with a Darwinian-like pressure surviving clones form big tumors with heterogeneity [252]. However, recent evidence suggests an alternative hierarchy model: some but not all cells have the capacity to form tumors, which are called cancer stem cells (CSCs) [253]. Tumor initiating cells (TICs) can form tumors in secondary recipients, which doesn't necessarily mean that they are CSCs. However, CSCs have more TIC capacity [254]. And finally, an alternative theory combines both stochastic and hierarchy model; cancer cells have the plasticity to interchange between CSC and non-CSC phenotypes, defining stemness as a "state" but not an "entity" [255].

Cancer stem cells have the potential to self-renew with unlimited proliferative capacity and differentiate into various progenies, like normal stem cells. Implanted CSCs can

form tumors with cellular heterogeneity of the primary tumor [255]. Next to metastasis and therapeutic resistance, EMT is also associated with CSC state [256,257]. However, the mechanistic links delineating the underlying interaction between CSC and EMT are yet not clear. It is determined that there is also a CSC heterogeneity, each mediating different aspects of cancer like tumorigenesis, tumor persistency, therapy resistance, and metastasis [258]. Additionally, how CSC subtypes are linked to EMT plasticity mechanistically and phenotypically are not clear [258]

Pancreatic CSCs are identified to have several markers, including CD24, CD133, CD44, EpCAM, CXCR4, ABCG2, ALDH-1, nestin, and c-Met [259–268]. There is a controversy regarding which markers are expressed alone or together in pancreatic CSCs [269]. The origin of pancreatic CSCs is not clarified, although they are hypothesized to derive from stem cells resident in healthy pancreatic tissue or bone marrow or de-differentiation of pancreatic cells via mutation [267]. Multiple techniques are employed to assess CSCness: detecting surface expression of CSC associated markers, sphere formation capacity, and tumor-initiating capacity. The sphere formation capacity of CSCs represents their self-renewal ability in non-adherent culturing conditions. Cultured to form spheres, human pancreatic cancer cells increase their expression of previously mentioned CSC surface markers [270–272]

Initially, pancreatic CSCs are isolated as triple-positiveCD44+, CD24+, EpCAM+ (0.2-0.8% ofthe whole population) population, which is showing 100 fold more tumor initiating capacity than triple negative counterpart [267] . CD133+ CSCs has been reported by multiple studies to possess pancreatic CSC properties [264,273,274]. Interestingly, 10- 40% of CD133+ subpopulation was also positive for aforementioned CD44+,CD24+, EpCAM+ triple positive population [264]. Within the same study, subpopulation CD133+,CXCR4+ is identified to possess high metastatic capacity.

An of note study is performed to check CSC marker expression in a cohort of 105 patients [275]. The surface expression of CD44, CD24, CXCR4, EpCAM, and nestin was shown to increase as the pancreatic carcinogenic transformation progressed from low-grade PanIN to cancer. CXCR4 and EpCAM expression showed a correlation with the differentiation grade of cancer.

Beyond the surface expression of CSC markers, there is additional heterogeneity linking EMT plasticity to CSC subtypes and eventual functional phenotype. Such a link is significant for the clear-cut understanding of the conclusion of this thesis work.

Therefore, we find it rather useful to discuss the EMT plasticity – CSC subtype link in detail after the presentation of the data we have.

3.5 Aim

Here in this work, we aim to understand the role of c-Rel in pancreatic cancer by using both *in vivo* and *in vitro* techniques. For this purpose, pancreas-specific c-Rel overexpression and knockout are achieved in preclinical pancreatic cancer mouse models. In comparison with *Rel* wild-type mice, pancreata of mice are analyzed histologically. Histopathological characterization of the tissues is performed with IHC stainings. Cancer cells from primary tumors are isolated to perform detailed *in vitro* analysis. Their EMT status, functional and descriptive CSC phenotype and, transcriptomics analysis delineated the mechanistic details of c-Rel impact. Furthermore, isolated cancer cells are used to model metastasis via intravenous injection.

4 MATERIALS AND METHODS

4.1 Mice

4.1.1 Mouse models

- Ptf1a$^{tm1(Cre)Hnak}$: *Cre* recombinase is knocked-in to exon-1 of *Ptf1a*. Ptf1a protein production is diminished, and *Cre* is expressed under the control of *Ptf1a* promoter/enhancer elements. It produces *Cre* specifically in the pancreas and additionally in the cerebellum, retina, partial duodenum, and neural tube. As part of this project, we also showed paternal transmission of germline recombination with the model. Therefore, in breedings, *Ptf1a-Cre* is transmitted to progeny always by mothers [77,276].
- Kras^{tm4Tyj}: This knock-in model possesses a Kras^{G12D} mutant allele in endogenous *Kras* locus, under the control of *lox-stop-lox* (LSL). Upon recombination, the stop cassette is deleted, allowing oncogenic Kras^{G12D} production [76].
- Trp53^{tm1Brn}: Exon-2 to 10 of the *Trp53* gene are flanked by *lox* sequences. Upon Cre recombination, the null allele is generated [78].
- Rel^{tm1Ukl}: Exon-1 of *Rel* is flanked by *lox*. Additionally, a promoterless *eGFP* gene is placed upstream of exon-1. Upon Cre recombination, the null allele is generated for *Rel*, and a *PGK* promoter meets with *eGFP* allowing reporter eGFP production in recombined cells [277].
- GFP-Rel: In this transgenic model, an N-terminus *eGFP*-tagged mouse *Rel* is randomly integrated into the genome with the use of a BAC clone. The locus contains an LSL downstream of the *CAG* promoter and upstream *eGFP*. Upon recombination, *CAG* induces overexpression of GFP-Rel protein. On C-terminus, the construct possesses a FLAG tag, followed by an IRES-Hygromycin resistance cassette [278]. The model was kindly provided by Prof. Dr. Marc Schmidt-Supprian.

- Multiple combinations are generated with the use of these models. The list of compound mutant mice and their abbreviations are shown in Table 2.

Table 2: List of mouse models used in this study along with their description and abbreviations

	Mouse Models	Description
CK	C: Ptf1a$^{tm1(cre)Hnak}$; K: Kras^{tm4Tyj}	Pancreas specific Ptf1a driven Cre expression causes oncogenic Kras^{G12D} expression.
CCK	C: Rel^{tm1Ukl}; CK	Pancreas specific knockout of c-Rel in CK.
GCK	G: GFP-Rel; CK	Pancreas specific overexpression of N' GFP-Tagged mouse c-Rel in CK.
CKP	P: Trp53^{tm1Brn}; CK	Pancreas specific Ptf1a driven Cre expression causes oncogenic Kras^{G12D} expression along with knocking out *Trp53.*
CCKP	C: Rel^{tm1Ukl}; CKP	Pancreas specific knockout of c-Rel in CKP.
GCKP	G: GFP-Rel; CKP	Pancreas specific overexpression of N' GFP-Tagged mouse c-Rel in CKP.

All mice are kept under specific pathogen-free conditions with access to water and food *ad-libitum* in accordance with the European Directive 2010/63/EU. All animal experiments were reviewed by Zentrum für Präklinische Forschung of the Technische Universität München, which adheres to the rules of federal German guidelines for ethical animal treatment, Regierung von Oberbayern.

4.1.2 Intravenous injection of cells

Littermates without the *Ptf1a-Cre* allele are used for tail-vein injection. 10^6 cells are collected and washed two times and resuspended in Mg/Ca^{++}-free PBS (200μL per injection), and injected with a 26G needle. Mice are sacrificed 28 days post-injection unless they show symptoms of burden. Pancreas, surrounding lymph nodes, liver, lung, duodenum, diaphragm, peritoneum, spleen, kidney, heart, and thymus are collected to analyze metastatic colonization histologically. Lung colonization is used as the primary output to assess differences in metastatic potential.

4.2 Molecular biology

4.2.1 Mouse genotyping

Ear clips and tail tips are used as the template for weekly genotyping and post-genotyping, respectively. Samples are lysed in tail lysis buffer (200uL DirectPCR lysis reagent-Viagen and 10μL Proteinase K-Roche) at 55°C shaker until dissolved. Proteinase K is inactivated by 85°C 1-hour incubation. For genotyping, 2μL from lysate is directly used as the template. GoTaq® Green Master Mix (Promega) is used for PCR reaction as follows: 7.5μL 2X GoTaq master mix, 0.6μL primer mix (10μM each),

4.9μL nuclease-free water and 2μL DNA template. The cycling protocol is as follows: 95°C-1 min, 40 cycles X (95°C-30 sec; 58°C 30 sec, 72°C 1.5 min), 72°C-10 min final elongation. All mice are genotyped for the respective floxed allele but also for their recombined product since paternally transmitted *Ptf1a-Cre* can cause germline recombination. Each mouse is validated to be germline recombination free also by post-genotyping. Primer sequences for genotyping are provided in Table 3.

Table 3: List of genotyping primers and theire respected band sizes

Name		Sequence	Expected sizes
Generic Cre	01	ACC AGC CAG CTA TCA ACT CG	wt: 350bp Cre/+: 200bp
	02	TTA CAT TGG TCC AGC CAC C	
	03	CTA GGC CAC AGA ATT GAA AGA TCT	
	04	GTA GGT GGA AAT TCT AGC ATC ATC C	
Kras	01	TGT CTT TCC CCA GCA CAG T	wt: 250bp flox: 100bp recombined: 300bp
	02	CTG CAT AGT ACG CTA TAC CCT GT	
	03	GCA GGT CGA GGG ACC TAA TA	
	01	GTC TTT CCC CAG CAC AGT G	wt: 622bp flox: 500bp recombined: 650bp
	02	CTC TTG CCT ACG CCA CCA GCT C	
	03	AGC TAG CCA CCA TGG CTT GAG TAA GTC TGC A	
Relb	01	AGG TTG ATG GTA ACT TTG GAT G	wt: 230bp flox: 270bp recombined: 186bp
	02	TCC AAA AAA ACC AAA CCA ACA AC	
	03	GTT TTC CCT GCT TGG TTC TGC	
Rel	01	CCA GCC AGG GTA AGT CTT CA	wt: 400bp flox: 266bp
	02	GCT AGG GGA AGG TGT CAC TGT	
	03	TCC AAA CTC ATC GAA GTT CCT	
	A	CAGGATGTTGCCGTCCTCCTTG	A+B recombined: 470bp A+C unrecombined: 470bp
	B	CCTGCAGCCAATAAGCTTATAAC	
	C	TATCATGTCTGGATCAATTCATAAC	
GFP-Rel	01	CTG CTG CAA GAT TGT GGT AAG A	wt: 290bp flox: 358bp
	02	AAT AGT GAG AGT GTG CGG GA	
	A	TGG GCA ACG TGC TGG TTA TT	flox: 385bp recombined: 584bp
	B	TTC TTC TGC TTG TCG GCC AT	
	C	TGC CTG CTT GCC GAA TAT CA	
Trp53	01	CAC AAA AAC AGG TTA AAC CCA G	wt: 288bp flox: 370bp
	02	AGC ACA TAG GAG GCA GAG AC	
	A	CAC AAA AAC AGG TTA AAC CCA G	recombined: 612bp
	B	GAA GAC AGA AAA GGG GAG GG	

4.2.2 RNA isolation and RT-qPCR

For RNA extraction, pancreatic tissues are freshly collected, homogenized and snap-frozen in 900μL RLT lysis buffer (1015762 Qiagen, Hilden, Germany) containing 1% β-mercaptoethanol (M6250 Sigma). For cells, the homogenization step is omitted. 200-300μL of lysates are used for RNA extraction via Maxwell® 16 LEV simplyRNA Purification Kit (Promega) for tissues and processed in Maxwell® 16 instrument (AS2000). RNA integrity and concentration are checked via NanoDrop 2000 spectrophotometer (Peqlab, Erlangen, Germany) and 1% agarose gel electrophoresis. 600ng RNA is used for cDNA synthesis by GoScript™ Reverse Transcriptase kit (Promega) with OligodT primer with manufacturer's recommended protocol. The 20μL cDNA final mix is diluted with 80μL nuclease-free water. 3μL of diluted cDNA mix is used per reaction for RT-qPCR. RT-qPCR is performed with LightCycler 480 machine (Roche) using Sybr Green Master Mix 1 (Roche) according to the recommended protocol of the manufacturer. A list of the primer sequences can be found in Table 4.

Table 4: Primer sequences used for mouse RT-qPCR

Gene	primer	Sequence 5'-3'
Rel	F	AGA CTG CG ACCT CAA TGT GG
	R	GCA CGG TTG TCA TAA ATT GGG TT
Cdh1	F	AGG TTT TCG GGC ACC ACT TA
	R	TGA TGT TGC TCT CCC CAA GT
Zeb1	F	CCA CTG TGG AGG ACC AGA AT
	R	CTC GTG AGG CCT CTT ACC TG
Zeb2	F	TAG CCG GTC CAG AAG AAA TG
	R	GGC CAT CTC TTT CCT CCA GT
Snai1	F	GGT CCC CAA CTA CGG GAA AC
	R	CTG TAG GGG CTC ACT GGG ATT
Snai2	F	TGG TCA AGA AAC ATT TCA ACG CC
	R	GGT GAG GAT CTC TGG TTT TGG TA

4.2.3 RNAseq analysis

Total RNA is isolated, and quality is assessed as described in section 4.2.2. RNAs are then sent to Novogene Europe Company Limited (Cambridge, United Kingdom). Further RNA sample quality check, mRNA library preparation with polyA enrichment,

sequencing with NovaSeq 6000 PE150 platform, and quality control of RNAseq are performed by the company. The results are further analyzed in collaboration with Dr. Mehmet Gönen for gene enrichment sets (Koc University, Istanbul, Turkey).

4.2.4 Protein extraction, SDS-Page, and Western blot

4.2.4.1 Protein extraction and Quantification

Collected tissues are homogenized and lysed in pre-chilled RIPA buffer (150mM NaCl, 1% NP-40, 0.5% Sodium deoxycholate, 50mM Tris pH:8.0) supplemented with fresh protease and phosphatase inhibitors (SERVA, Heidelberg, Germany). Cell pellets are only lysed without homogenization. Lysates are incubated on ice for 20 min, sonicated, and centrifuged at 13.200 rpm, 20min, 4°C. Supernatants are collected, and protein quantification is performed with Bradford Assay (Bio-Rad, Munich, Germany). Basically, Bradford stock solution is diluted 1:5 in water and aliquoted as 250μL per well/sample to the clear-bottomed micro-well plate. 2μL of each protein lysate is put to wells as triplicates and mixed. BSA (1mg/mL, Sigma) with 2uL RIPA buffer is used for standard curve generation. Optical-Density (OD) values are measured by Multiskan™ FC Microplate Photometer at 595nM. Based on the standard curve, protein concentrations are quantified and diluted accordingly. Lysates are also supplemented with 6X Laemmi Buffer and boiled for 5 min at 95°C, cooled down immediately on ice, centrifuged at room temperature (RT) for 5 min at maximum speed, and stored at -20°C for further use.

4.2.4.2 SDS-PAGE Gel

SDS-Polyacrylamide gel preparation and electrophoresis is performed with Mini-Protean® 3 Cell System (Bio-Rad). Depending on the target protein molecular weight, separating gel concentration is arranged. Per well, 30-50μg of each protein lysate is loaded to gel with 5μL reference protein ladder (26619, PageRuler™ Plus Prestained Protein Ladder, 10 to 250 kDa, ThermoFisher Scientific). The gel is run at 90V and 145V in stacking and separating gels, respectively. The recipe for 2x 1.5mm varying concentrations of separating and stacking gels are given below in Tables 5 and 6.

Table 5: Recipe for two separating gel for given concentrations.

Separating Gel Concentration	**7.5%**	**10%**	**12%**	**15%**
dH_2O (mL)	7.4	6.2	5.1	3.8
Tris-Cl 1.5M, pH:8.8 (mL) (Sigma)	3.9			
30/0.8% Acrylamid/Bis solution (Roth, Karlsruhe, Germany)	3.8	5	6	7.5
10% SDS (μL) (Sigma)	150			
10% APS (μL) (Sigma)	75			
TEMED (μL) (Fluka, Buchs, Schweiz)	23			

Table 6: Recipe for two stacking gel for given concentrations.

Stacking Gel	
dH_2O (mL)	4.5
Tris-Cl 0.5M, pH:6.8 (mL)	2
30/0.8% Acrylamid/Bis solution	1.1
10% SDS (μL)	75
10% APS (μL)	38
TEMED (μL)	15

4.2.4.3 Western Blot

The proteins are transferred to either PVDF or nitrocellulose membranes (0.2-0.45μm, Merck-Millipore) by Mini Trans-Blot Cell™ System (Bio-Rad). PVDF membrane is incubated in methanol for 1.5 min before transfer. Blotting is performed with prechilled transfer buffer (3.025gr Tris, 14.4gr Glycine, 200mL Methanol, up to 1L dH_2O), 100V for 90-120 min on ice. Membranes are blocked 1 hour at RT with either 5% milk or BSA in TBS-t (2.4gr Tris, 8.3gr NaCl, up to 1L dH_2O, pH:7.6, 1mL Tween-20). Membranes were then incubated with primary antibody solutions (Table 7) over night at four °C, on a shaker. The next day membranes are washed 3 x 15 min with TBS-t at RT on the shaker. Then membranes are incubated with HRP-conjugated secondary antibody solutions for 1 hour at RT and washed again. Signal development is performed with Amersham ECL™ or ECL™-prime reagent, Amersham Hyperfilm™, and Amersham Hyperprocessor™ (GE Healthcare, Buckinghamshire, UK). Exposure times are set according to the target protein.

Table 7: List of antibodies used for western blot.

Antibody	Catalog #	Company
c-Rel	Sc-71	Santa Cruz Biotechnology
	AF-2699-SP	R&D Biotechnology
β-Actin	A2228	Sigma Aldrich
ERK-1/2	Sc-514302	Santa Cruz Biotechnology
RelA	Sc-372	Santa Cruz Biotechnology
RelB	Sc-226	Santa Cruz Biotechnology
Zeb1	A301-922A	Bethyl Laboratories
E-cadherin	610181	BD-Biosciences
β-Catenin	9562	Cell Signaling
HSP90	Sc-7947	Santa Cruz Biotechnology
N-cadherin	610921	BD-Biosciences
Vimentin	Ab8978	Abcam
Slug	9585	Cell signaling

4.2.5 Co-immunoprecipitation assay

Cultured cells (~50x10^6cells) are washed twice with ice-cold PBS in 10cm cell culture dishes, and 1 mL Co-IP lysis buffer (1% Triton-X, 150mM NaCl, 2mM EDTA, 50mM Tris-Cl pH:8, fresh protease/phosphatase inhibitors, fresh 0.5mM DTT, Fresh 100μM PMSF) is added and incubated on ice for 30 minutes to allow lysis. The lysed sample is scraped and collected in a 1.5mL Eppendorf tube, and sonicated for 3x3 pulse after cooling down the sonication probe, and passed through a syringe for few times until smooth. The lysate is centrifuged for 15min at max speed, 4°C. Now on all centrifuge steps are performed at 2500g, 4°C, 3 min unless indicated. The lysate is pre-cleared for unspecific binding to protein A/G microbeads (20241, Pierce Protein A/G Agarose, Thermo Scientific) with the addition of pre-washed 20μL bead (bead solution has 50-50% bead and slurry). Finally, the volume is adjusted to 1mL mL. 10% of the whole lysate is separated as input. Protein concentration is calculated with Bradford assay. The remaining lysate is split into 4 parts to be incubated with primary antibodies at 4°C on a rotator. 1-2mg of protein per cell lysate is incubated 2 hours at 4°C rotator with 2μg antibody. The antibodies are anti-c-Rel sc-71, anti p65 sc-372, anti-RelB sc-226, Rabbit IgG. Meanwhile, the beads are equilibrated with wash buffer and blocked with 1% BSA in lysis buffer for 1hr. The lysate-antibody mix then put-on blocked beads for incubation on rotator at 4°C. The next day, the bead-lysate-antibody mixture is

centrifuged, and the supernatant is collected as flow-through for quality check of IP. The beads are washed 2x with 500μL lysis buffer and 2x with 1mL PBS-TritonX 0.1%. The beads are then resuspended in 100μL lysis buffer + 20μL Laemmi Buffer mix, boiled and centrifuged for further use in western blot.

4.3 Histology

4.3.1 Tissue sectioning

Collected tissue samples are fixed in 4% PFA (Merck, Darmstadt, Germany) in PBS for 48h, dehydrated, and embedded in paraffin. The tissues are sectioned as 2μm slices with a microtome (HM 355 S, MICROM, Walldorf, Germany) and collected to adhesive-coated slides (SuperFrost® Plus, Menzel, Braunschweig, Germany). Slides then dried at RT and stored for further use. For cryosectioning, fresh tissue samples are snap-frozen in O.C.T. Compound (Tissue-Tek, Weckert Labortechnik, Kitzingen, Germany) and stored at -80°C. They are sliced with cryotome with 10μm thickness, mounted, and stored in -20°C for further use.

4.3.2 Haematoxylin and Eosin Staining (H&E)

Paraffin sections are deparaffinized with two changes of ROTI®Histol 5 min each (Carl ROTH), rehydrated by 2X 3 min incubation in 100%-96%-70% ethanol, and dH_2O in order. The slides are incubated in hematoxylin solution (Merck Millipore, Billerica, MA) for 3.5 min, washed under running tap water for 10 min. Then slides are incubated in eosin solution (Merck) for 3.5 min and dehydrated by 25 seconds incubation in 96% ethanol and isopropanol. Slides then passed through two changes of ROTI®Histol and mounted with Pertex (Medite GmbH) with coverslips. Microscopic histological analysis is performed with Axiostar Plus (Carl Zeiss, Göttingen, Germany).

4.3.3 Immunohistochemistry staining

Tissue sections are deparaffinized and rehydrated, as explained in 4.3.2. Heat-induced antigen retrieval (HIAR) is performed either by microwave (3 min 900W, 3 min 120w, 14min 360W) or water bath incubation (96°C). Depending on the antibody, a different antigen retrieval solution is used. Slides are cooled down 20 min to RT washed twice for 5 min in dH_2O and incubated in 3% hydrogen peroxide to block endogenous peroxidase activity. The slides were then washed with water and specified washing buffer two times at RT. Blocking is performed with diluted (5% in selected washing buffer) serum of species, which secondary antibody is raised in and avidin drops (4 drops in 1mL, SP-2001 Vector Laboratories, CA), at RT for 1 hour.

After 5 min X 3 wash, primary antibody solution (diluted in blocking solution with biotin) is added and incubated overnight at 4°C. The next day, slides are washed with wash buffer and incubated for 1 hour at RT with respective biotinylated secondary antibody. Meanwhile, the avidin-biotin complex is prepared according to the manufacturer's protocol (PK6200, VECTASTAIN elite ABC-HRP kit, VECTOR Laboratories). Slides are washed 3X with wash buffer and incubated for 30 minutes with ABC solution at RT. Finally, slides are washed 3X with dH_2O, and the signal is developed with DAB reagent (Vector Laboratories, CA), counterstained with hematoxylin, dehydrated, and mounted as explained in section 4.3.2. The list of antibodies, their respective HIAR protocol, and washing buffers can be obtained in Table 8.

Table 8: List of antibodies and their respective HIAR protocols for IHC.

Antibody target	Company Catalog number	Dilution factor	HIAR	Wash buffer
c-Rel	R&D AF-2699	1:25	Citrate buffer pH:6	BondRxm (Leica, Wetzlar, Germany)
GFP	0R-GRO11	1:2500	EDTA pH:9	
Integrin β3	Novus NBP2-67416	1:200	Tris-EDTA pH:9	TBS-t
Gata-6	CST 5851	1:200	Vector antigen unm. solution (H-3300)	
CD44	SantaCruz sc18849	1:100		
Vimentin	Abcamab8978	1:200	Tris-EDTA pH:8	
β- Catenin	CST 9562	1:200	Citrate buffer pH:6	
P-ERK 1/2	CST 4376	1:100		
E-cadherin	BD 610181	1:100		0.3% Triton-X & TBS-t
BrdU	Bio-Rad MCA2483T	1:1000		PBS
CK-19	Troma III	1:300		PBS
Fibronectin	Abcam ab199056	1:250		TBS

4.3.4 Sirius Red Staining

Slides are deparaffinized and rehydrated as described previously. Nuclei are stained with Weigert's Haematoxylin for 8 minutes and washed under running tap water for 10 minutes. Slides are then stained with the pico-Sirius red solution (0.5gr Sirius Red F3B (C.I. 35782), 0.5L saturated aqueous solution of picric acid) for one hour at RT. Slides are then washed twice with acidified water (0.5% glacial acetic acid in water), dehydrated by multiple changes of ethanol and histoclear, and mounted with Pertex.

4.3.5 Histological quantification and statistics

The stained slides are scanned by the pathology department, and histological quantifications are performed by either Aperio ImageScope (Leica), QuPath, or

ImageJ (NIH) software. Representative images are either taken from scanned slides or by microscope Axiostar Plus (Carl Zeiss, Göttingen, Germany).

4.4 *In vitro* cell culture experiments

4.4.1 Isolation of tumor cells from mice and their cultivation

Mouse primary pancreatic tumor cells are isolated from fresh tumor tissues. Small pieces of tumor tissues from different locations are minced and incubated in cell culture medium (Dulbecco's modified Eagle medium (DMEM) supplemented with 10%FBS (#10082147; Gibco), 1% PenStrep (#1500-063; Gibco), 1% Non-Essential-Amino-Acids (NEAA #11140050; Gibco) and incubated in humidified 37°C incubators with 5% CO_2 supply. GCKP cells are passed through Hygromycin selection to eliminate cells without *GFP-Rel* recombination. The cell lines are validated to have c-Rel overexpression and knockout in GKCP and CKCP, respectively. These cells are also validated to possess an eGFP signal by flow cytometry.

4.4.2 Sphere formation assay

Adherent cells are trypsinized as single cells and counted as usual. Cells are then diluted in sphere culture medium as 2000 cells/mL and seeded in 2mL medium on Corning ULTRA low Cell culture 6-well plates (Corning, 3471). Cells are fed every 2-3 days with a fresh medium. 7-10 days after seeding, cells form 1st generation of spheres to be quantified. Pictures of the whole well area are taken. Their size and numbers are quantified by ImageJ software. Sphere culture medium is prepared as given: 500mL cDMEM/F12 (1:1) (Gibco, 21331-020), 5mL Pen/Strep (Gibco, 1500-063), 2mL fungizone (Gibco, 15290-018), 5mL L-Glutamine (Gibco, 25030-024), 10mL B-27 supplement (Gibco, 17504-044), 10μg FGF-β (BioLegend, 579602).

4.4.3 Extreme limiting dilution assay (ELDA)

For the extreme limiting dilution assay (ELDA), tumor cells were seeded in a density of 0.75, 3, 10, and 20 cells in 20μL of matrigel per well with seven replicates in a 96-well plate. After solidification, 80μL of media was added to each well, and cells were kept for seven days in the incubator. Thereafter, each well was evaluated regarding spheroid formation (yes or no), and the free online ELDA software was used for detailed analysis [279]. The experiment is performed by Katja Peschke in collaboration with the laboratory of Prof. Dr. med. Maximilian Reichert in Klinikum rechts der Isar.

4.4.4 Flow cytometry

Cultured cells are collected as single-cell suspension after washing and trypsinization as usual. All centrifugation steps are performed at 4°C, 300rcf, 5 min unless indicated. All steps are performed on ice. After multiple PBS wash, cells are re-suspended in 250μL FACS buffer (PBS,0.1%FBS, 0.5mM EDTA) and blocked with Fc-block (14-0161-85 eBioscience) with 1:200 dilution for 20 min. After 3x wash with 1mL FACS buffer, cells are incubated with antibodies with the manufacturer's recommended dilution (Table 9). Single and multi stains of each antibody are performed for proper compensation. Stained cells are washed 1x wash with 250μL FACS buffer and 2x with PBS to remove remaining FBS. Cells are finally resuspended in 300μL PBS. Zombie Red™ (423110, BioLegend) is added to appropriate samples with 1:500 dilution 15 minutes before analysis. Each sample is passed through 20μm cell strainer before analysis with Gallios Flow Cytometer (Beckman Coulter). Further analysis is performed with FlowJo software.

Table 9: List of antibodies used for flow cytometry experiment

Antibody	Conjugate	Catalog #	Company
CD133	AlexaFluor 647	141216	BioLegend
CD44	Pacific Blue	103019	BioLegend
Sca-1	AlexaFluor 700	108142	BioLegend
CXCR4	PE	130-118-682	MiltenyiBiotec

4.4.5 Image-stream flow cytometry

For the intracellular staining of cells eBioscience™ Foxp3 / Transcription Factor Staining Buffer Set (00-5523-00, ThermoFisher Scientific) is used. Each centrifugation step is performed at 300rcf, 5 min unless indicated. Collected single cells are fixed at RT in the dark for 1 hour on a rotator, then washed with 500μL permeabilization buffer for two times and finally resuspended in 50μL permeabilization buffer. Antibodies are added to be incubated overnight at 4°C (RelA, sc-372 1:800 dilution; RelB sc-226 1:100 dilution; c-Rel sc-71 1:200 dilution). The next day, cells are washed twice with permeabilization buffer and incubated with 1:500 diluted secondary antibody (Anti-Rabbit AlexaFluor 488 conjugated, Invitrogen) for 30min at 4°C in the dark. After washing three times, cells are resuspended in 25μL permeabilization buffer with or without DAPI. Further analysis is performed with ImageStream MKII (Luminex Corp.)

and analyzed with IDEAS software having an integrated module scoring nuclear translocation [280]

4.4.6 Nuclear fractionation

Sub-confluent adherent cells on a 10cm dish are washed twice with ice-cold PBS, lysed with pre-chilled 1mL hypotonic buffer on ice for 30 minutes, and collected to a 1.5mL tube after scraping. The lysate is centrifuged at 13200rpm for 15 min at 4°C. The supernatant is saved as cytoplasmic fraction. The pellet is washed 5x with 300μL hypotonic buffer, and each time, the supernatant is discarded. Finally, the nuclear pellet is dissolved in 200μL nuclear buffer to concentrate the nuclear fraction. The fraction is passed through a 31G syringe multiple times to break down the nuclear envelope and incubated with 0.5μL benzonase (9025-65-4, Sigma) for 20 min on ice to cut DNA and release bound proteins. Finally, the fraction is centrifuged at max for 15 min, and the supernatant is denatured with boiling with laemmi buffer. Hypotonic buffer contains 10mM HEPES, 1.5mM $MgCl_2$, 10mM KCl, 0.5mM DTT, 0.1% NP40 and freshly added protease/phosphatase inhibitors. Nuclear buffer contains 20mM HEPES, 100mM KCl, 100mM NaCl, 0.1% NP40, 0.5mM DTT and freshly added protease/phosphatase inhibitors.

4.4.7 Immunocytochemistry

Cells are seeded on 8-well chambers (94.6140.802, x-well, Sarstedt) in the full culture medium. After the proper treatment, cells are washed with Hank's Balanced Salt Solution (HBSS) supplemented with Ca/Mg^{++}, fixed with 4% PFA diluted in HBSS at 37°C for 10 min, and washed 3x with HBSS at RT. For cell permeabilization, fixed cells are washed one time with PBS/Triton-X 0.1% for 5-7 minutes at room temperature and washed again. Each staining is blocked with 2% BSA (pre-filtrated to remove speckles) for 1 hour at RT. Cells are incubated overnight at 4°C with diluted primary antibody solution (c-Rel antibody R&D AF2699, 1:100 dilution in blocking solution). The next day after three washes, cells are incubated with Alexa-Fluor 568 conjugated anti-goat antibody (1:1000 dilution in 2% BSA, Thermo Fisher Scientific) for 1 hour at RT. After three washes, cells are mounted with DAPI medium (H-1200, Vector Laboratories). Slides are analyzed by fluorescence microscopy (Axiostar Plus FL, Carl Zeiss).

4.4.8 Collagen contraction assay

Rattail collagen type 1 (9007-34-5, Corning) is diluted in 0.1% sterile acetic acid as 3mg/mL. for Collagen solidification, a NaOH titration assay is performed. 76μL 0.036N

NaOH is selected to solidify 1.5mL collagen/cell culture solution. Per well, 200.000 cells in 1mL full culture medium, 0.5mL collagen mix, and NaOH are mixed immediately and put on each well of 24 well plates (3524, Corning). For each cell, technical triplicates are prepared. After polymerization (20 min at RT), each well is humidified with 0.6mL full culture medium. Each gel is dissociated from well gently by running a 10μL tip around. Contraction of gels is observed 2-5 days after seeding. Plates are then scanned, and the surface area of each gel is quantified with ImageJ software.

4.4.9 Viability Assay

Cells are seeded to black-flat bottomed 96w well-plates (3916, Corning) as 5000 cells/well, 100μL, as technical triplicates. For each day, one plate is prepared. At every time point, culture media is discarded, and the plate is stored at -80°C. After each plate is collected, DNA quantification is performed. Frozen plates are thawed, and 100μL AT extraction buffer supplemented with 5μM Nuclear Green™ DCS1 (AAT Bioquest) is put to each well. The plates are covered in dark and incubated 15min at 37°C. Then, 150μL AT dilution buffer is put into each well and mixed. Fluorescence reads are taken by a microplate reader (BMG LabTech). The fluorescent AU of each day is normalized to the first plate, which is taken one day after seeding to quantify relative viability change. AT extraction buffer: 1N NH_4OH, 0.2% Triton-X 100. AT dilution buffer: 100mM NaCl, 10mM EDTA, 10mM Tris pH:7.

4.4.10 Fibronectin coating

Human fibronectin (1918-FN-02M, R&D Systems) is stored as 2μg/μL in at -80°C and thawed before use. Fibronectin (FN) is diluted as 2μg/mL in PBS (supplemented with 0.5mM Mg^{++} and 0.9mM Ca^{++}) and aliquoted as 100μL per well onto black/flat bottom plates (3916, Corning) under sterile conditions. The plates are then incubated overnight at 4°C. The next day, FN media is removed and dried in a running hood for 1 min. Each well is blocked 30 min at RT with 200μL 1% Fraction V BSA (10735078001, Merck) in PBS. The coated plates are used either for FN adhesion assay or immunofluorescence staining.

4.4.11 Fibronectin adhesion assay

Adherent cells are prepared as a single cell suspension in PBS with Mg/Ca^{++} with a concentration of 10^6/mL. 100μL of cell suspension is aliquoted onto each well, and the plate is spun down for 2 min at 411g with a slow brake. After 3-5 hours incubation in

cell culture incubator, unattached cells are discarded by 2x wash with PBS. Cell number in each well is quantified by a slightly modified viability assay protocol (section 4.4.8). A plate without wash is used as seeding control. Wells with BSA blocking without FN coating is also used as a negative control.

4.4.12 Cytokine array

2x 10^6 cells are seeded to 10cm dishes in the full culture medium. The next day, the plates are washed twice with PBS and refed with 6mL full culture medium. After two days of conditioning, mediums are collected and centrifuged at 1000rcf for 5 minutes to remove cell debris. For each plate, the cell number is re-quantified for normalization of difference in proliferation. Cytokine array is performed with Proteome Profiler Mouse Cytokine Array Kit, Panel A (ARY0006, R&D Systems) as manufacturer's protocol. The integrated density of each dot is quantified by ImageJ software and normalized to cell number.

4.4.13 Viral packaging and lentiviral transduction

For lentiviral packaging, psPAX2 (Addgene: 12260), pMD2.G (Addgene: 12259), and shRNA expressing pLKO vectors purchased from Sigma Aldrich. Mouse *Rel*, TRCN:0000218674 (catalog number: SHCLNG), and negative control non-targeting MISSION shRNAs (catalog number: SHC016-1EA) are used. 4922ng psPAX2, 2760ng pMD2.G, and 3220ng shRNA-pLKO1-puro are co-transfected to HEK-293T cells via Jet-PRIME transfection reagent (Polyplus) per manufacturer's protocol. Medium is changed twice 4-18 hours post-transfection. Post-18h, 30% FBS containing full supplemented medium is put for viral production. After 48 hours, the medium is collected, and the virus is concentrated via Lenti-X-Concentrator (631232, TAKARA) as the manufacturer's protocol. Virus amount is titrated, and 200.000 cells per well in 6-well plates are transduced with a selected volume of the virus along with 2μL polybrene (TR-1003-G, Sigma Aldrich) in 500μL full supplement medium. After two days, cells are washed and put in selection with puromycin (concentration is pre-determined for each CKP cell). Selected cells are expanded and validated for knockdown with western blot.

4.5 Statistics

Prism 5 software (GraphPad Software, Inc) is used for statistical analysis. All statistics are performed with One-way analysis of variance ANOVA test and Tukey's multiple

comparison test ($p<0.05$ *, $p<0.01$ **, $p<0.001$***) unless indicated. The data are displayed as mean ± standard error means (SEM).

5 RESULTS

5.1 c-Rel in human pancreatic cancer

An oncogenic function of c-Rel in multiple human solid tumors has already been studied. We stratified patients based on *REL* mRNA expression and copy-number-variation (CNV) in the human TCGA (The Cancer Genome Atlas Program) dataset with the help of an exploration tool UCSC-Xena [281]. Results indicate no statistically significant difference in overall survival (Figure 3A). Additional patient stratification based on the mutational status of *KRAS* and *TP53* also has no significant difference (Figure 3A). With the use of the GEPIA exploration tool compiling TCGA and GTEx data, we analyzed *REL* levels [282]. Data indicates that *REL* expression increases in tumor samples compared to healthy tissues (Figure 3B). Importantly, *REL* level is significantly higher in the last stage tissues of patient tumors (Figure 3C). Moreover, we compiled other transcriptomics datasets using various patient cohorts with the help of ONCOMINE tool [283] (Table 10). In two of the datasets (marked in grey), *REL* expression is significantly higher in tumor cells than healthy counterparts. We validated the ubiquitous protein expression of c-REL *in vitro* human pancreatic cancer cell lines (Figure 3D) and *in vivo* human PDAC patient samples (Figure 3E). c-REL protein is not only localized into premalignant/malignant cells but also in tumor microenvironment cells (arrows).

Table 10: List of pancreatic cancer datasets analyzing REL mRNA expression

Analysis	Reference	# of Pancreatic Samples		Statistics	
		Cancer	Normal	Fold change	p-value
Logsdon	[284]	10	5	-1.186	0.698
Pei	[285]	36	16	1.456	0.005
Iacobuzio-Donahue	[286]	12	5	1.379	0.125
Grutzmann	[287]	11	11	1.407	0.151
Buchholz	[288]	8	6	1.035	0.312
Segara	[289]	11	6	1.094	0.29
Badea	[290]	39	39	1.434	0.002
Ishikawa	[291]	24	25	1.044	0.328

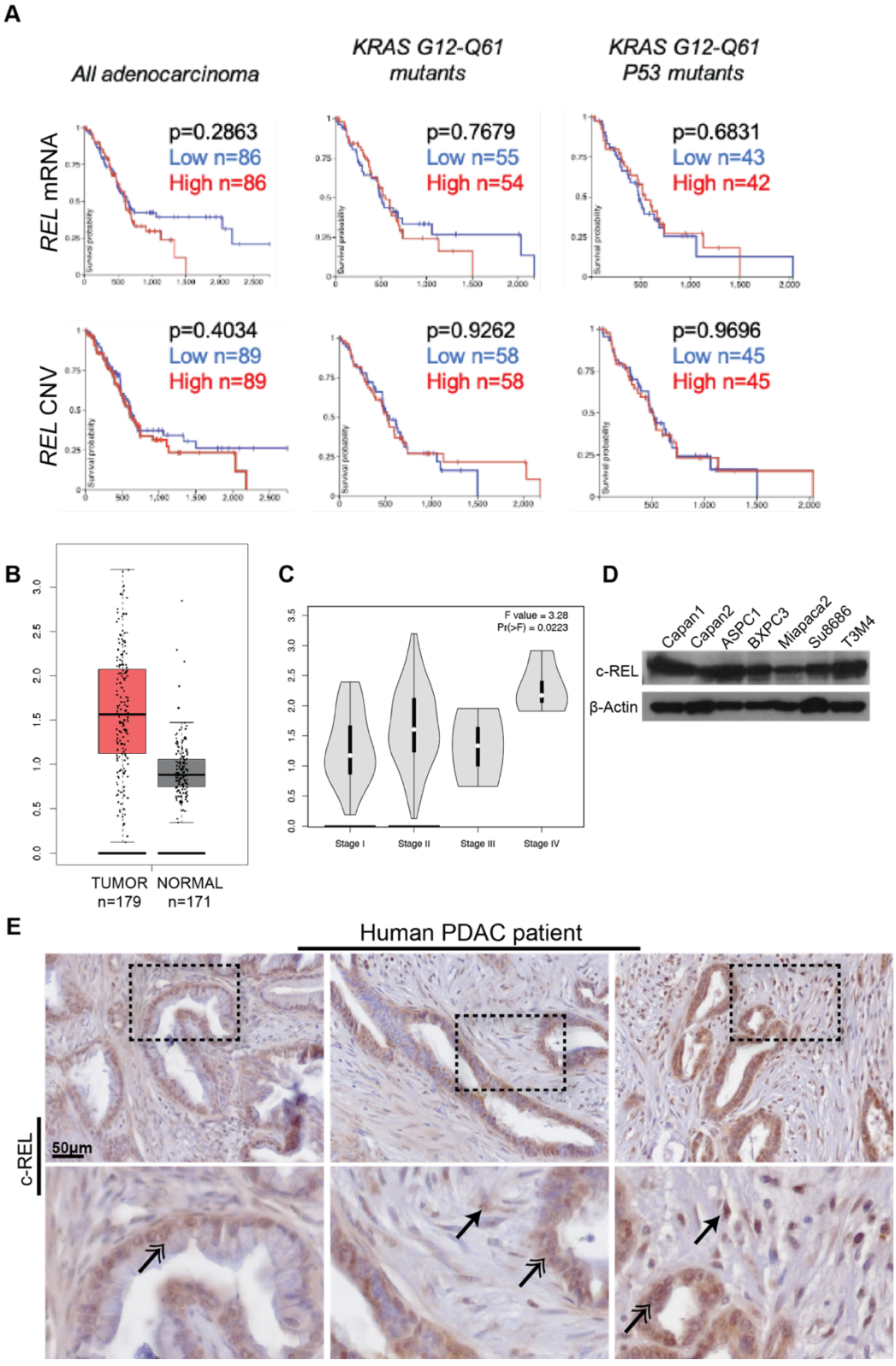

Figure 3: c-REL in human pancreatic cancer. A) TCGA dataset Kaplan-Meier survival curve analysis for *REL* mRNA and CNV in unstratified and stratified patient cohorts. B) *REL* mRNA expression in tumor vs normal pancreatic tissue within TCGA and GTEx dataset. C) *REL* mRNA expression level in different stages of human pancreatic cancer in TCGA dataset. D) Expression of c-REL in isolated human pancreatic cancer cell lines. E) c-REL IHC staining in human pancreatic cancer tissue.

5.2 c-Rel in mouse pancreatic cancer

5.2.1 c-Rel expression in mouse PDAC samples

In order to study c-Rel in murine pancreatic cancer, we utilized the highly used PDAC mouse models CK and CKP. CK model harbors a *Ptf1a-Cre*; *Kras*^{G12D} alleles allowing pancreas-specific expression of oncogenic-mutant Kras^{G12D}. This model recapitulates PDAC progression from ADM structures to cancer. Additional *Trp53*^{floxflox} allele (CKP) allows pancreas-specific knockout of *Trp53*, which generates a rather aggressive tumor with a swift tumorigenesis process. c-Rel is expressed in both cancer cells isolated from tumors and tissue samples, as shown by western blot analysis (Figure 4A). Additionally, IHC results indicate that c-Rel is expressed in both premalignant lesions (CK 18w) and cancer cells (CK tumor), along with cells in tumor microenvironment (Figure 4B).

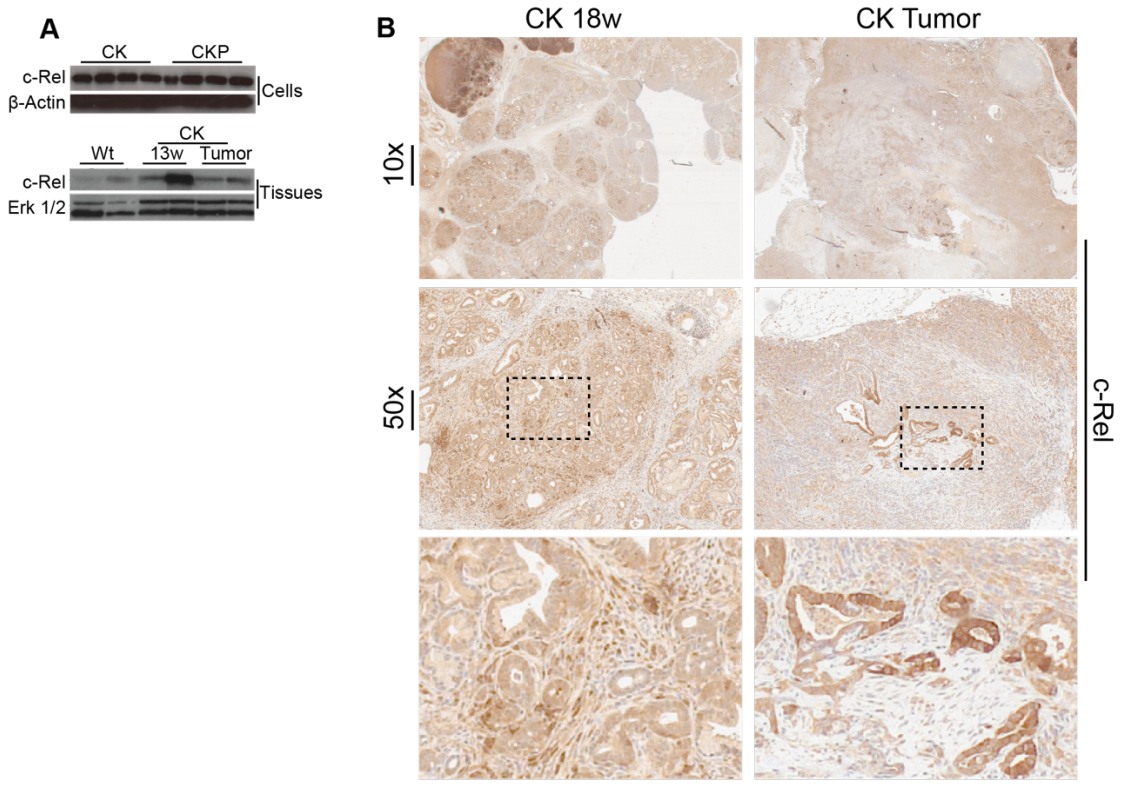

Figure 4: c-Rel is expressed in Mouse pancreatic cancer. A) western blot analysis for c-Rel expression in isolated CK and CKP cancer cells (top panel), and c-Rel expression in pancreata of wt, 13w old mice containing premalignant lesions, and tumor. B) c-Rel IHC stainings in 18w old and end-point sacrificed mouse pancreata from CK. IHC qualitity is assessed by a pathologist.

5.2.2 Activation of c-Rel in NF-κB signaling pathway

c-Rel nuclear localization has been reported to be very dynamic [292,293], which can be used as an indication for its transcription factor activity in NF-κB signaling. Hence, we used leptomycin-B, a nuclear export inhibitor, to check c-Rel nuclear localization in basal conditions. With both TNFα and leptomycin-B treatment, c-Rel nuclear localization is increased in KPC cells (Figure 5A). We validated these results with imaging flow cytometry in which nuclear localization can be quantified. Eight hours of TNFα treatment increased both RelA and c-Rel nuclear localization, unlike RelB (Figure 5B). Additionally, a co-immunoprecipitation experiment identified RelA as a c-Rel binding partner in basal conditions in different CKP cell lines, in accordance with the previous reports (Figure 5C).

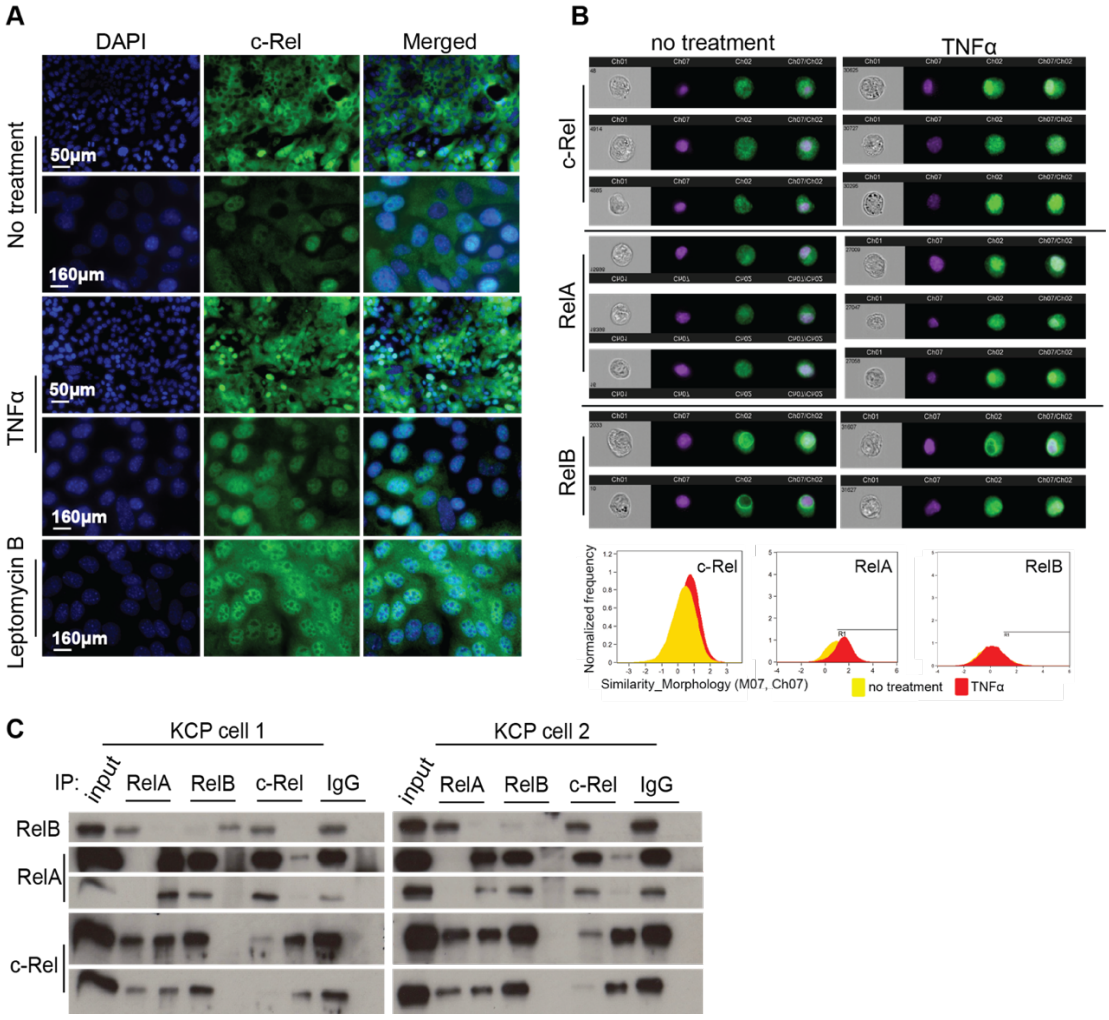

Figure 5: Activation of c-Rel within NF-κB signaling. A) Immunofluorescence staining of c-Rel in mouse CKP cells with TNFα and leptomycin-b treatment. B) Image stream analysis of c-Rel, RelA and RelB nuclear translocation upon 8 hours TNFα treatment. C) Co-immunoprecipitation analysis of c-Rel, RelA and RelB, with two CKP cells cultured under standard conditions.

5.2.3 Genetic Manipulation of Rel in PDAC mouse models

To elaborate c-Rel function in murine pancreatic cancer, we knocked-out and overexpressed *Rel* in the CKP model. Now on, *Rel* knockout and overexpression models will be named CCKP and GCKP, respectively. A depiction of both models can be found in (Figure 6A). Due to the possibility of paternal germline recombination observed in the *Ptf1a-Cre* model, we post-genotyped all of the mice accordingly (Figure 6B-C). The models are additionally validated by eGFP and c-Rel IHC stainings (Figure *6D*). In CCK tissues, robust c-Rel expression as observed only in the cells of TME as also validated by a pathologist (Figure 6D). In western blot, eGFP tagged c-Rel gave an expected shift of ~33kDa in c-Rel blots of bulk pancreatic tissue (Figure 6E). In parallel, reduction of c-Rel expression is also validated in bulk pancreatic tissue (Figure 6F).

5.2.4 c-Rel level regulates pancreatic histopathology

The survival graph of CKP, CKP, and GCKP indicates that c-Rel broadly acts as an oncogene in pancreatic cancer. With the overexpression of c-Rel, survival gets significantly shorter, whereas with c-Rel knockout, survival gets significantly longer (Figure 7A). There was no difference in the pancreatic weight/ body weight ratio (Figure 7B). However, histological morphology showed a remarkable difference, especially in c-Rel overexpression mice (Figure 7C). Classification of the tumor types revealed a higher incidence of undifferentiated tumor formation as c-Rel level increases (Figure 7D). Additionally, the proliferation rate of cells is increasing in parallel to the c-Rel level (Figure 7E).

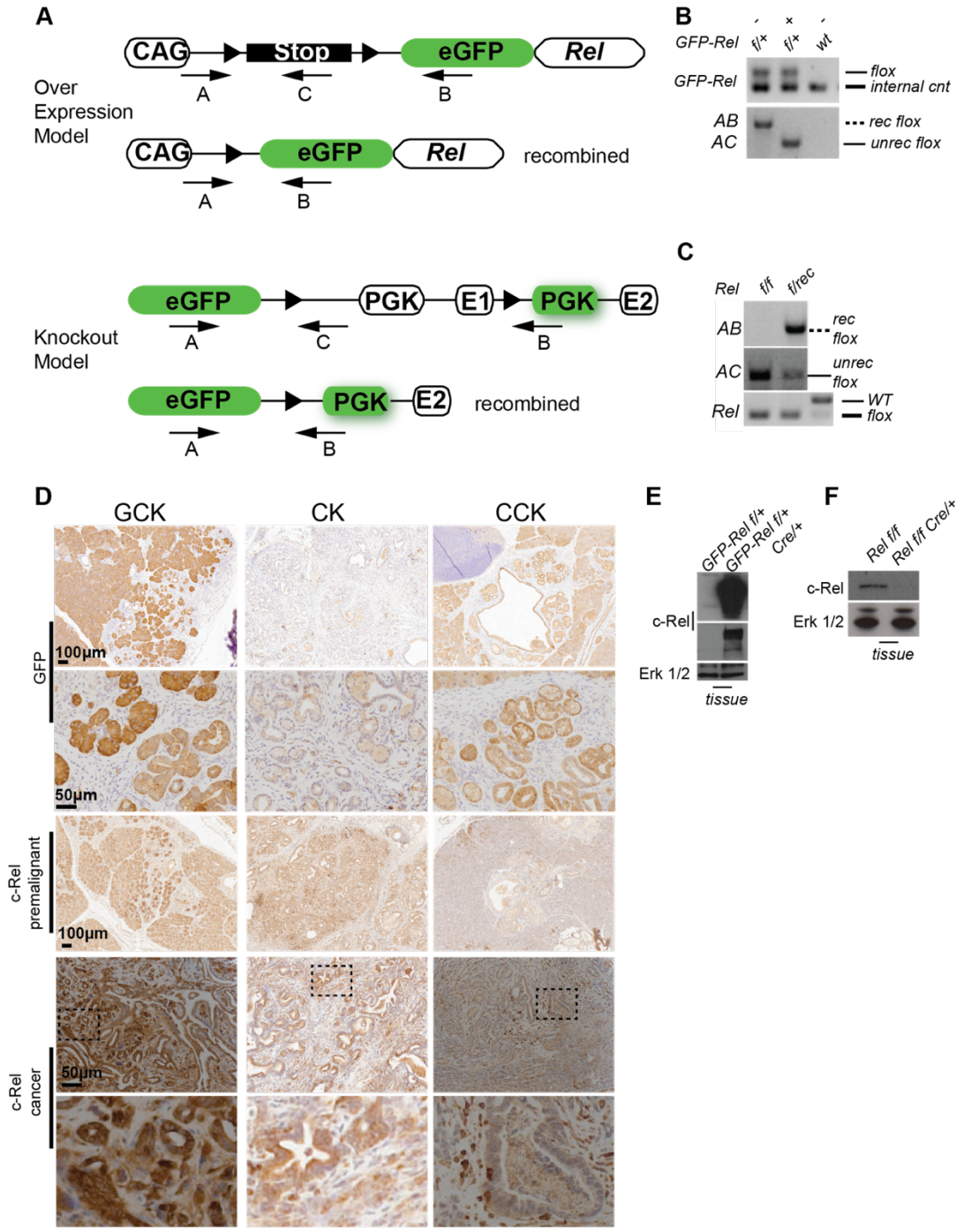

Figure 6: A) Schematics for both *Rel* knockout and overexpression models. In overexpression model (GFP-Rel) After recombination N-terminus eGFP tagged c-Rel meets with CAG promoter driving overexpression (Top). In knockout model, a promoterless eGFP gene meets with PGK promoter after recombination of *Rel*'s exon-1. Arrows indicate locations of primers, which are designed to test recombination. B-C) Representative genotyping PCR results for overexpression model recognizing wt/flox and recombined/unrecombined flox alleles and for knockout model recognizing wt/flox and recombined/unrecombined flox alleles. D) IHC staining for eGFP in GCK (overexpression), CK (c-Rel wildtype control) and CCK (knockout) tissues. E-F) c-Rel western blot results of pancreata with c-Rel overexpression and knockout.

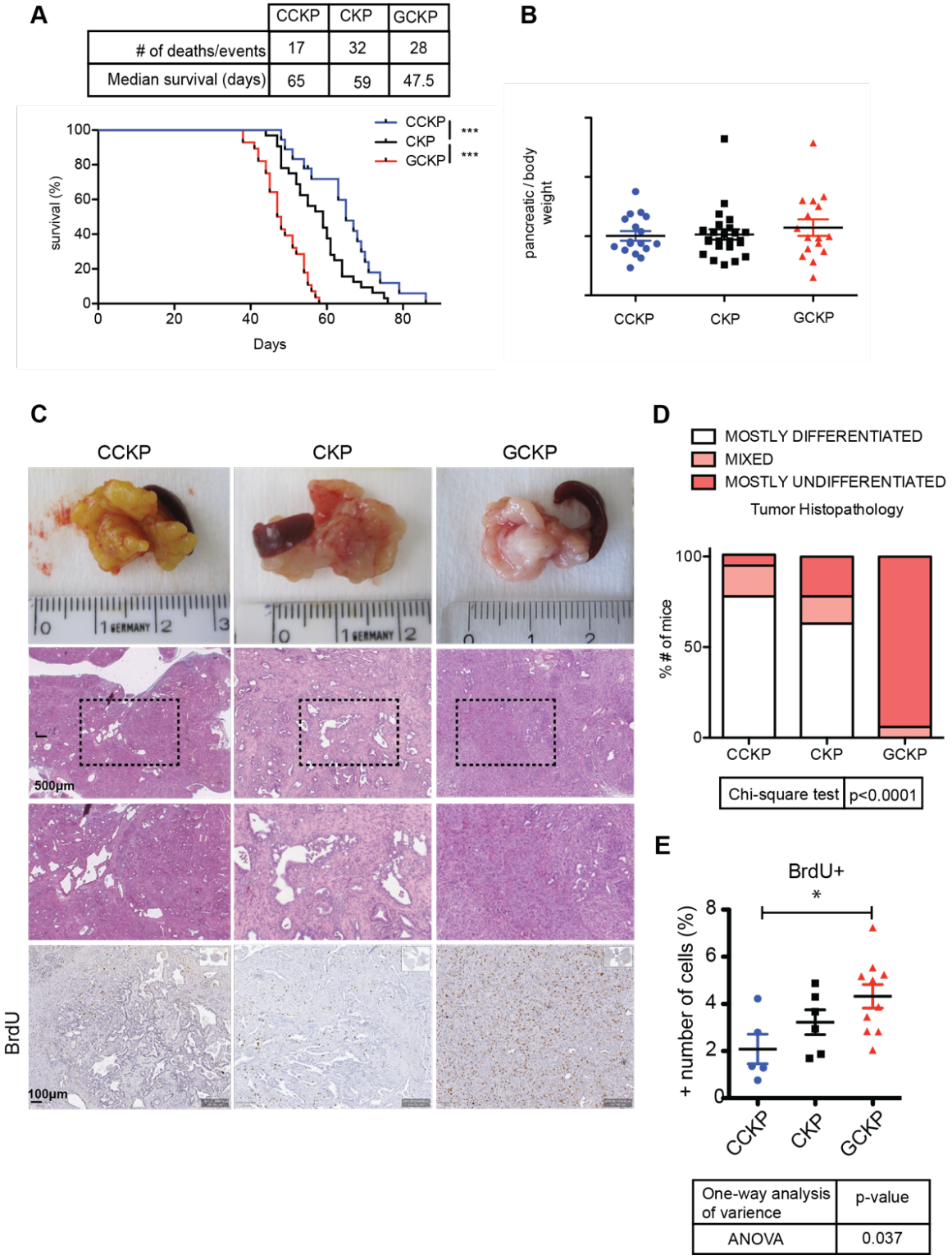

Figure 7: c-Rel acts as an oncogene in CKP model. A) Kaplan-Meier survival analysis for CCKP, CKP and GCKP mice. Statistical analysis is performed with log-rank (Mantel-Cox) test. B) Pancreas/body weight ratio for CCKP, CKP and GCKP tumors. C) Representative macroscopic and microscopic H&E images are given. D) Quantification of histological tumor types are given. CCKP n=18, CKP n=27, GCKP n=17. E) Proliferation analysis based on BrdU+ IHC staining.

5.2.5 c-Rel level regulates EMT in pancreatic cancer

Undifferentiated tumor formation is coupled with EMT. Therefore, we analyzed markers associated with EMT in CCKP, CKP, and GCKP tissues. As various IHC stainings indicate (Figure 8A), increased c-Rel expression from CCKP, CKP to GCKP tissues showed a negative correlation with epithelial markers' level (CK-19, E-cadherin, membrane β-Catenin expression). In parallel, increasing c-Rel level positively correlated with mesenchymal marker expression (Vimentin). The results obtained from IHC stainings are further validated by western blot of bulk pancreatic tumor tissues from CCKP, CKP, and GCKP mice (Figure 8B). E-cadherin and β-Catenin expression decreases along with an increase in Zeb1 levels in especially GCKP tissues. Of note, c-Rel protein level was not absent in CCKP tissues, likely due to high c-Rel expression in TME cells, since cancer cells isolated from these cells have no c-Rel expression *in vitro*. RT-qPCR analysis performed with RNA isolated from bulk tumor tissue validated gradual increase of *Rel* mRNA levels in CCKP-CKP-GCKP samples (Figure 8C). In parallel, epithelial marker *cdh1* is decreased while mesenchymal markers *Zeb1, Zeb2, Snai2* are increased. Of note, *Snai1* showed a significant decrease, unlike other mesenchymal markers. Additionally, *Rel* mRNA level is significantly higher in squamous subtype (~QM-PDA) compared to progenitor group in Bailey dataset (Figure 8D). Multiple studies associated GATA-6 decrease along with ΔNp63 increase with poorly differentiated squamous/ QM-PDA/ Basal-like molecular subtype of human pancreatic cancer as explained in introduction section 3.1.1. Gata-6 levels was significantly less in GCKP tumors (Figure 8E). Total p63 level in nucleus showed a trend to be higher in GCKP tumors (Figure 8E).

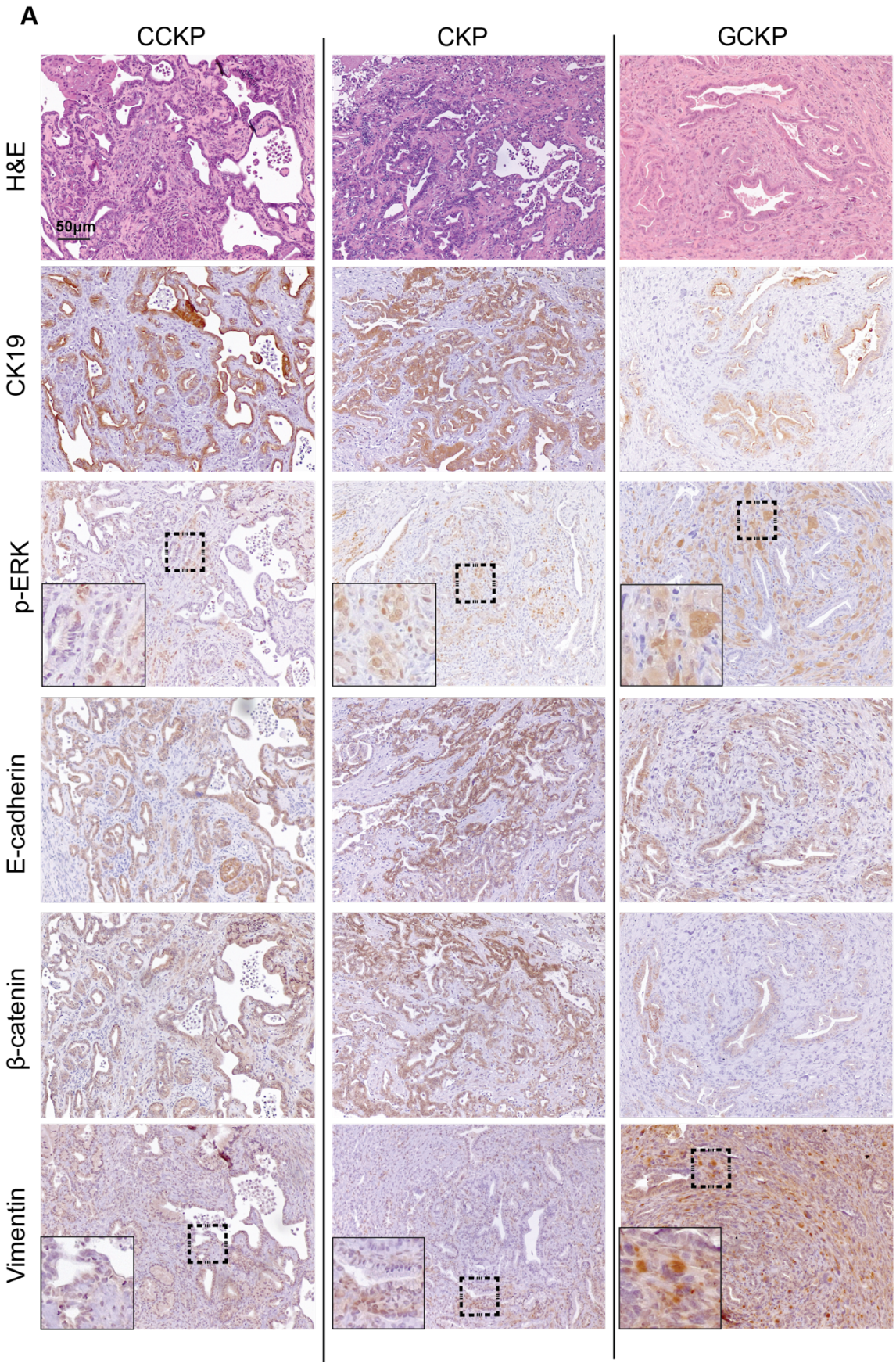
A
CCKP
CKP
GCKP
H&E
CK19
p-ERK
E-cadherin
β-catenin
Vimentin
50μm

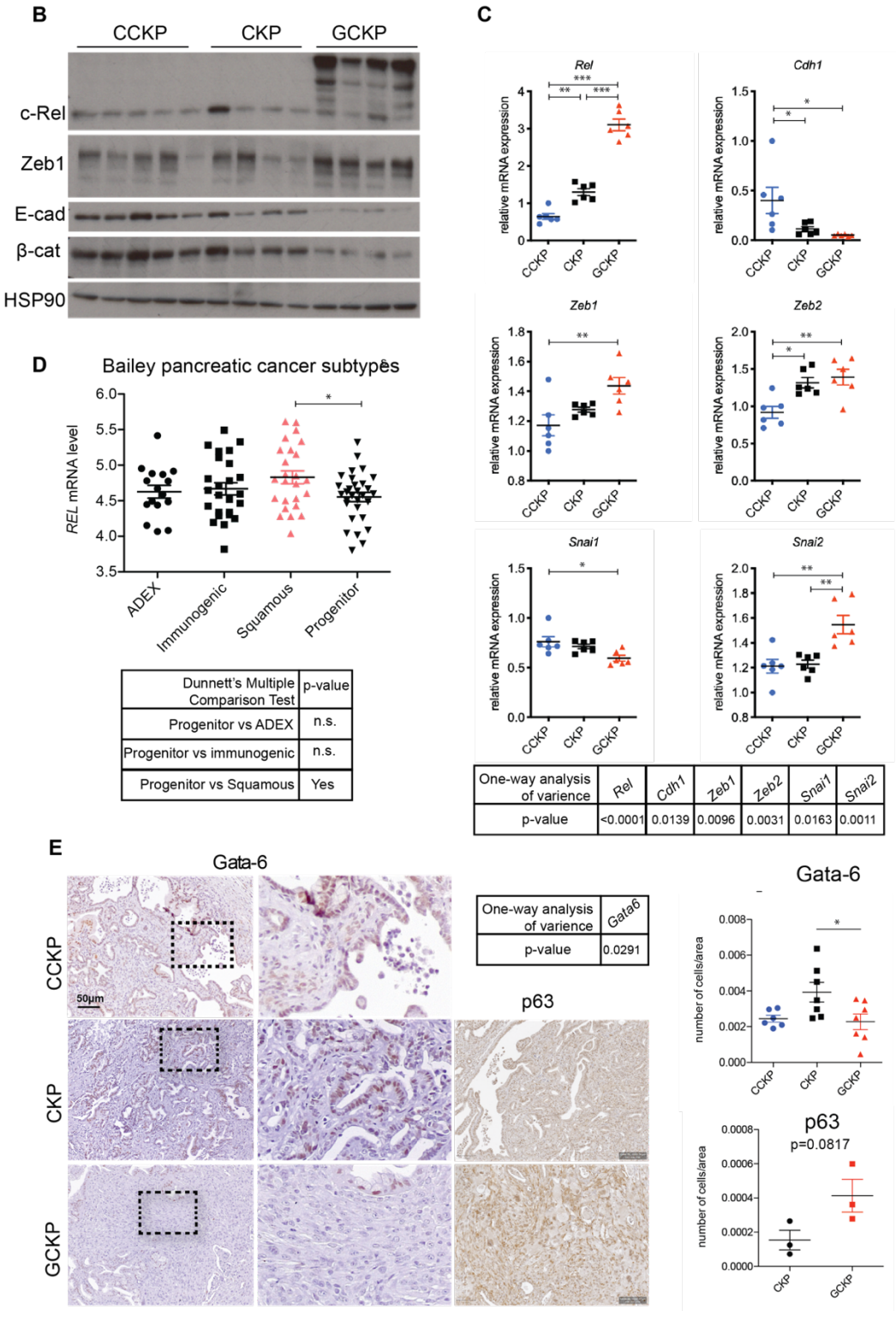

Figure 8: EMT is regulated by c-Rel level in CKP model *in vivo*. A) an IHC panel for EMT markers in CCKP, CKP and GCKP tissues. 6 samples from each genotype are stained and quantified. B) Western blot analysis for EMT markers in bulk tumor tissues of CCKP, CKP and GCKP. C) RT-qPCR results of EMT markers from RNA isolated from bulk tumor tissues of CCKP, CKP and GCKP mice. n=6 for each genotype. D) *REL* mRNA expression in Bailey molecular subtypes of human pancreatic cancer. E) GATA-6 and p63 IHC staining in CCKP, CKP and GCKP tissues. Quantification is made based on nuclear localization. For p63 student's t-test is applied.

We analyzed EMT also *in vitro* with the use of cancer cells isolated from murine tumors. Morphologically, GCKP cells showed a rather mesenchymal structure, whereas both CCKP and CKP cells are mostly epithelial (Figure 9A). Expression levels of EMT markers are analyzed in isolated cancer cells (Figure 9B). In parallel with the *in vivo* results, E-cadherin level decreased, and Vimentin level increased gradually from c-Rel knockout to overexpression cells. Mesenchymal N-cadherin levels didn't show any difference, but an additional smaller band in GCKP cells is observed. To further elaborate these results, we knockdown *Rel* in six different CKP cells (Figure 9C). While 4/6 of these cells showed reduced Zeb1 and Slug expression, there was no notable change in the expression of other markers. Analysis of cellular proliferation showed no significant difference except day 3 (Figure 9D). However, there is a trend for a higher rate in CCKP and GCKP cells compared to CKP. Additionally, *Rel* knockdown didn't impact CKP cell proliferation significantly (Figure 9E).

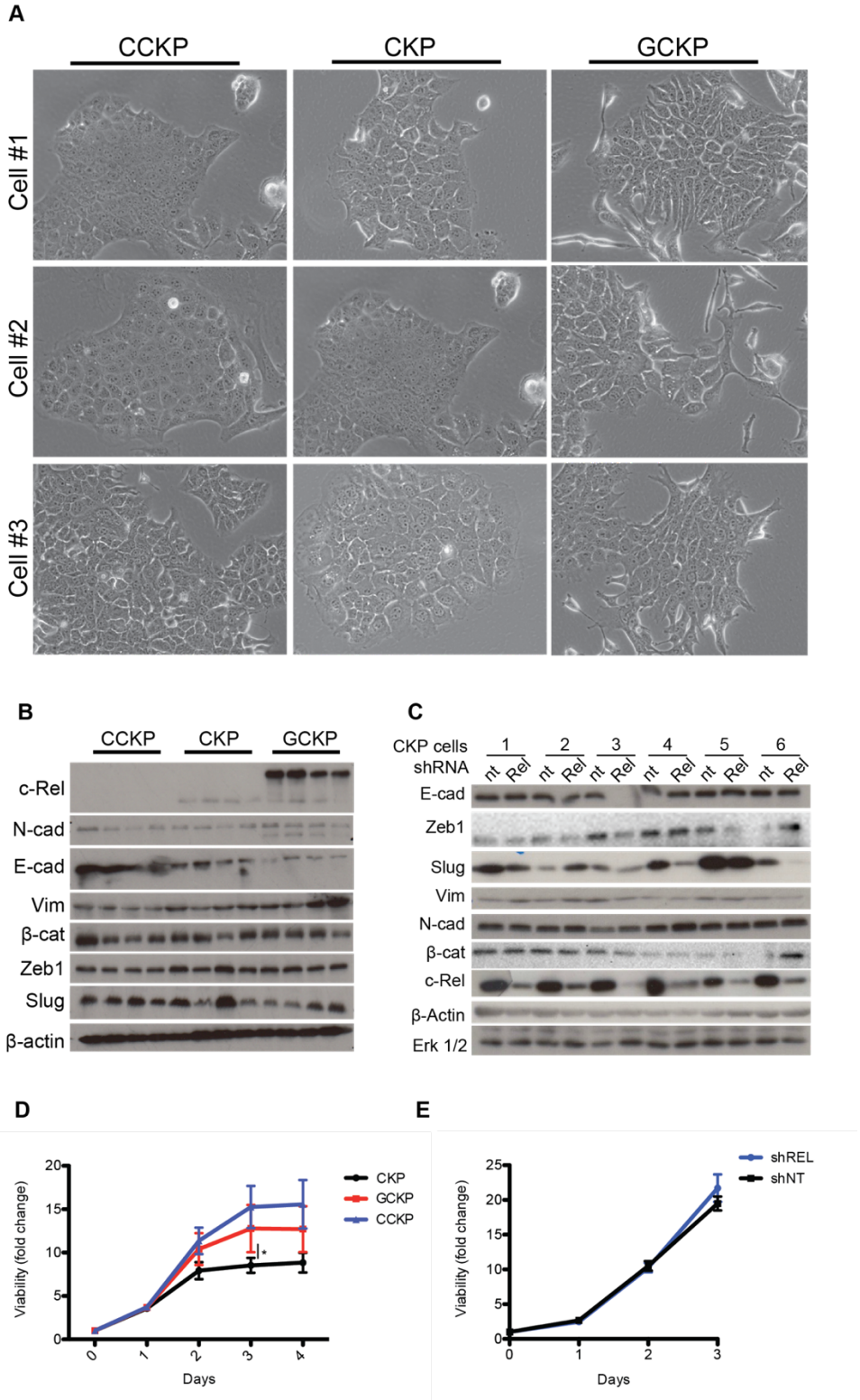

Figure 9: EMT is regulated by c-Rel level *in vitro*. A) Representative bright-field images of isolated CCKP, CKP and GCKP cells in 2D cell culture. B) Western blot analysis for c-Rel and various EMT markers in isolated cancer cells. C) CKP cells transduced with shRel and shNt (non-targeting control) with lentivirus and are analyzed by western blot for c-Rel and EMT markers' expression. D) Proliferation assay for CCKP n=6, CKP n=5 and GCKP n=5 cells with technical triplicates. E) Proliferation assay for RNAi transduced CKP cells n=6 for each group with technical triplicates.

With the use of an online exploration tool EMTome [294], we checked *REL* mRNA level correlation with EMT signature in human pancreatic cancer samples (Figure 10). *REL* expression significantly correlated with both Aiello EMT signature and expression of top-50 genes associated with EMT [295].

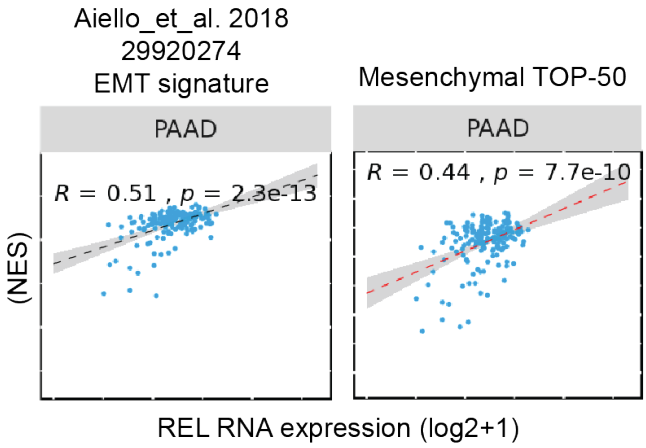

Figure 10: Correlation of *REL* mRNA expression with Aiello et al. EMT signature within human samples. Graph is adapted from EMTome database. On the right, *REL* correlation with TOP-50 mesenchymal genes is displayed.

5.2.6 c-Rel regulates CSC phenotype

EMT and CSC phenotypes are considered to be associated, as elaborated in the introduction part. Our preliminary data indicated a decrease in NF-κB signaling signature in CSCs isolated from various human tissues (Figure 11A). Basically, RNAseq analysis was performed in these cells, which are maintained *in vitro* either via conventional 2D cell culture or in an unattached spheroid culture medium (enriched for CSCs). Interestingly, unlike other NF-κB transcription factors, *REL* mRNA level is increased in CSCs (Figure 11A). Encouraged by these results, we performed a spheroid formation assay in CCKP, CKP, and GCKP cells. To our surprise, while CCKP cells had higher spheroid number compared to CKP and GCKP cells, GCKP cells had a bigger spheroid size compared to CCKP and CKP cells (Figure 11B). Additionally, we performed flow cytometry analysis to check the surface expression levels of CSC markers. Overall, the trend indicated a gradual decrease in individual CSC markers CD133, Sca-1, CD44, and CXCR4 from c-Rel knockout out to overexpression cells (Figure 11C). Co-expression analysis indicated a similar decrease in Sca1+CD133+ double-positive and CD44+Sca1+CD133+ triple positive (TP) population (Figure 11D). Interestingly, amount of CD44+Sca1-CD133-

population, which was previously identified to have higher tumor-initiating capacity than TP, was getting higher in parallel to increasing c-Rel expression (Figure 11E) [296].

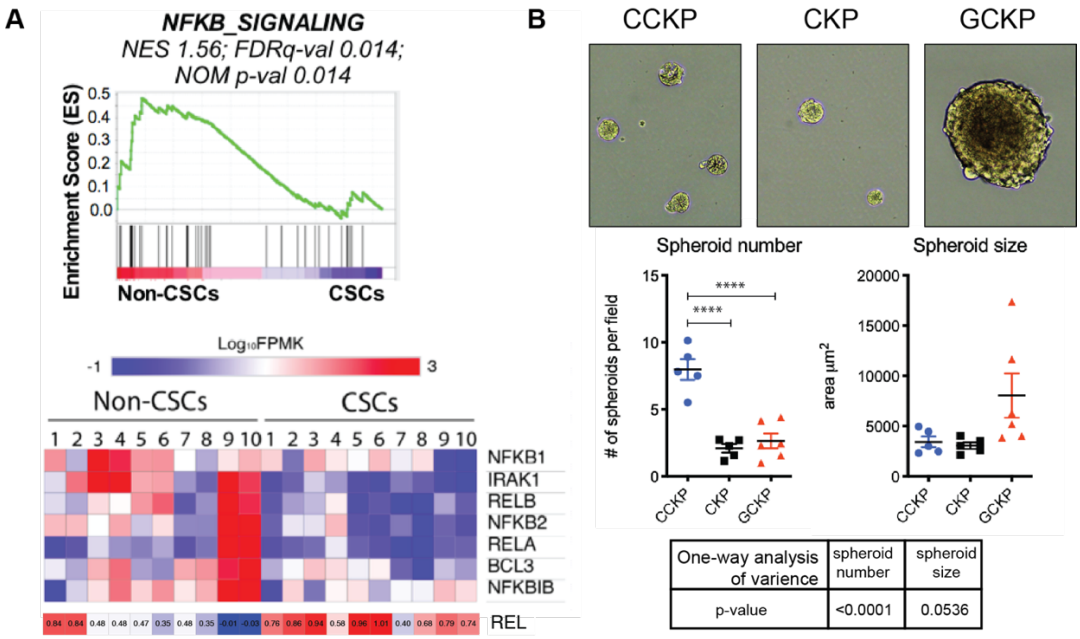

One-way analysis of varience	spheroid number	spheroid size
p-value	<0.0001	0.0536

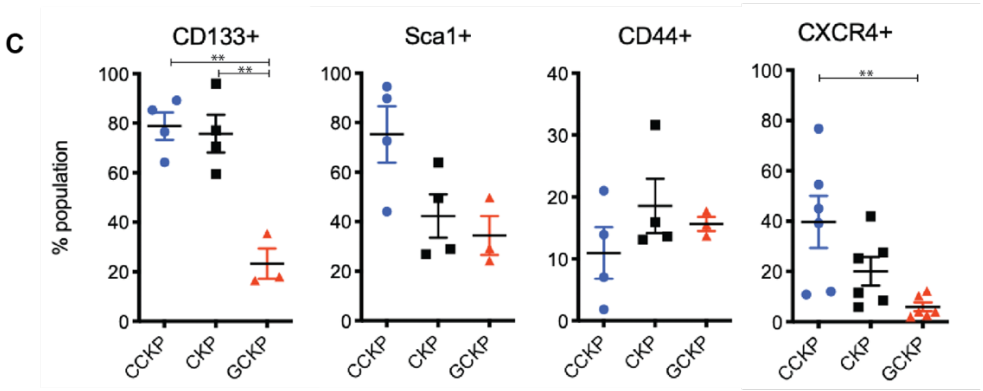

One-way analysis of varience	CD133+	Sca1+	CD44+	CXCR4+
p-value	0.0008	0.0419	0.3941	0.0118

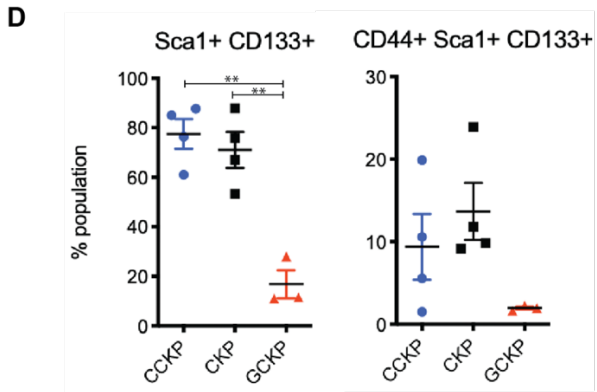

One-way analysis of varience	CD133+ Sca1+	CD44+ CD133+ Sca1+
p-value	0.0005	n.s.

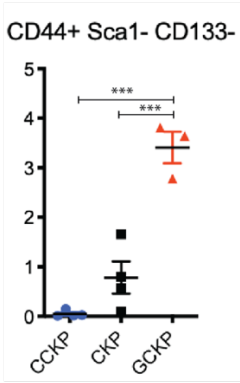

One-way analysis of varience	CD44+ CD133- Sca1-
p-value	0.0001

Figure 11: c-Rel regulates CSCness in pancreatic cancer. A) RNAseq analysis is shown as heat-map for various NF-κB components along with NF-κB enrichment score. Cells are isolated from human tissues and enriched for CSCs under spheroid culture. B) Spheroid formation assay for CCKP n=5, CKP n=5 and GCKP n=6 cells, with technical duplicates of each cell line. C) Flow cytometry analysis of surface expression for previously identified CSC markers. D) Flow cytometry analysis for co-expression of CSC markers. E) A previously identified CSC subtype showing high tumor initiating capacity. For figures C-E, CCKP n=4, CKP n=4 and GCKP n=3 except CXCR4 in which n=6 for each group.

Additionally, we functionally tested the colony-forming capacity of CCKP, CKP, and GCKP cells by extreme limiting dilution assay (ELDA). Basically, each cell line is seeded in small numbers to be tested for their colony-forming capacity, which is associated with stemness. GCKP cells had higher stem cell frequency than both CCKP and CKP cells (Figure 12A-B). There was no significant difference for CCKP cells compared to CKP.

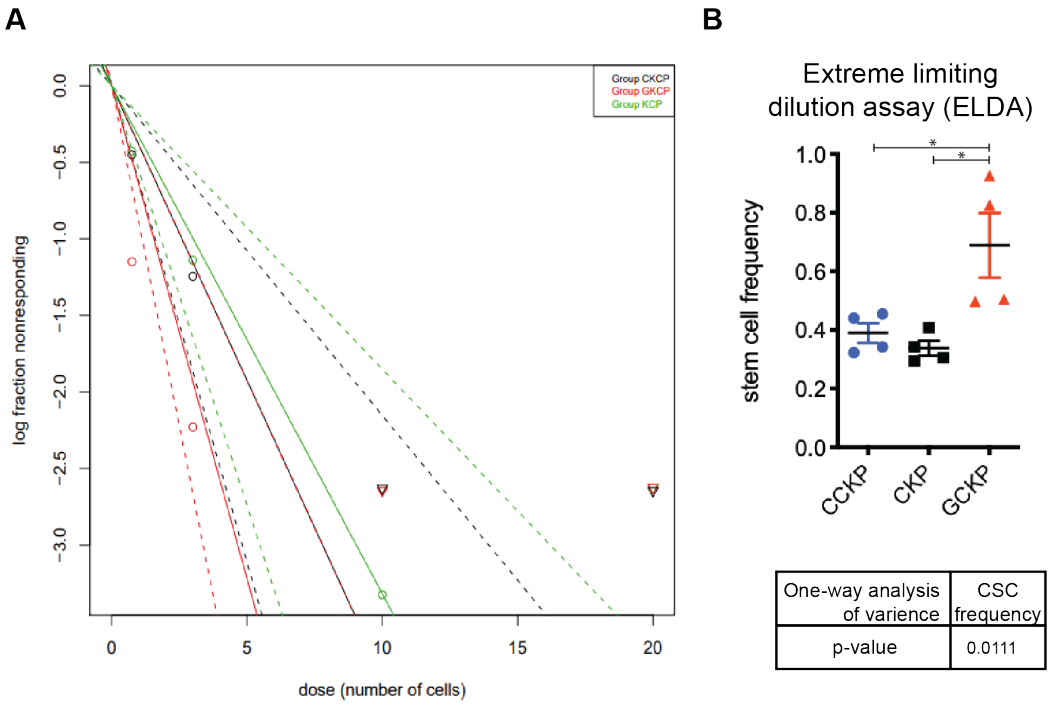

Figure 12: c-Rel regulates stem cell numbers *in vitro*. A) Extreme limiting dilution analysis graph for stem cell frequency in CCKP, CKP and GCKP cells. N=4 for each group. B) Stem cell frequency displayed in chart graph for statistical analysis.

5.2.7 c-Rel regulates CSC subtypes

As mentioned in the introduction part, there are previous studies reporting c-Rel as a downstream transcription factor of integrin-β3-Kras-TBK1 signaling axis. Basically, c-Rel activation by this pathway had been associated with EGFRi resistance with an

increased CSC phenotype. Based on these reports and our results, we analyzed this axis in CCKP, CKP, and GCKP tissues. IHC analysis revealed that in GCKP tumors, integrin-β3 expression is more (Figure 13). The staining also showed a pattern for integrin-β3 expression in invasive cancer cells dissociated from basal lamina in CKP and CCKP tissues along with stromal cells. Interestingly, collagen deposition decreased with more c-Rel implying a stromal remodeling (Figure 13). These results may indicate that cancer cells with high c-Rel expression may maintain their CSC phenotype by FN-integrin-β3 axis although they express less CSC markers individually.

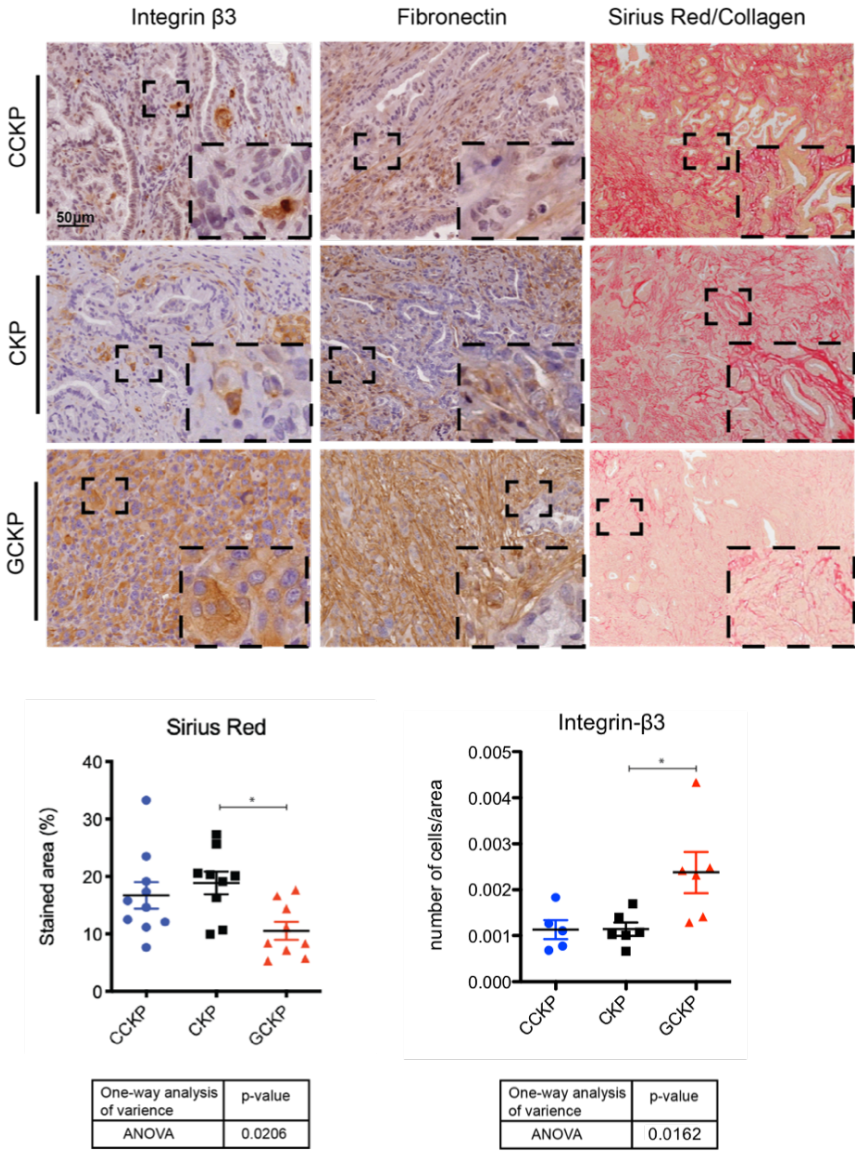

Figure 13: Analysis of c-Rel function in fibronectin-integrin-β3 signaling axis *in vivo*. IHC stainings indicate fibronectin and integrin-β3 expression in especially around/in invasive cells detached from basal lamina. Colagen deposition and integrin-β3 is also quantified as in the graphs.

We analyzed the signaling axis also by *in vitro* assays. CKP cells are seeded on fibronectin to analyze c-Rel nuclear translocation/activation (Figure 14A). In the cells seeded on the fibronectin coated wells, there was significantly higher c-Rel nuclear localization along with RelA. Additionally, cells with high c-Rel expression had faster ability to bind fibronectin (Figure 14B). Moreover, cells with high c-Rel expression had more contractility (Figure 14C).

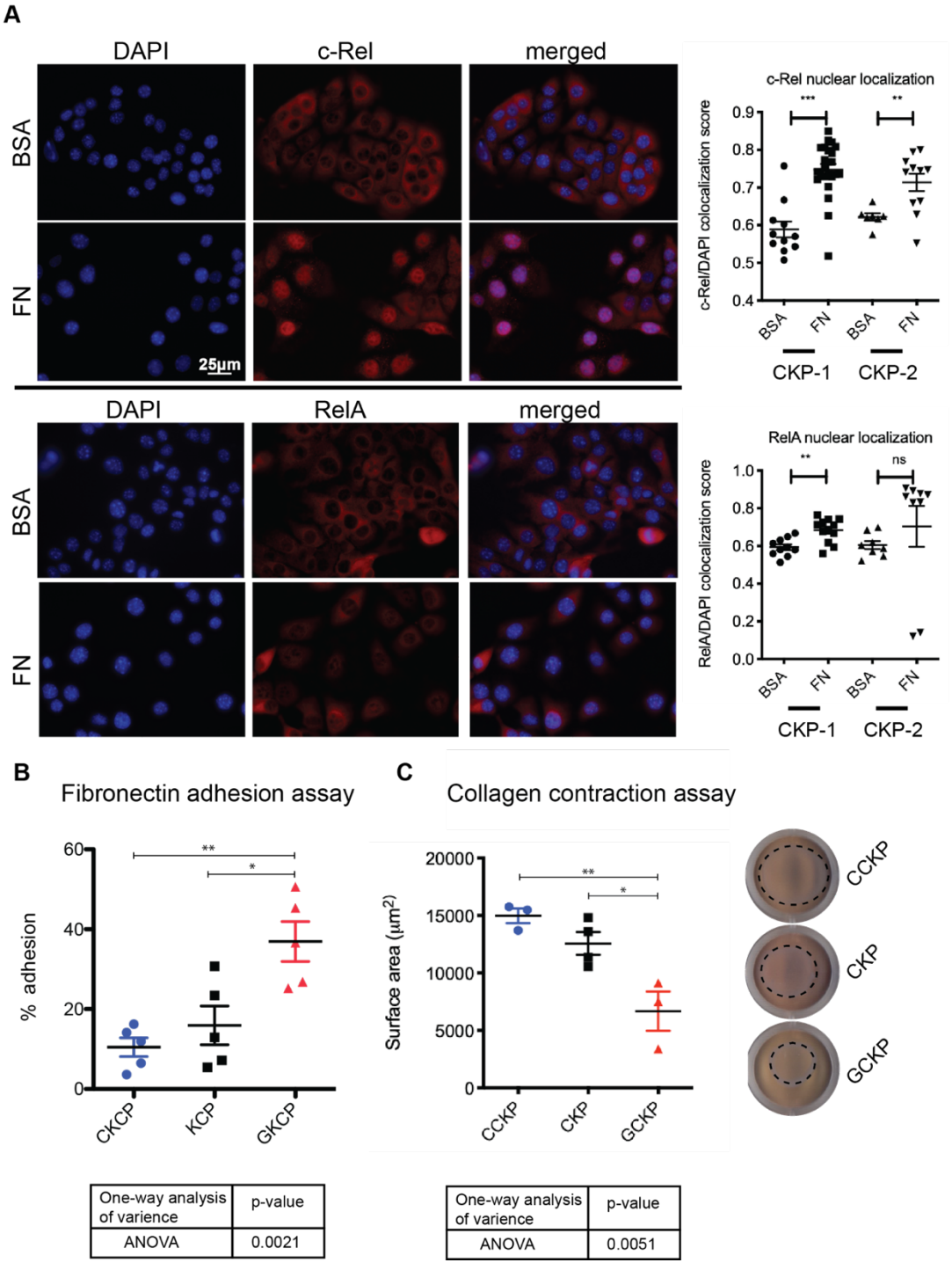

One-way analysis of varience	p-value
ANOVA	0.0021

One-way analysis of varience	p-value
ANOVA	0.0051

Figure 14: Analysis of c-Rel function in fibronectin-integrin-β3 signaling axis *in vitro*. A) Immunofluorescence staining for c-Rel and RelA for cells seeded on fibronectin or BSA coated wells. Quantification results are indicated on the graphs, right side. B) Fibronectin adhesion assay quantifications for CCKP, CKP and GCKP cells each seeded as technical triplicates. C) Contractility of cells are compared based on surface area of collagen gels. CCKP n=3, CKP n=4 and GCKP n=3 cells are seeded as technical triplicates. A representative image is put on right side.

5.2.8 c-Rel level regulates metastatic capacity

Up to now, cumulative evidence suggests that c-Rel regulates EMT and CSC subtypes. To understand its functional relevance *in vivo*, we tested these cells' ability to metastasize through intravenous injection of CCKP, CKP, and GCKP cells into wildtype littermates. From each CCKP, CKP, and GCKP genotype, 5-6 different cells are injected into two different mice each. Results indicate that the lung/body weight ratio was higher for CCKP cells compared to CKP and GCKP cells (Figure 15B). Next to macroscopic observation (Figure 15A), we performed metastatic colony area quantification in histology slides. Results indicate that both CCKP and GCKP cells metastasize higher compared to CKP cells (Figure 15C). We also performed intravenous injection of 6 different CKP cells with either *Rel* and non-targeting shRNA knockdown, each to 2-3 different mice. However, there was no significant difference in the metastatic capacity of these cells (Figure 15D). These results indicate that both absence and overexpression of c-Rel increases the metastatic capacity of mouse pancreatic cancer cells. Although, the low but present c-Rel level may still be efficient enough to rescue knockout cells' metastatic phenotype.

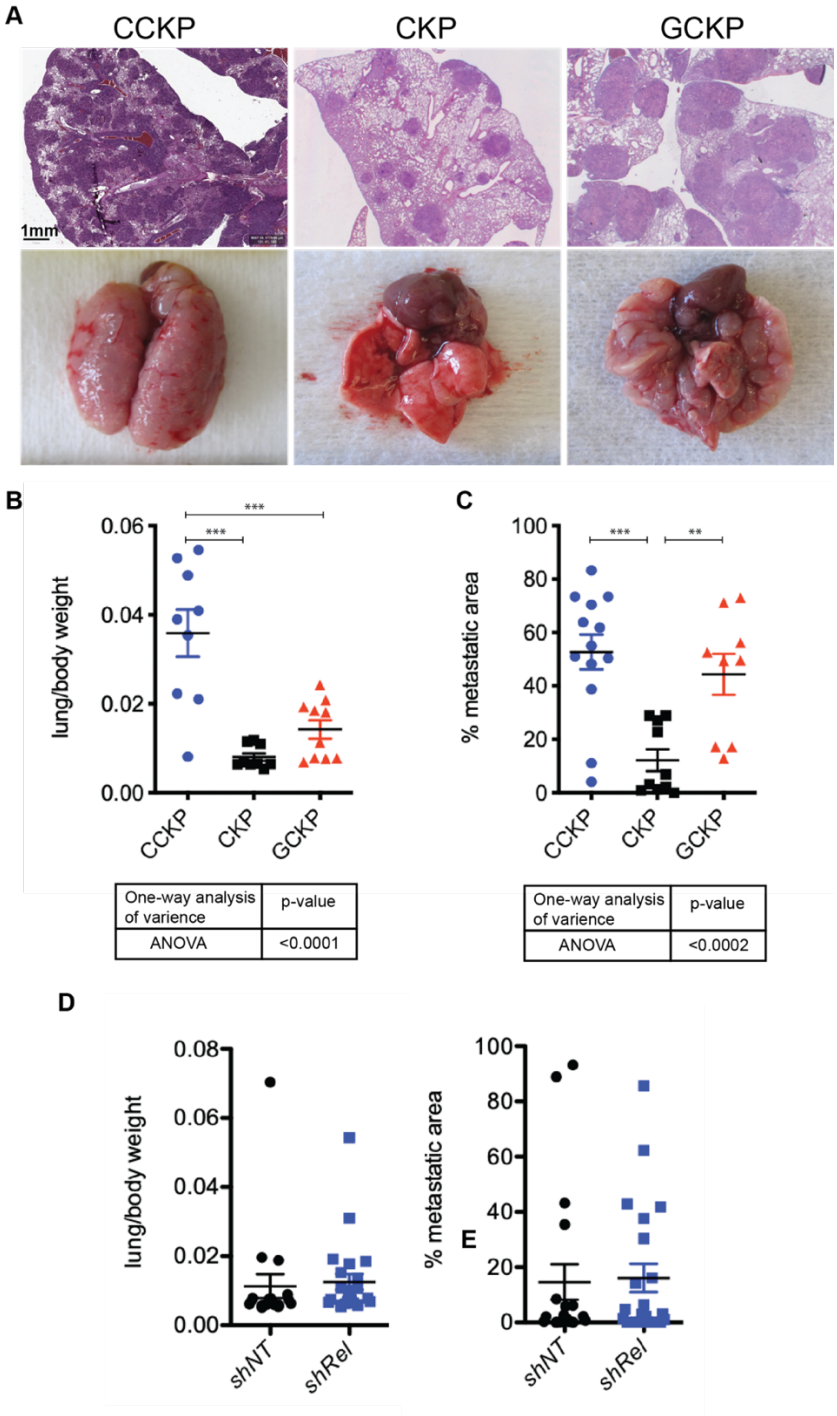

Figure 15: c-Rel regulates metastatic potential of CKP cells. A) Representative H&E microscopic and macroscopic images of lungs from littermate mice, which are injected with indicated cells lines. B) lung/body weight ratio is compared between groups. C) Percent metastatic colony area is estimated by average area quantification of both metastasis and whole lung with 2 different lung sections for each mouse. For A-C 6, 5 and 5 different CCKP, CKP and GCKP cell lines respectively are injected to individual mice (2-3 mice per cell lines). D) lung/body weight ratio and E) % metastatic area quantification for wildtype mice, which are tail-vein injected with RNAi CKP cells. 6 different CKP cells transduced either with shRel or shNt are injected 3-4 mice.

To dissect the mechanistic details about how c-Rel regulates EMT, CSC, and metastatic capacity, we performed RNAseq analysis with five different cells from each CCKP, CKP, and GCKP groups with technical duplicates. The analysis revealed that GCKP cells had 562 upregulated and 192 downregulated transcripts compared to CKP cells. On the other hand, CCKP cells had 405 upregulated and 199 downregulated transcripts. Among these, we analyzed the number of common products (Figure 16A). To our surprise, there were 165 upregulated and 38 downregulated common transcripts in both GCKP and CCKP cells compared to CKP cells. 26 common transcripts were downregulated in CCKP and upregulated in GCKP, while 14 transcripts were upregulated in CCKP and downregulated in GCKP compared to CKP control. Of note, *Rel* was upregulated in GCKP and downregulated in CCKP significantly. Gene set enrichment analysis in the KEGG pathway database showed multiple outputs consistent with the phenotypes observed (Figure 16B).

Focal adhesion and TGF-beta signaling pathway are commonly enriched in both GCKP and CCKP up. However, there is a clear difference in the statistical significance level of enrichment based on the difference in their $-\log_{10}$FDR values. Basically, these pathways are enriched more significantly in GCKP cells compared to CCKP cells. These enrichments can be reasoned with the differences in EMT, contractility, and metastatic capacity level in GCKP vs. CCKP cells. Some genes within these sets are common, while some are not. Although the enrichment is common, their phenotypic output might be different in combination with other factors. For example, in CCKP samples, cell-cell adhesion-related- Rap1 signaling pathway, cell adhesion molecules, and Gap junction- are enriched. These pathways are associated with a rather epithelial morphology. This may explain why CCKP cells show high metastatic capacity despite that they are not as contractile as GCKP cells.

In parallel to the observation we had, e.g., high undifferentiated pathology of GCKP tumor and high *REL* expression in Bailey's squamous molecular subtype in PDAC, basal cell carcinoma pathway is enriched in GCKP up. In parallel to the high fibronectin-integrinβ3 expressions in GCKP, there is an enrichment for ECM-receptor interaction in GCKP up.

In CCKP down, signaling pathways regulating pluripotency of stem cells are enriched. This result is in parallel to the high surface expression of common CSC markers in CCKP cells compared to CKP cells. PI3K-Akt signaling pathway and melanogenesis

pathways are enriched in GCKP up and CCKP down, indicating a positive correlation between c-Rel and PI3K signaling pathway.

Commonly enriched chemokine signaling pathway and cytokine-cytokine receptor activation sets in GCKP and CCKP up are further supported by a cytokine array experiment we performed (Figure 17). Interestingly, in both GCKP and CCKP cells, the levels of multiple inflammatory cytokines/chemokines are increased compared to CKP control.

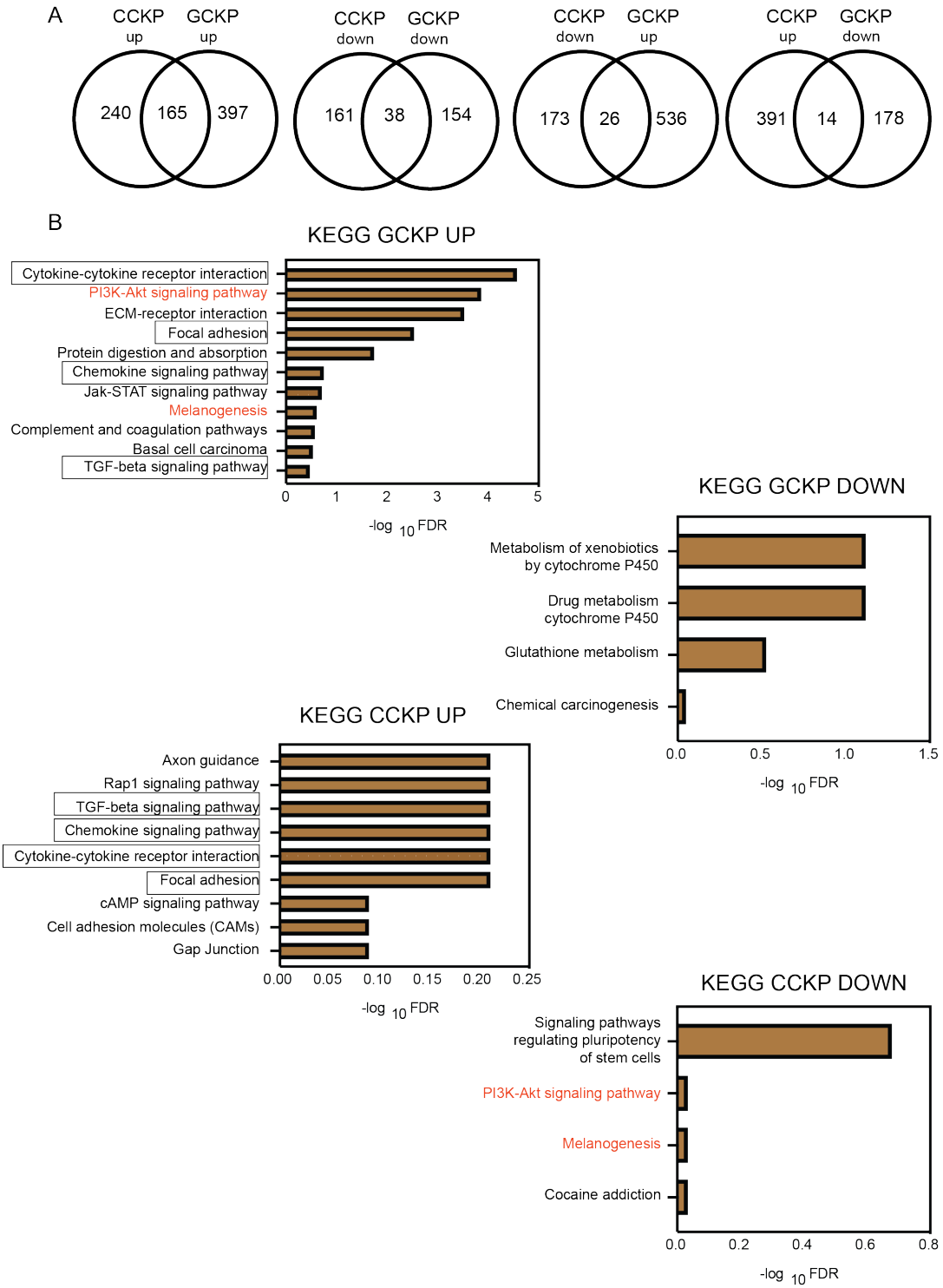

Figure 16: RNAseq analysis of CCKP, CKP and GCKP cells. A) Wenn-diagrams show number of commonly upregulated and downregulated genes in GCKP and CCKP cells compared CKP controls. B) The KEGG pathway-enrichment sets are displayed in order based on each enrichment's FDR values. UP-DOWN enrichments are calculated based on upregulated and downregulated genes respectively, in GCKP and CCKP cells compared to CKP controls. The commonly upregulated pathways in GCKP and CCKP cells are marked in black bow, while upregulated in GCKP and downregulated in CCKP are marked in red color.

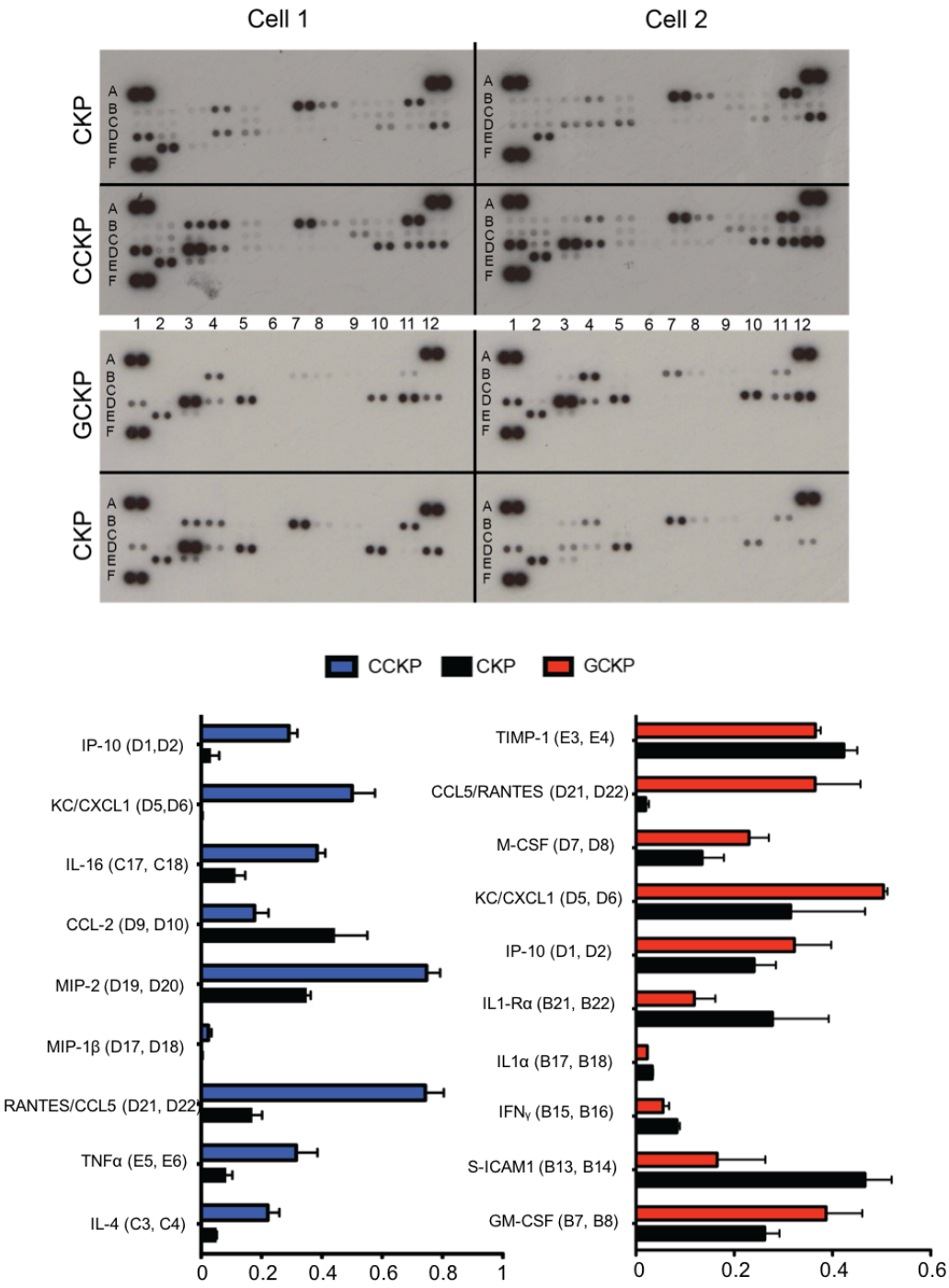

Figure 17: Cytokine array blot of CCKP and GCKP cells using CKP cells as control. 2 individual experiments are performed each with 4 membranes. In each experiment, two cell lines from each genotype are used. The dot blots are quantified with ImageJ software for integrated density values. As CKP controls, same cell lines are used in each experiment.

5.2.9 p53 status regulates c-Rel function

The CKP model is great for modeling spontaneous primary tumor formation in the pancreas. However, these mice die too early (8-10 weeks) before detecting metastasis in distant organs. To circumvent this obstacle, the $CKP^{lox/+}$ model (*trp53* is deleted heterozygously) is highly utilized. Therefore, we generated *Rel* knockout and overexpression in $CKP^{lox/+}$ background. To our surprise, $CCKP^{lox/+}$ mice showed significantly shorter survival compared to both $CKP^{lox/+}$ and $GCKP^{lox/+}$ mice (Figure 18A). There was no difference between the survival days of $CKP^{lox/+}$ and G $CKP^{lox/+}$ mice (Figure 18A). There was also no difference between the pancreas/body weight ratio between the models (Figure 18B). While both $CCKP^{lox/+}$ and $CKP^{lox/+}$ mice had full penetrance in tumor formation, tumor incidence was lower in $GCKP^{lox/+}$ (Figure 18C). On the contrary to the CKP model, both c-Rel knockout and overexpression models showed higher metastatic incidence (Figure 18D). However, diaphragm invasion incidence was higher with increasing c-Rel levels in $CKP^{lox/+}$ mice (Figure 18E). All of these results indicate that the c-Rel function is context-dependent, as shown with the p53 case.

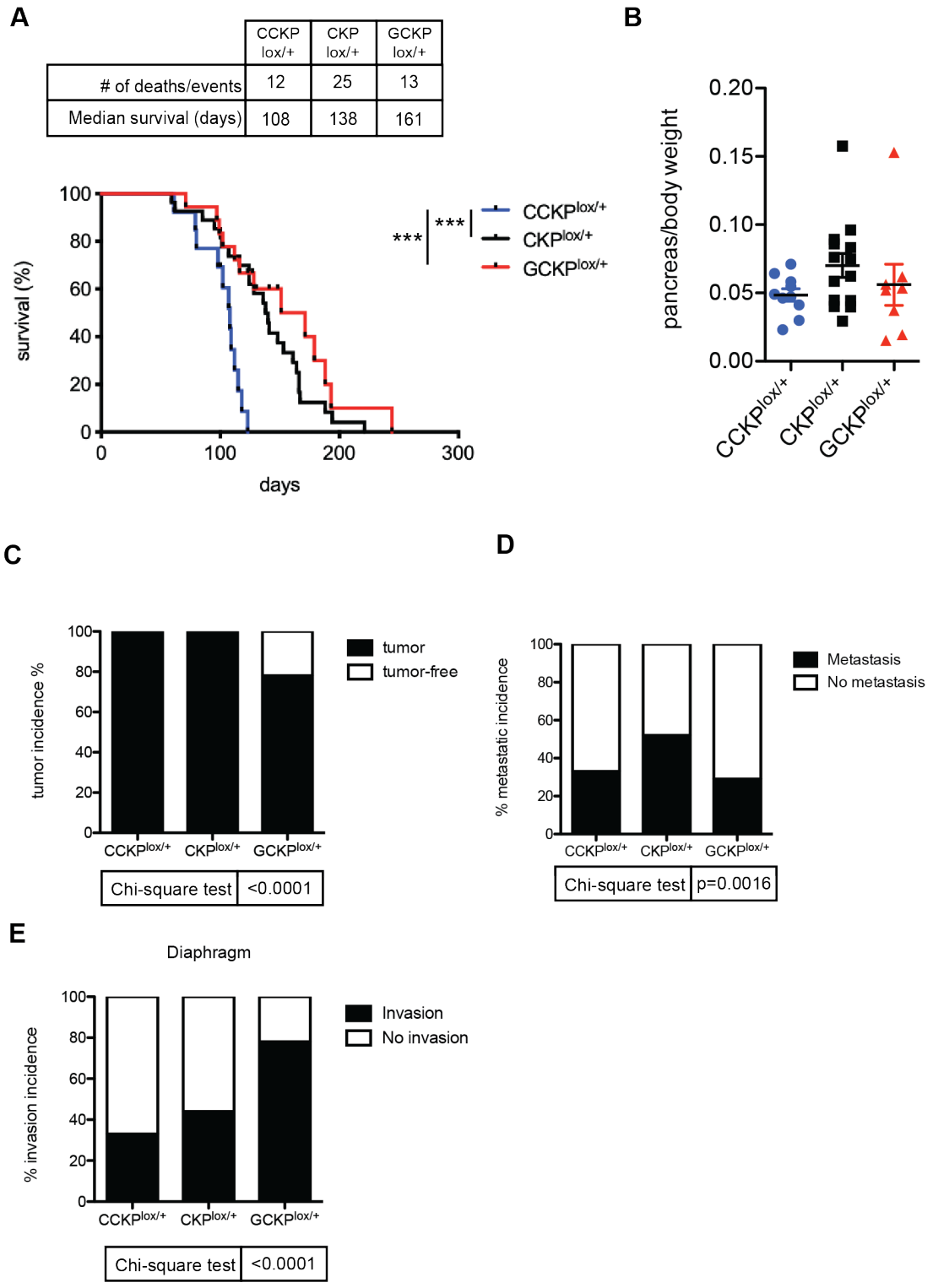

Figure 18: c-Rel function is regulated by p53 status. A) Kaplan-Meier survival analysis for $CCKP^{lox/+}$, $CKP^{lox/+}$ and $GCKP^{lox/+}$ mice. Statistical analysis is performed with log-rank (Mantel-Cox) test. B) pancreas/body weight ratio. C) Tumor incidence in $CCKP^{lox/+}$ n=12 $CKP^{lox/+}$ n=25 $GCKP^{lox/+}$ n=18 mice. D-E) Metastatic (to liver, lung and distant lymph node) and duodenal invasion incidence calculation is made only with tumor bearing mice with $CCKP^{lox/+}$ n=12 $CKP^{lox/+}$ n=25 $GCKP^{lox/+}$ n=14 mice

6 DISCUSSION

NF-κB signaling components have been shown to be both oncogenic and tumor suppressors in pancreatic cancer [194]. There is a significant number of studies delineating the function of RelA and RelB in pancreatic cancer, both *in vitro* and *in vivo*. However, the role of c-Rel in solids tumors as the least studied component of NF-κB has not been well elaborated in pancreatic cancer. Still, existing data, as compiled in the introduction part, mostly *in vitro*, already defined an anticipated oncogenic function of c-Rel in pancreatic cancer.

Herein, we analyzed the impact of c-Rel knockout and overexpression in various pancreatic cancer *in vivo* and *in vitro* mouse models. In parallel to the existing literature, our *in vivo* mouse models in which c-Rel is genetically manipulated reveals a broadly oncogenic function of c-Rel. In pancreatic cancer as reflected in the Kaplan-Meier survival curve of the CKP mouse model high c-Rel expression decreases survival, while its knockout increases it. From absence to overexpression of c-Rel, undifferentiated tumor formation frequency increased, while the differentiated type was reduced. Additionally, we provided evidence for which EMT is positively regulated by c-Rel expression. Based on the results from existing literature correlating c-Rel function with CSCness and, RNAseq results from CSC enriched human pancreatic cancer cells, we analyzed CSC characteristics in isolated mouse pancreatic cancer cells. To our surprise, both c-Rel knockout and overexpression cells showed enhanced CSC characteristics, but with different phenotypic outputs. Molecularly, CCKP cells showed increased surface expression of conventional CSC markers. On the other hand, GCKP cells had higher fibronectin-integrin-β3 expression. These results imply that the heterogeneity in CSC molecular subtypes may be reflected in heterogeneity in CSC phenotype. Particularly, c-Rel might be involved in the pivotal point of CSC subtype selection. Associated with the EMT and CSC phenotype, we checked the impact of c-Rel in the metastatic potential of cancer cells. In both CCKP and GCKP cells, metastasis degree was increased compared to control CKP cells. However, these results were not reflected in the results obtained from *Rel* RNAi knockdown CKP cells. To dissect the mechanistic details of the aforementioned phenotypes, we performed RNAseq analysis on CCKP, CKP, and GCKP cells. The enriched datasets actually supported most of the phenotypes we already observed. There were some unanticipated enrichment results, such as PI3K-Akt signaling and melanogenesis in

GCKP up and CCKP down, which might be the core signaling pathways involved in the phenotype formation. Additionally, cytokine array results surprisingly showed quite an increase in most of the inflammatory cytokines and chemokines in both GCKP and CCKP cells. This result is also in line with the RNAseq results.

And finally, we provided evidence that p53 status can impact the role of c-Rel in pancreatic cancer. When mice possess one intact *Trp53* allele, c-Rel knockout mouse survival got shorter. Additionally, in both c-Rel overexpression and knockout mice, the metastatic incidence was lower compared to control mice. Overall, these results imply that c-Rel has the potential to be used as a marker for patient stratification and targeted therapeutically in a context specific manner.

6.1 c-Rel impacts histopathology of primary pancreatic cancer

Adenosquamous carcinoma of the pancreas in humans is characterized by 30% of the tumor being with squamous differentiation [297]. In parallel, undifferentiated tumor type has more anaplastic differentiated morphology. Both tumor types are associated with reduced survival in human patient cohorts [298,299]. These subtypes are defined based on the morphological properties of the tumors.

In anaplastic-undifferentiated tumors of humans, tumor cells grow in dispersal with a polymorphous structure (like multinucleated giant cells), express a high amount of vimentin, and lack E-cadherin expression [298]. These properties are associated with EMT as observed in epithelial tumors. These tumors are generally diagnosed in the late stages when the tumor is already locally advanced and invaded the local environment. Although the incidence is low (2-7%), there is an urgent need for the identification of therapeutic options, especially for this aggressive form of tumor [300]. Additionally, *REL* mRNA expression is higher in the last stage of tumors (Figure 3C), which is locally advanced and spread to nearby tissues.

In mouse tumors with c-Rel overexpression, we observed increased incidence for undifferentiated tumor formation. Of note, none of the tumors in GCKP mice formed the classical type of PDAC. On the other hand, CCKP tumors developed more the classical type of tumors compared to both CKP control and GCKP.

Next to morphological classification, we also checked c-Rel association with molecular subtypes of pancreatic cancer. As expected, Bailey squamous subtype (named QM-PDA, basal-like subtypes by other groups) showed high *REL* expression compared to

the progenitor subtype (called classical subtype by other groups) (Figure 7). To test these results in mouse models, we checked the expression levels of Gata-6 and p63 levels in CCKP, CKP, and GCKP tumors (Figure 7). Squamous subtype is defined with low Gata-6 and high ΔNp63 expression. IHC results confirmed a statistically significant decrease of Gata-6 expression in GCKP tissues compared to CKP. Interestingly, Gata-6 also showed lower expression in CCKP tissues, although not significant. As a preliminary result, the trend indicates a higher total p63 expression in GCKP compared to CKP. For a clear-cut understanding of p63 correlation, an IHC staining testing not total p63 but only for ΔNp63 levels in CCKP, CKP, and GCKP tissues is required.

Existing literature already suggests the involvement of c-Rel regulation in p63 isoforms' function in head and neck squamous cell carcinoma (HNSCC) [216,301]. In their model, TAp73 is a tumor suppressor occupying p63/p53 transcription factor binding sites on target genes, especially in p53 mutant HNSCC. After TNFα induction, c-Rel translocate to the nucleus to bind ΔNp63, and the dimer replaces tumor suppressor TAp73 from AP-1 promoter to rather activate it. Overall, c-Rel activation results in redistribution of p63-p73 isoforms on target genes, eventually increasing inflammation. In parallel, RNAseq analysis showed increased basal carcinoma signature in GCKP cells along with a high cytokine-chemokine signaling signature. Increased cytokine-chemokine expression was further validated by cytokine array supporting increased inflammation, which is possibly mediated by c-Rel&ΔNp63 co-activity. Their results suggest a similar pattern for c-Rel involvement in squamous differentiation of pancreatic cancer.

6.2 c-Rel expression regulates EMT plasticity

Previous studies suggested c-Rel involvement in EMT regulation in multiple cell types [302–305]. Among these, especially the study done by Liu et al. highlighted the importance of c-Rel in human pancreatic cancer cells' EMT and CSCness *in vitro*. Additionally, *REL* expression showed a very high correlation with EMT signature in human pancreatic cancer samples.

In parallel to the observed histopathological properties, we also observed a gradual decrease in E-cadherin expression from c-Rel knockout to overexpression samples both *in vivo* and *in vitro*. However, as mentioned in the introduction part, EMT is a dynamic process and can't be defined only by an increase or decrease of single components [231]. As highly recommended by the EMT consensus community, it is

essential to characterize the panel of EMT-associated proteins along with its associated phenotypes. Accordingly, we analyzed the expression of multiple EMT transcription factors. Zeb1 and Zeb2 expression showed a positive correlation with c-Rel level as shown in western blot and RT-qPCR results. Unlike *Snai2*, the *Snai1* level decreased as the c-Rel level increased. Most of the studies focusing on Snai transcription factors define their joint function. On the other hand, a recent study determined their opposite roles during dynamic EMT progress of breast cancer cells [306]. In early EMT with a less invasive phenotype, Snail suppresses PLD2 levels. As the EMT progresses to a more invasive phenotype, increased Slug expression induces PLD2 transcription, which in turn can inhibit Snail expression. This implies possible positive/negative feedback loops between Snail-Slug transcription factors depending on the EMT stage. Vimentin expression is also increased with increasing c-Rel levels in both tissues and cells. Interestingly, unlike *in vivo*, levels of β-catenin, Zeb1, and Slug didn't show a consistent expression change in isolated CCKP cancer cells. The E-cadherin and vimentin levels were consistent with *in vivo* results.

Of note, total N-cadherin level didn't change in cancer cells, but in GCKP cells, there was an additional low molecular weight N-cadherin band observed in western blots (Figure 9B). this might be a result of different *Cdh2* mRNA isoform or truncation of existent N-cadherin protein. Unfortunately, the literature search didn't come up with an explanation for the observed bands. Further analysis is required to understand this difference. Rt-qPCR expression analysis for mRNA isoforms or isolation of the low molecular weight band for mass spectrometry analysis is the future option to characterize the function of this product.

Microscopically, isolated cancer cells in 2D cell culture demonstrated that GCKP cells show a rather mesenchymal phenotype. These cells are not fully mesenchymal, as western blot analysis also shows co-expression of epithelial E-cadherin expression. Such cells showing both mesenchymal and epithelial characteristics are named quasi-mesenchymal (QM) cells with partial differentiation. Cells in these hybrid state can lower but not diminish epithelial characteristics either transcriptionally or post-translationally [231]. In a noted study [295], Aiello et al. showed that cancer cells with partial EMT programs disseminate collectively and harbor a special endosome recycling program by which they reduce surface E-cadherin occupancy. On the other hand, they

experimentally show that cells with a full EMT program disseminate as single cells diminishing cell-cell adhesion with the absence of E-cadherin.

A partial EMT program is not only important for metastatic potential but also it can create a difference in therapy response. For example, FOLFIRINOX treatment in epithelial or base QM tumor cells results in more QM cells, whereas Vitamin D treatment increases epithelial and base QM states [307]. These results suggest that therapy selection according to the initial status of the tumor may impact not only primary tumor growth but also their metastatic potential with the EMT plasticity.

Unlike knock out cancer cells, *Rel* knockdown in CKP cells didn't show a very consistent phenotype regarding EMT change. Strikingly, Slug and Zeb1 expression is decreased in 5 and 4 out of 6 cell lines upon c-Rel knockdown, respectively. However, these changes were not reflected in the total expression of E-cadherin, N-cadherin, β-catenin, and Vimentin levels. These results can be explained by two reasons. Firstly, although c-Rel levels are reduced after RNAi administration, remaining might still be adequate to execute its activity for epithelial phenotype maintenance. Secondly, c-Rel knockout cells are isolated from primary tumors in which cells underwent a Darwinian-like selection *in vivo*, which may not be reflected in RNAi knockdown *in vitro*. Additionally, in isolated CCKP, CKP, and GCKP cells *in vitro,* although the EMT characteristics were mostly maintained, the phenotype observed was more prominent *in vivo*. This may imply that possible crosstalk with the TME *in vivo* may augment cell-autonomous c-Rel mediated EMT phenotype in cancer cells.

6.3 c-Rel expression level regulates CSC subtypes

Our group identified Bcl3 as a negative regulator for CSCness in pancreatic cancer (manuscript under revision), which was a hit in the RNAseq experiment performed with human cell lines *in vitro*. In the same experiment, *REL* was another hit but this time as a positive regulator with the stemness. Basically, spheroid cells (assumed ot be enriched for CSCs) had more *REL* expression compared to their 2D cultured counterparts. Since the validity of the RNAseq experiment was elaborated and validated in deep for the case of Bcl3, we were encouraged to check the same for c-Rel.

Each of the CSC experiment is performed with 4-6 different cell lines per genotype, each isolated from an individual mouse. In terms of statistics, the high number of biological replicates increases the reliability of the results. The spheroid formation

experiment revealed that CCKP cells form a higher number of spheroids compared to CKP, while GCKP didn't show a difference. In contrast, GCKP cells formed bigger spheroids than CKP control, while CCKP showed no difference. For such a difference, multiple reasons can be speculated. Big spheroids can maintain the diffusion of material from outside to the inside of the spheroids [308]. Such an ability would require a leaky cell-cell contract between cells of a spheroid. In GCKP cells, epithelial characteristics are reduced (not diminished), which would provide the optimal conditions for spheroid growth. On the other hand, CCKP cells have high cell-cell contact limiting paracellular material transfer, as experimentally shown by both protein expression and RNAseq. Due to this fact, the formation of bigger spheroids is likely not favored in these cells.

Secondly, GCKP cells produce a high amount of ECM constituents like fibronectin and collagen-I *in vitro* as quantified by RNAseq experiment. Such scaffolding proteins can generate interconnected micropores for nutrient and oxygen transfer towards the inside of the spheroid, additionally providing support for optimal cell attachment and proliferation [308]. Of note, fibronectin overexpression of GCKP cells was evident also by IHC, unlike collagen *in vivo*. It is likely that despite that GCKP tumors have high collagen production; their remodeling may reduce bulk collagen deposition *in vivo*. Nevertheless, *in vitro,* functional assays proposed a positive feedback loop between fibronectin-induced c-Rel activation additionally, as the c-Rel level increased contractility of cancer cells increased on collagen suggesting a possible method for collagen fiber remodeling *in vivo.*

And finally, the proliferation rate was higher in GCKP CKP and CCKP in order *in vivo*, as assessed by BrdU+ incorporation. However, when these cells are cultured in 2D system, the proliferative capacity of CCKP cells increased as much as GCKP cells. These results indicate that c-Rel regulated proliferation is influenced by the 3D microenvironment. Accordingly, with the high rate of proliferation in GCKP cells, spheroids can get bigger in a period of time.

While we proposed multiple mechanisms explaining how GCKP cells can form bigger spheroids, explaining how CCKP cells creating a higher number of spheroids is more challenging. Flow cytometry analysis revealed that CCKP cells express conventional CSC markers (alone or in combination) on cell surfaces more than CKP and GCKP cells. These results can entirely explain why CCKP can form more spheroids. QM phenotype of GCKP cells along with high ECM constituent expression may

compensate for low surface expression of common CSC markers for spheroid formation capacity. Although surface expression of CSC markers decreases as the c-Rel level increases, number of cell in a subpopulation with CD44+;Sca1-;CD133- increases. This subpopulation is identified for its high tumor-initiating capacity in mouse pancreatic tumor model [296].

Previously, integrin-β3 is identified to promote cell survival and CSCness in anchorage-independent cultures without ECM engagement [204,309]. We provided evidence that *in vivo*, GCKP cells possess more fibronectin and integrin-β3 expression. Additionally, *in vitro* GCKP cells can respond faster to fibronectin presence as assessed by adhesion assay. In the spheroid culture medium (anchorage-independent) of GCKP cells, high integrin-β3 activity may explain large spheroid formation despite these cells possess less surface expression of common CSC markers. Additionally, *in vitro,* ELDA revealed higher CSC frequency in GCKP cells compared to CKP and CCKP cells. *In vitro,* ELDA has Matrigel as an ECM constituent, which may activate integrin-β3 signaling in an anchorage-dependent manner. These results imply that in c-Rel overexpressing cells, integrin-β3 signaling can increase CSCness anchorage dependently or independently.

Further rescue experiments with genetic manipulation of integrin-β3 in GCKP cells will help us understand the functional importance of this pathway in CSCness. Since *in vivo* tumors have a lot of fibronectin deposition, unlike *in vitro* cultures, it is of the question whether the CSC phenotype observed *in vitro* will also be retained *in vivo*. For this, flow cytometry analysis for CSC markers with the use of freshly dissected tumors of CCKP, CKP, and GCKP mice are ongoing. Additionally, *in vivo,* ELDA assay with the use of immunocompromised mice is required to functionally validate the current information.

Compiling evidence suggests that the bridge between EMT and CSC is not established in a straightforward way. In order to elaborate on this controversy, we will compile the evidence from how healthy epithelial cells are connected to various CSC states [258]. Epithelial lining can be divided into two groups: simple epithelia (in colon, pancreas, etc.) or stratified epithelia (in mammary and prostate glands). Simple epithelia are composed of a single lining of epithelial cells, as such observed in pancreatic ducts. Whereas in stratified epithelia, the epithelial lining is multilayered with luminal cells and additional basal-type cells.

In stratified epithelia, basal type cells are known to express EMT-TFs, of which the most prominent one is Slug [310,311]. Mammary stem cells (MaSC) are formed within Slug expressing mammary cells [256]. Evidently, re-introduction of high Slug expression to epithelia can increase MaSC frequency while its knockout reduces MaSC numbers [312]. Slug has been shown to maintain a basal-type state rather than luminal differentiation in the stratified epithelial lining [313]. Interestingly, basal MaSCs are multipotent, which can give rise to luminal epithelia through a hybrid EMT program. Next to hybrid EMT acquisition (involving Slug), these cells also rely on the activity of basal-type transcription factor ΔNp63. Still, how Slug and ΔNp63 networks are connected is not clear for maintenance of MaSC multipotency [314]. Additionally, basal type stem cells are predicted to rely on ECM-integrin signaling, maintaining a partial EMT phenotype [258]. In simple epithelia, stem cells seem to demonstrate no EMT signature, broadly [315]. However, some studies demonstrated Snail expression in mouse intestinal stem cells [316,317]. These results suggest a dual preference for subtypes of stem cells towards the necessity of EMT acquisition. Tissues composed of both epithelia ad basal-type cells possess stem cell subtypes, which rely on the acquisition of ΔNp63 and Slug mediated EMT signature. Whereas stem cells in simple epithelial tissues don't rely on broad EMT plasticity, but maybe snail.

Mentioned stem cell heterogeneity may also reflect heterogeneity in CSCs, which we will name as basal-CSC and epithelial-CSC from now on. GCKP cells with high p63-Slug and low Snail expression may possess a rather basal-CSC phenotype. On the other hand, CCKP cells may maintain their epithelial-CSC phenotype through an EMT-independent fashion. Of note, Zeb1 ablation in epithelial mouse pancreatic cancer cells is reported to reduce CSCness while the surface expression of CSC markers is not changed [318]. These results suggest that different EMT-TFs might still be involved in the stemness of epithelial-CSCs.

Cumulatively, these results propose that there is heterogeneity in CSCness associated phenotypes, especially in spheroid forming modalities. Although not studied deeply in pancreatic cancer, CSC subtypes and their different phenotypic outcomes are briefly defined in other entities [319–321] c-Rel might be holding, if not pivotal, at least a defining position for the CSC subtype determination in association with EMT in pancreatic cancer.

6.4 Pathological c-Rel levels increase metastatic potential

Tail-vein injection of both CCKP and GCKP cells showed higher colonization in littermate mice. These results again re-question a previously widely accepted hypothesis in which more EMT means more metastasis. As recently started to be widely accepted, rather than a full EMT program, the partial transition to mesenchymal phenotype is accepted to be more aggressive in terms of metastasis [231]. QM phenotype observed in GCKP cells can explain their high metastatic potential.

The real surprising result is observed with CCKP cells as they also show quite high metastatic incidence. Although these cells are more epithelial, they also possess high CSC numbers. Additionally, CCKP cells produce a lot of inflammatory cytokines, which are also enriched in RNAseq data. Paracrine crosstalk with metastatic niche microenvironment might be increasing metastatic colonization ability in cancer cells. This hypothesis will be further tested by intravenous injection of the cancer cells to immunocompromised mice. In case that cytokine network is important, we expect to see less change of metastatic colonization in immunocompromised mice. Interestingly, CCKP mice survive significantly longer than GCKP and CKP mice, although they have more metastatic potential. The difference here lies in the functional heterogeneity of c-Rel in primary vs. metastatic cells. CKP model is not good to quantify spontaneous metastasis formation for the reasons described in the introduction part. Of note, one of the CCKP mice developed liver metastasis, which is an infrequent event to see in this model.

After RNAi knockdown of c-Rel, no change in the metastatic capacity of CKP cells was observed. This is not surprising since no remarkable difference was also observed in EMT markers. Nevertheless, the change in cytokine/chemokine expression is to be tested. The lack of phenotype in RNAi cells can be due to similar reasons, as explained in section 6.2.

6.5 c-Rel as an NF-κB signaling component

RNAseq results revealed many common genes upregulated in both CCKP and GCKP cells. NF-κB transcription factors are known to compensate for each other's absence, as described in the introduction part. While one would expect high NF-κB activation due to high c-Rel expression, it is also customary to observe more RelA or p50 activation due to c-Rel absence. The absence of c-Rel may release more RelA and

p50 proteins free to dimerize and translocate to the nucleus as active transcription complexes.

Further investigation is required to understand such crosstalk with other components. For this, molecular assays like ChIP-seq together with *in vivo* models combining RelA, with c-Rel mouse models are necessary.

6.6 The c-Rel function is dependent on p53 status

Unlike CKP, in the $CKP^{lox/+}$ model, c-Rel knockout reduces survival while overexpression has no impact on it. On the other hand, c-Rel overexpression reduces tumor formation incidence. Strikingly, in both $CCKP^{lox/+}$ and $GCKP^{lox/+}$ mice, the metastatic incidence in tumor mice was lower than in control $CKP^{lox/+}$. Basically, there is a complete reversal of the phenotype in the model where one allele of *Trp53* is wild type. This result is actually not surprising considering the previous study from our group delineating RelA function in pancreatic cancer [182]. In this study, RelA was shown to act as a tumor suppressor during tumorigenesis, where p53 can still induce senescence. RelA was shown to activate a senescence induced secretory phenotype (SASP) in premalignant lesions supporting senescence. Therefore, RelA knockout in the CK model caused a significantly shorter survival compared to the CK model. On the other hand, RelA knockout in the CKP model resulted in prolonged survival since, due to the absence of the p53 senescence barrier is exceeded, leaving no room for the tumor suppressor function of RelA. Such a phenotype is also possibly expected in c-Rel function considering the high cooperation between RelA and c-Rel. In the RelA study, JSH-023 treatment of HPDE cells (human pancreatic ductal epithelial cells) resulted in reduced SASP components, as shown by cytokine array analysis. JSH023 in pancreatic cancer cells inhibits not only RelA nuclear localization but also c-Rel (Data not shown). Therefore, c-Rel action in canonical NF-κB signaling regulating senescence is highly probable.

6.7 c-Rel as a therapeutic target

c-Rel is therapeutically targetable with the use of pentoxifylline and IT-901 (IT-603) drugs, as shown by multiple studies mentioned in the introduction part. In solid tumors, c-Rel function in Treg and MDSCs was rather targeted for therapeutics. However, targeting c-Rel in solids tumors pharmacologically was not tested for its impact on cancer cells per se.

Our results show that stratification based on p53 status will be important for patient selection. Firstly, this will inform us whether inhibiting c-Rel will be favorable for primary tumor targeting. In the case of p53 full inactivation, we show that c-Rel is an oncogene for primary tumor formation and both an oncogene and tumor-suppressor for metastasis. But importantly, in c-Rel RNAi knockdown cells, there was no increase in CKP cells metastatic potential. These cells already have high c-Rel expression, and further knockdown to a certain level didn't increase their metastatic potential. Therefore, c-Rel inhibition in patients with high c-Rel expression and p53 inactivation might hold promise for primary tumor therapy. Nevertheless, for metastatic tumors with high c-Rel expression, c-Rel inhibition to a steady-state level might also be beneficial for anti-metastatic treatment.

A critical approach to delineate context-specific c-Rel targeting would be to perform rescue experiments in CCKP and GCKP cells by overexpressing and knocking down c-Rel, respectively. We would anticipate a reduction in the metastatic potential of both groups of cells upon c-Rel rescue. The results would help us define a better strategy for patient stratification together with c-Rel targeting.

We will also test the importance of c-Rel in other compartments in pancreatic cancer metastasis by using the c-Rel whole-body knockout mouse model to transplant c-Rel wild type cells both orthotopically and intravenously. We are in the process of generating a c-Rel whole-body knockout model with the use of a pancreas-specific *Ptf1a-Cre* model, which transfers germline recombination paternally.

7 SUMMARY

In the present study, we aimed to analyze the function of NF-κB transcription factor c-Rel in pancreatic cancer. Firstly, we investigated whether c-Rel is expressed in human pancreatic cancer samples. Results indicated no correlation between *REL* mRNA/ CNV levels and survival in human pancreatic cancer. Still, tumor samples expressed more *REL* mRNA than healthy tissue in the pancreas. Most importantly, late-stage (locally advanced and invasive) tumors express more *REL* mRNA than earlier stages. Additionally, we observed ubiquitous c-Rel production in both human and mouse pancreatic cancer samples.

Encouraged by these results, we decided to use the CKP mouse model, harboring pancreas-specific expression of $Kras^{G12D}$ and knockout of p53, to dissect the function c-Rel in pancreatic cancer. We both overexpressed and knocked out c-Rel in CKP mice by genetic manipulation of *Rel*. In this autochthonous model, pancreas-specific overexpression of c-Rel (GCKP) reduced survival, while knockout (CCKP) prolonged it. Histopathological analysis demonstrated that from CCKP to CKP to GCKP mice, the incidence of undifferentiated tumor formation increased. Following that, *REL* was expressed more in Bailey's molecular squamous subtype than the progenitor. In support of these results, EMT plasticity was shifted towards a mesenchymal type with increasing c-Rel level *in vivo* tumors and *in vitro* isolated cancer cells.

Based on our preliminary results in which *REL* mRNA expression is increased in CSC enriched human cell lines, we analyzed CSC related characteristics in isolated murine pancreatic cancer cells. GCKP cells formed bigger spheroids, while CCKP cells formed a higher number of spheroids compared to CKP control cells. Furthermore, the surface expression of CSC markers increased from GCKP to CKP to CCKP cells. However, GCKP cells had more cells of a previously identified subpopulation (CD44+;Sca1-;CD133-) with high tumor-initiating capacity. Furthermore, GCKP tumors showed more elevated fibronectin-integrin signaling, which is known to induce stemness in various settings.

To further characterize the consequences of c-Rel manipulation in EMT and CSC associated metastasis *in vivo*, we performed intravenous injection of the cells. Both CCKP and GKCP cells showed higher metastatic potential than CKP control cells. RNAseq analysis revealed that both CCKP and GCKP cells possess transcription enrichment sets associated with their elaborated phenotypes. Inflammatory cytokine

expression is increased in both CCKP and GCKP cells experimentally shown by RNAseq and cytokine array experiments. Finally, we provide evidence that the function of c-Rel gets reversed by the presence of a single *Trp53* allele.

Overall, cumulative results suggest that c-Rel expression can be used as a biomarker for tumor type classification. While pharmacological inhibition of c-Rel is possible, it is crucial to identify the context to utilize such therapeutic intervention.

8 REFERENCES

1. Longnecker, D. *Anatomy and Histology of the Pancreas*. (The University of Michigan Library, 2014). at <http://pancreapedia.org/?q=node/8098>
2. Siegel, R. L., Miller, K. D. & Jemal, A. Cancer statistics, 2020. *CA Cancer J Clin* **70,** 7–30 (2020).
3. Kleeff, J. *et al.* Pancreatic cancer. *Nat. Rev. Dis. Primers* **2,** 16022 (2016).
4. Siegel, R. L., Miller, K. D. & Jemal, A. Cancer statistics, 2018. *CA Cancer J Clin* **68,** 7–30 (2018).
5. Bedard, P. L. *et al.* A phase Ib dose-escalation study of the oral pan-PI3K inhibitor buparlisib (BKM120) in combination with the oral MEK1/2 inhibitor trametinib (GSK1120212) in patients with selected advanced solid tumors. *Clin. Cancer Res.* **21,** 730–738 (2015).
6. Bodoky, G. *et al.* A phase II open-label randomized study to assess the efficacy and safety of selumetinib (AZD6244 [ARRY-142886]) versus capecitabine in patients with advanced or metastatic pancreatic cancer who have failed first-line gemcitabine therapy. *Invest. New Drugs* **30,** 1216–1223 (2012).
7. Infante, J. R. *et al.* A randomised, double-blind, placebo-controlled trial of trametinib, an oral MEK inhibitor, in combination with gemcitabine for patients with untreated metastatic adenocarcinoma of the pancreas. *Eur. J. Cancer* **50,** 2072–2081 (2014).
8. Ko, A. H. *et al.* A Multicenter, Open-Label Phase II Clinical Trial of Combined MEK plus EGFR Inhibition for Chemotherapy-Refractory Advanced Pancreatic Adenocarcinoma. *Clin. Cancer Res.* **22,** 61–68 (2016).
9. Tolcher, A. W. *et al.* A phase IB trial of the oral MEK inhibitor trametinib (GSK1120212) in combination with everolimus in patients with advanced solid tumors. *Ann. Oncol.* **26,** 58–64 (2015).
10. Wolpin, B. M. *et al.* Oral mTOR inhibitor everolimus in patients with gemcitabine-refractory metastatic pancreatic cancer. *J. Clin. Oncol.* **27,** 193–198 (2009).
11. Conroy, T. *et al.* FOLFIRINOX versus gemcitabine for metastatic pancreatic cancer. *N. Engl. J. Med.* **364,** 1817–1825 (2011).
12. Von Hoff, D. D. *et al.* Increased survival in pancreatic cancer with nab-paclitaxel plus gemcitabine. *N. Engl. J. Med.* **369,** 1691–1703 (2013).
13. Goldstein, D. *et al.* nab-Paclitaxel plus gemcitabine for metastatic pancreatic cancer: long-term survival from a phase III trial. *J. Natl. Cancer Inst.* **107,** (2015).

14. Kabacaoglu, D., Ciecielski, K. J., Ruess, D. A. & Algül, H. Immune checkpoint inhibition for pancreatic ductal adenocarcinoma: current limitations and future options. *Front. Immunol.* **9,** 1878 (2018).
15. Cascinu, S., Falconi, M., Valentini, V., Jelic, S. & ESMO Guidelines Working Group. Pancreatic cancer: ESMO Clinical Practice Guidelines for diagnosis, treatment and follow-up. *Ann. Oncol.* **21 Suppl 5,** v55-8 (2010).
16. Bosetti, C. *et al.* Cigarette smoking and pancreatic cancer: an analysis from the International Pancreatic Cancer Case-Control Consortium (Panc4). *Ann. Oncol.* **23,** 1880–1888 (2012).
17. Aune, D. *et al.* Body mass index, abdominal fatness and pancreatic cancer risk: a systematic review and non-linear dose-response meta-analysis of prospective studies. *Ann. Oncol.* **23,** 843–852 (2012).
18. Bosetti, C. *et al.* Nutrient-based dietary patterns and pancreatic cancer risk. *Ann Epidemiol* **23,** 124–128 (2013).
19. Larsson, S. C. & Wolk, A. Red and processed meat consumption and risk of pancreatic cancer: meta-analysis of prospective studies. *Br. J. Cancer* **106,** 603–607 (2012).
20. Rohrmann, S. *et al.* Meat and fish consumption and risk of pancreatic cancer: results from the European Prospective Investigation into Cancer and Nutrition. *Int. J. Cancer* **132,** 617–624 (2013).
21. Duell, E. J. *et al.* Pancreatitis and pancreatic cancer risk: a pooled analysis in the International Pancreatic Cancer Case-Control Consortium (PanC4). *Ann. Oncol.* **23,** 2964–2970 (2012).
22. Ben, Q. *et al.* Diabetes mellitus and risk of pancreatic cancer: A meta-analysis of cohort studies. *Eur. J. Cancer* **47,** 1928–1937 (2011).
23. Jones, S. *et al.* Exomic sequencing identifies PALB2 as a pancreatic cancer susceptibility gene. *Science* **324,** 217 (2009).
24. Roberts, N. J. *et al.* Whole genome sequencing defines the genetic heterogeneity of familial pancreatic cancer. *Cancer Discov.* **6,** 166–175 (2016).
25. Waddell, N. *et al.* Whole genomes redefine the mutational landscape of pancreatic cancer. *Nature* **518,** 495–501 (2015).
26. Hu, Z. I. *et al.* Evaluating mismatch repair deficiency in pancreatic adenocarcinoma: challenges and recommendations. *Clin. Cancer Res.* **24,** 1326–1336 (2018).
27. Golan, T. *et al.* Maintenance Olaparib for Germline BRCA-Mutated Metastatic Pancreatic Cancer. *N. Engl. J. Med.* **381,** 317–327 (2019).

28. Le, D. T. *et al.* Mismatch repair deficiency predicts response of solid tumors to PD-1 blockade. *Science* **357,** 409–413 (2017).
29. Ryan, D. P., Hong, T. S. & Bardeesy, N. Pancreatic adenocarcinoma. *N. Engl. J. Med.* **371,** 1039–1049 (2014).
30. Pishvaian, M. J. & Brody, J. R. Therapeutic Implications of Molecular Subtyping for Pancreatic Cancer. *Oncology (Williston Park)* **31,** 159–166, 168 (2017).
31. Aguirre, A. J. *et al.* Real-time Genomic Characterization of Advanced Pancreatic Cancer to Enable Precision Medicine. *Cancer Discov.* **8,** 1096–1111 (2018).
32. Qian, Z. R. *et al.* Association of alterations in main driver genes with outcomes of patients with resected pancreatic ductal adenocarcinoma. *JAMA Oncol.* **4,** e173420 (2018).
33. Smit, V. T. *et al.* KRAS codon 12 mutations occur very frequently in pancreatic adenocarcinomas. *Nucleic Acids Res.* **16,** 7773–7782 (1988).
34. Biankin, A. V. *et al.* Pancreatic cancer genomes reveal aberrations in axon guidance pathway genes. *Nature* **491,** 399–405 (2012).
35. Jones, S. *et al.* Core signaling pathways in human pancreatic cancers revealed by global genomic analyses. *Science* **321,** 1801–1806 (2008).
36. Collisson, E. A., Bailey, P., Chang, D. K. & Biankin, A. V. Molecular subtypes of pancreatic cancer. *Nat. Rev. Gastroenterol. Hepatol.* **16,** 207–220 (2019).
37. Pylayeva-Gupta, Y., Grabocka, E. & Bar-Sagi, D. RAS oncogenes: weaving a tumorigenic web. *Nat. Rev. Cancer* **11,** 761–774 (2011).
38. Yachida, S. *et al.* Clinical significance of the genetic landscape of pancreatic cancer and implications for identification of potential long-term survivors. *Clin. Cancer Res.* **18,** 6339–6347 (2012).
39. Mueller, S. *et al.* Evolutionary routes and KRAS dosage define pancreatic cancer phenotypes. *Nature* **554,** 62–68 (2018).
40. Quelle, D. E., Zindy, F., Ashmun, R. A. & Sherr, C. J. Alternative reading frames of the INK4a tumor suppressor gene encode two unrelated proteins capable of inducing cell cycle arrest. *Cell* **83,** 993–1000 (1995).
41. Schutte, M. *et al.* Abrogation of the Rb/p16 tumor-suppressive pathway in virtually all pancreatic carcinomas. *Cancer Res.* **57,** 3126–3130 (1997).
42. Makohon-Moore, A. & Iacobuzio-Donahue, C. A. Pancreatic cancer biology and genetics from an evolutionary perspective. *Nat. Rev. Cancer* **16,** 553–565 (2016).
43. Vogelstein, B., Lane, D. & Levine, A. J. Surfing the p53 network. *Nature* **408,** 307–310 (2000).

44. Hahn, S. A. *et al.* DPC4, a candidate tumor suppressor gene at human chromosome 18q21.1. *Science* **271,** 350–353 (1996).
45. Whittle, M. C. *et al.* RUNX3 controls a metastatic switch in pancreatic ductal adenocarcinoma. *Cell* **161,** 1345–1360 (2015).
46. Siegel, P. M. & Massagué, J. Cytostatic and apoptotic actions of TGF-beta in homeostasis and cancer. *Nat. Rev. Cancer* **3,** 807–821 (2003).
47. Kretzschmar, M., Doody, J., Timokhina, I. & Massagué, J. A mechanism of repression of TGFbeta/ Smad signaling by oncogenic Ras. *Genes Dev.* **13,** 804–816 (1999).
48. Saha, D., Datta, P. K. & Beauchamp, R. D. Oncogenic ras represses transforming growth factor-beta /Smad signaling by degrading tumor suppressor Smad4. *J. Biol. Chem.* **276,** 29531–29537 (2001).
49. Cordenonsi, M. *et al.* Links between tumor suppressors: p53 is required for TGF-beta gene responses by cooperating with Smads. *Cell* **113,** 301–314 (2003).
50. Cordenonsi, M. *et al.* Integration of TGF-beta and Ras/MAPK signaling through p53 phosphorylation. *Science* **315,** 840–843 (2007).
51. Hruban, R. H., Goggins, M., Parsons, J. & Kern, S. E. Progression model for pancreatic cancer. *Clin. Cancer Res.* **6,** 2969–2972 (2000).
52. Hruban, R. H. *et al.* Pancreatic intraepithelial neoplasia: a new nomenclature and classification system for pancreatic duct lesions. *Am. J. Surg. Pathol.* **25,** 579–586 (2001).
53. Maitra, A. *et al.* Multicomponent analysis of the pancreatic adenocarcinoma progression model using a pancreatic intraepithelial neoplasia tissue microarray. *Mod. Pathol.* **16,** 902–912 (2003).
54. Kanda, M. *et al.* Presence of somatic mutations in most early-stage pancreatic intraepithelial neoplasia. *Gastroenterology* **142,** 730–733.e9 (2012).
55. Hong, S.-M. *et al.* Genome-wide somatic copy number alterations in low-grade PanINs and IPMNs from individuals with a family history of pancreatic cancer. *Clin. Cancer Res.* **18,** 4303–4312 (2012).
56. Wilentz, R. E. *et al.* Loss of expression of Dpc4 in pancreatic intraepithelial neoplasia: evidence that DPC4 inactivation occurs late in neoplastic progression. *Cancer Res.* **60,** 2002–2006 (2000).
57. Wang, L., Xie, D. & Wei, D. Pancreatic Acinar-to-Ductal Metaplasia and Pancreatic Cancer. *Methods Mol. Biol.* **1882,** 299–308 (2019).
58. Parsa, I. *et al.* Ductal metaplasia of human exocrine pancreas and its association with

carcinoma. *Cancer Res.* **45,** 1285–1290 (1985).

59. Liu, J. *et al.* TGF-β1 promotes acinar to ductal metaplasia of human pancreatic acinar cells. *Sci. Rep.* **6,** 30904 (2016).
60. Notta, F. *et al.* A renewed model of pancreatic cancer evolution based on genomic rearrangement patterns. *Nature* **538,** 378–382 (2016).
61. Eldredge, N. & Gould, S. J. Punctuated equilibria: the tempo and mode of evolution reconsidered. *Paleobiology* (1977).
62. Collisson, E. A. *et al.* Subtypes of pancreatic ductal adenocarcinoma and their differing responses to therapy. *Nat. Med.* **17,** 500–503 (2011).
63. Moffitt, R. A. *et al.* Virtual microdissection identifies distinct tumor- and stroma-specific subtypes of pancreatic ductal adenocarcinoma. *Nat. Genet.* **47,** 1168–1178 (2015).
64. Bailey, P. *et al.* Genomic analyses identify molecular subtypes of pancreatic cancer. *Nature* **531,** 47–52 (2016).
65. Cancer Genome Atlas Research Network. Electronic address: andrew_aguirre@dfci.harvard.edu & Cancer Genome Atlas Research Network. Integrated genomic characterization of pancreatic ductal adenocarcinoma. *Cancer Cell* **32,** 185–203.e13 (2017).
66. Aung, K. L. *et al.* Genomics-Driven Precision Medicine for Advanced Pancreatic Cancer: Early Results from the COMPASS Trial. *Clin. Cancer Res.* **24,** 1344–1354 (2018).
67. Hingorani, S. R. *et al.* Preinvasive and invasive ductal pancreatic cancer and its early detection in the mouse. *Cancer Cell* **4,** 437–450 (2003).
68. Siveke, J. T. *et al.* Concomitant pancreatic activation of Kras(G12D) and Tgfa results in cystic papillary neoplasms reminiscent of human IPMN. *Cancer Cell* **12,** 266–279 (2007).
69. Clark, C. E. *et al.* Dynamics of the immune reaction to pancreatic cancer from inception to invasion. *Cancer Res.* **67,** 9518–9527 (2007).
70. Erkan, M. *et al.* The impact of the activated stroma on pancreatic ductal adenocarcinoma biology and therapy resistance. *Curr. Mol. Med.* **12,** 288–303 (2012).
71. Kawaguchi, Y. *et al.* The role of the transcriptional regulator Ptf1a in converting intestinal to pancreatic progenitors. *Nat. Genet.* **32,** 128–134 (2002).
72. Ahlgren, U., Jonsson, J. & Edlund, H. The morphogenesis of the pancreatic mesenchyme is uncoupled from that of the pancreatic epithelium in IPF1/PDX1-deficient mice. *Development* **122,** 1409–1416 (1996).
73. Offield, M. F. *et al.* PDX-1 is required for pancreatic outgrowth and differentiation of the

rostral duodenum. *Development* **122,** 983–995 (1996).

74. Krapp, A. *et al.* The p48 DNA-binding subunit of transcription factor PTF1 is a new exocrine pancreas-specific basic helix-loop-helix protein. *EMBO J.* **15,** 4317–4329 (1996).
75. Krapp, A. *et al.* The bHLH protein PTF1-p48 is essential for the formation of the exocrine and the correct spatial organization of the endocrine pancreas. *Genes Dev.* **12,** 3752–3763 (1998).
76. Jackson, E. L. *et al.* Analysis of lung tumor initiation and progression using conditional expression of oncogenic K-ras. *Genes Dev.* **15,** 3243–3248 (2001).
77. Nakhai, H. *et al.* Ptf1a is essential for the differentiation of GABAergic and glycinergic amacrine cells and horizontal cells in the mouse retina. *Development* **134,** 1151–1160 (2007).
78. Marino, S., Vooijs, M., van Der Gulden, H., Jonkers, J. & Berns, A. Induction of medulloblastomas in p53-null mutant mice by somatic inactivation of Rb in the external granular layer cells of the cerebellum. *Genes Dev.* **14,** 994–1004 (2000).
79. Whatcott, C. J. *et al.* Desmoplasia in primary tumors and metastatic lesions of pancreatic cancer. *Clin. Cancer Res.* **21,** 3561–3568 (2015).
80. Apte, M. V. *et al.* Pancreatic stellate cells are activated by proinflammatory cytokines: implications for pancreatic fibrogenesis. *Gut* **44,** 534–541 (1999).
81. Provenzano, P. P. *et al.* Enzymatic targeting of the stroma ablates physical barriers to treatment of pancreatic ductal adenocarcinoma. *Cancer Cell* **21,** 418–429 (2012).
82. Jacobetz, M. A. *et al.* Hyaluronan impairs vascular function and drug delivery in a mouse model of pancreatic cancer. *Gut* **62,** 112–120 (2013).
83. Ramanathan, R. K. *et al.* Phase IB/II randomized study of FOLFIRINOX plus pegylated recombinant human hyaluronidase versus FOLFIRINOX alone in patients with metastatic pancreatic adenocarcinoma: SWOG S1313. *J. Clin. Oncol.* **37,** 1062–1069 (2019).
84. Hingorani, S. R. *et al.* HALO 202: Randomized Phase II Study of PEGPH20 Plus Nab-Paclitaxel/Gemcitabine Versus Nab-Paclitaxel/Gemcitabine in Patients With Untreated, Metastatic Pancreatic Ductal Adenocarcinoma. *J. Clin. Oncol.* **36,** 359–366 (2018).
85. Van Cutsem, E. *et al.* Randomized Phase III Trial of Pegvorhyaluronidase Alfa With Nab-Paclitaxel Plus Gemcitabine for Patients With Hyaluronan-High Metastatic Pancreatic Adenocarcinoma. *J. Clin. Oncol.* **38,** 3185–3194 (2020).
86. Linder, S., Castaños-Velez, E., von Rosen, A. & Biberfeld, P. Immunohistochemical

expression of extracellular matrix proteins and adhesion molecules in pancreatic carcinoma. *Hepatogastroenterology* **48,** 1321–1327 (2001).

87. Ohlund, D. *et al.* Type IV collagen is a tumour stroma-derived biomarker for pancreas cancer. *Br. J. Cancer* **101,** 91–97 (2009).
88. Leppänen, J. *et al.* Tenascin C, Fibronectin, and Tumor-Stroma Ratio in Pancreatic Ductal Adenocarcinoma. *Pancreas* **48,** 43–48 (2019).
89. Hu, D. *et al.* Stromal fibronectin expression in patients with resected pancreatic ductal adenocarcinoma. *World J Surg Oncol* **17,** 29 (2019).
90. Hiroshima, Y. *et al.* Novel targets identified by integrated cancer-stromal interactome analysis of pancreatic adenocarcinoma. *Cancer Lett.* **469,** 217–227 (2020).
91. Lynch, M. D. & Watt, F. M. Fibroblast heterogeneity: implications for human disease. *J. Clin. Invest.* **128,** 26–35 (2018).
92. Omary, M. B., Lugea, A., Lowe, A. W. & Pandol, S. J. The pancreatic stellate cell: a star on the rise in pancreatic diseases. *J. Clin. Invest.* **117,** 50–59 (2007).
93. Hwang, R. F. *et al.* Cancer-associated stromal fibroblasts promote pancreatic tumor progression. *Cancer Res.* **68,** 918–926 (2008).
94. Özdemir, B. C. *et al.* Depletion of Carcinoma-Associated Fibroblasts and Fibrosis Induces Immunosuppression and Accelerates Pancreas Cancer with Reduced Survival. *Cancer Cell* **28,** 831–833 (2015).
95. Rhim, A. D. *et al.* Stromal elements act to restrain, rather than support, pancreatic ductal adenocarcinoma. *Cancer Cell* **25,** 735–747 (2014).
96. Feldmann, G. *et al.* Hedgehog inhibition prolongs survival in a genetically engineered mouse model of pancreatic cancer. *Gut* **57,** 1420–1430 (2008).
97. Bailey, J. M. *et al.* Sonic hedgehog promotes desmoplasia in pancreatic cancer. *Clin. Cancer Res.* **14,** 5995–6004 (2008).
98. Catenacci, D. V. T. *et al.* Randomized phase ib/ii study of gemcitabine plus placebo or vismodegib, a hedgehog pathway inhibitor, in patients with metastatic pancreatic cancer. *J. Clin. Oncol.* **33,** 4284–4292 (2015).
99. Öhlund, D. *et al.* Distinct populations of inflammatory fibroblasts and myofibroblasts in pancreatic cancer. *J. Exp. Med.* **214,** 579–596 (2017).
100. Bernard, V. *et al.* Single-Cell Transcriptomics of Pancreatic Cancer Precursors Demonstrates Epithelial and Microenvironmental Heterogeneity as an Early Event in Neoplastic Progression. *Clin. Cancer Res.* **25,** 2194–2205 (2019).
101. Elyada, E. *et al.* Cross-Species Single-Cell Analysis of Pancreatic Ductal

Adenocarcinoma Reveals Antigen-Presenting Cancer-Associated Fibroblasts. *Cancer Discov.* **9,** 1102–1123 (2019).

102. Dominguez, C. X. *et al.* Single-Cell RNA Sequencing Reveals Stromal Evolution into LRRC15+ Myofibroblasts as a Determinant of Patient Response to Cancer Immunotherapy. *Cancer Discov.* **10,** 232–253 (2020).
103. Dunn, G. P., Bruce, A. T., Ikeda, H., Old, L. J. & Schreiber, R. D. Cancer immunoediting: from immunosurveillance to tumor escape. *Nat. Immunol.* **3,** 991–998 (2002).
104. Dunn, G. P., Old, L. J. & Schreiber, R. D. The three Es of cancer immunoediting. *Annu. Rev. Immunol.* **22,** 329–360 (2004).
105. Gabrilovich, D. I. Myeloid-Derived Suppressor Cells. *Cancer Immunol Res* **5,** 3–8 (2017).
106. Sica, A., Schioppa, T., Mantovani, A. & Allavena, P. Tumour-associated macrophages are a distinct M2 polarised population promoting tumour progression: potential targets of anti-cancer therapy. *Eur. J. Cancer* **42,** 717–727 (2006).
107. Lankadasari, M. B., Mukhopadhyay, P., Mohammed, S. & Harikumar, K. B. TAMing pancreatic cancer: combat with a double edged sword. *Mol. Cancer* **18,** 48 (2019).
108. DeNardo, D. G. *et al.* CD4(+) T cells regulate pulmonary metastasis of mammary carcinomas by enhancing protumor properties of macrophages. *Cancer Cell* **16,** 91–102 (2009).
109. Kuang, D.-M. *et al.* Activated monocytes in peritumoral stroma of hepatocellular carcinoma foster immune privilege and disease progression through PD-L1. *J. Exp. Med.* **206,** 1327–1337 (2009).
110. Rodriguez, P. C. *et al.* Arginase I production in the tumor microenvironment by mature myeloid cells inhibits T-cell receptor expression and antigen-specific T-cell responses. *Cancer Res.* **64,** 5839–5849 (2004).
111. Murai, M. *et al.* Interleukin 10 acts on regulatory T cells to maintain expression of the transcription factor Foxp3 and suppressive function in mice with colitis. *Nat. Immunol.* **10,** 1178–1184 (2009).
112. Curiel, T. J. *et al.* Specific recruitment of regulatory T cells in ovarian carcinoma fosters immune privilege and predicts reduced survival. *Nat. Med.* **10,** 942–949 (2004).
113. Leliefeld, P. H. C., Koenderman, L. & Pillay, J. How neutrophils shape adaptive immune responses. *Front. Immunol.* **6,** 471 (2015).
114. Fridlender, Z. G. *et al.* Polarization of tumor-associated neutrophil phenotype by TGF-beta: "N1" versus "N2" TAN. *Cancer Cell* **16,** 183–194 (2009).

115. Reid, M. D. *et al.* Tumor-infiltrating neutrophils in pancreatic neoplasia. *Mod. Pathol.* **24,** 1612–1619 (2011).
116. Shen, M. *et al.* Tumor-associated neutrophils as a new prognostic factor in cancer: a systematic review and meta-analysis. *PLoS One* **9,** e98259 (2014).
117. Gabrilovich, D. I. *et al.* The terminology issue for myeloid-derived suppressor cells. *Cancer Res.* **67,** 425; author reply 426 (2007).
118. Rodriguez, P. C. *et al.* Arginase I in myeloid suppressor cells is induced by COX-2 in lung carcinoma. *J. Exp. Med.* **202,** 931–939 (2005).
119. Donkor, M. K. *et al.* Mammary tumor heterogeneity in the expansion of myeloid-derived suppressor cells. *Int. Immunopharmacol.* **9,** 937–948 (2009).
120. Youn, J.-I., Collazo, M., Shalova, I. N., Biswas, S. K. & Gabrilovich, D. I. Characterization of the nature of granulocytic myeloid-derived suppressor cells in tumor-bearing mice. *J. Leukoc. Biol.* **91,** 167–181 (2012).
121. Li, Q., Pan, P.-Y., Gu, P., Xu, D. & Chen, S.-H. Role of immature myeloid Gr-1+ cells in the development of antitumor immunity. *Cancer Res.* **64,** 1130–1139 (2004).
122. Narita, Y., Wakita, D., Ohkur, T., Chamoto, K. & Nishimura, T. Potential differentiation of tumor bearing mouse CD11b+Gr-1+ immature myeloid cells into both suppressor macrophages and immunostimulatory dendritic cells. *Biomed. Res.* **30,** 7–15 (2009).
123. Gabrilovich, D. I., Ostrand-Rosenberg, S. & Bronte, V. Coordinated regulation of myeloid cells by tumours. *Nat. Rev. Immunol.* **12,** 253–268 (2012).
124. Pardoll, D. M. The blockade of immune checkpoints in cancer immunotherapy. *Nat. Rev. Cancer* **12,** 252–264 (2012).
125. Gao, G. F., Rao, Z. & Bell, J. I. Molecular coordination of alphabeta T-cell receptors and coreceptors CD8 and CD4 in their recognition of peptide-MHC ligands. *Trends Immunol.* **23,** 408–413 (2002).
126. Steimle, V., Siegrist, C. A., Mottet, A., Lisowska-Grospierre, B. & Mach, B. Regulation of MHC class II expression by interferon-gamma mediated by the transactivator gene CIITA. *Science* **265,** 106–109 (1994).
127. Stout, R. D. & Bottomly, K. Antigen-specific activation of effector macrophages by IFN-gamma producing (TH1) T cell clones. Failure of IL-4-producing (TH2) T cell clones to activate effector function in macrophages. *J. Immunol.* **142,** 760–765 (1989).
128. Crespo, J., Sun, H., Welling, T. H., Tian, Z. & Zou, W. T cell anergy, exhaustion, senescence, and stemness in the tumor microenvironment. *Curr. Opin. Immunol.* **25,** 214–221 (2013).

129. Tanaka, A. & Sakaguchi, S. Regulatory T cells in cancer immunotherapy. *Cell Res.* **27,** 109–118 (2017).
130. Sen, R. & Baltimore, D. Multiple nuclear factors interact with the immunoglobulin enhancer sequences. *Cell* **46,** 705–716 (1986).
131. Williams, L. M. & Gilmore, T. D. Looking Down on NF-κB. *Mol. Cell. Biol.* **40,** (2020).
132. Zhang, Q., Lenardo, M. J. & Baltimore, D. 30 Years of NF-κB: A Blossoming of Relevance to Human Pathobiology. *Cell* **168,** 37–57 (2017).
133. Bours, V., Villalobos, J., Burd, P. R., Kelly, K. & Siebenlist, U. Cloning of a mitogen-inducible gene encoding a kappa B DNA-binding protein with homology to the rel oncogene and to cell-cycle motifs. *Nature* **348,** 76–80 (1990).
134. Ghosh, S. *et al.* Cloning of the p50 DNA binding subunit of NF-kappa B: homology to rel and dorsal. *Cell* **62,** 1019–1029 (1990).
135. Kieran, M. *et al.* The DNA binding subunit of NF-kappa B is identical to factor KBF1 and homologous to the rel oncogene product. *Cell* **62,** 1007–1018 (1990).
136. Meyer, R. *et al.* Cloning of the DNA-binding subunit of human nuclear factor kappa B: the level of its mRNA is strongly regulated by phorbol ester or tumor necrosis factor alpha. *Proc. Natl. Acad. Sci. USA* **88,** 966–970 (1991).
137. Schmid, R. M., Perkins, N. D., Duckett, C. S., Andrews, P. C. & Nabel, G. J. Cloning of an NF-kappa B subunit which stimulates HIV transcription in synergy with p65. *Nature* **352,** 733–736 (1991).
138. Neri, A. *et al.* B cell lymphoma-associated chromosomal translocation involves candidate oncogene lyt-10, homologous to NF-kappa B p50. *Cell* **67,** 1075–1087 (1991).
139. Mercurio, F., Didonato, J., Rosette, C. & Karin, M. Molecular cloning and characterization of a novel Rel/NF-kappa B family member displaying structural and functional homology to NF-kappa B p50/p105. *DNA Cell Biol* **11,** 523–537 (1992).
140. Bours, V. *et al.* A novel mitogen-inducible gene product related to p50/p105-NF-kappa B participates in transactivation through a kappa B site. *Mol. Cell. Biol.* **12,** 685–695 (1992).
141. Baeuerle, P. A. & Baltimore, D. Activation of DNA-binding activity in an apparently cytoplasmic precursor of the NF-kappa B transcription factor. *Cell* **53,** 211–217 (1988).
142. Baeuerle, P. A. & Baltimore, D. I kappa B: a specific inhibitor of the NF-kappa B transcription factor. *Science* **242,** 540–546 (1988).
143. Haskill, S. *et al.* Characterization of an immediate-early gene induced in adherent monocytes that encodes I kappa B-like activity. *Cell* **65,** 1281–1289 (1991).

144. Link, E. *et al.* Purified I kappa B-beta is inactivated upon dephosphorylation. *J. Biol. Chem.* **267,** 239–246 (1992).
145. Jacobs, M. D. & Harrison, S. C. Structure of an IkappaBalpha/NF-kappaB complex. *Cell* **95,** 749–758 (1998).
146. Hayden, M. S. & Ghosh, S. NF-κB, the first quarter-century: remarkable progress and outstanding questions. *Genes Dev.* **26,** 203–234 (2012).
147. Ohno, H., Takimoto, G. & McKeithan, T. W. The candidate proto-oncogene bcl-3 is related to genes implicated in cell lineage determination and cell cycle control. *Cell* **60,** 991–997 (1990).
148. Nolan, G. P. *et al.* The bcl-3 proto-oncogene encodes a nuclear I kappa B-like molecule that preferentially interacts with NF-kappa B p50 and p52 in a phosphorylation-dependent manner. *Mol. Cell. Biol.* **13,** 3557–3566 (1993).
149. Franzoso, G. *et al.* The oncoprotein Bcl-3 can facilitate NF-kappa B-mediated transactivation by removing inhibiting p50 homodimers from select kappa B sites. *EMBO J.* **12,** 3893–3901 (1993).
150. Fujita, T., Nolan, G. P., Liou, H. C., Scott, M. L. & Baltimore, D. The candidate proto-oncogene bcl-3 encodes a transcriptional coactivator that activates through NF-kappa B p50 homodimers. *Genes Dev.* **7,** 1354–1363 (1993).
151. Hatada, E. N. *et al.* The ankyrin repeat domains of the NF-kappa B precursor p105 and the protooncogene bcl-3 act as specific inhibitors of NF-kappa B DNA binding. *Proc. Natl. Acad. Sci. USA* **89,** 2489–2493 (1992).
152. Inoue, J., Kerr, L. D., Kakizuka, A. & Verma, I. M. I kappa B gamma, a 70 kd protein identical to the C-terminal half of p110 NF-kappa B: a new member of the I kappa B family. *Cell* **68,** 1109–1120 (1992).
153. Wulczyn, F. G., Naumann, M. & Scheidereit, C. Candidate proto-oncogene bcl-3 encodes a subunit-specific inhibitor of transcription factor NF-kappa B. *Nature* **358,** 597–599 (1992).
154. Naumann, M., Wulczyn, F. G. & Scheidereit, C. The NF-kappa B precursor p105 and the proto-oncogene product Bcl-3 are I kappa B molecules and control nuclear translocation of NF-kappa B. *EMBO J.* **12,** 213–222 (1993).
155. Perkins, N. D. The diverse and complex roles of NF-κB subunits in cancer. *Nat. Rev. Cancer* **12,** 121–132 (2012).
156. Connelly, M. A. & Marcu, K. B. CHUK, a new member of the helix-loop-helix and leucine zipper families of interacting proteins, contains a serine-threonine kinase

catalytic domain. *Cell Mol Biol Res* **41,** 537–549 (1995).

157. DiDonato, J. A., Hayakawa, M., Rothwarf, D. M., Zandi, E. & Karin, M. A cytokine-responsive IkappaB kinase that activates the transcription factor NF-kappaB. *Nature* **388,** 548–554 (1997).
158. Zandi, E., Rothwarf, D. M., Delhase, M., Hayakawa, M. & Karin, M. The IkappaB kinase complex (IKK) contains two kinase subunits, IKKalpha and IKKbeta, necessary for IkappaB phosphorylation and NF-kappaB activation. *Cell* **91,** 243–252 (1997).
159. Mercurio, F. *et al.* IkappaB kinase (IKK)-associated protein 1, a common component of the heterogeneous IKK complex. *Mol. Cell. Biol.* **19,** 1526–1538 (1999).
160. Mercurio, F. *et al.* IKK-1 and IKK-2: cytokine-activated IkappaB kinases essential for NF-kappaB activation. *Science* **278,** 860–866 (1997).
161. Yamaoka, S. *et al.* Complementation cloning of NEMO, a component of the IkappaB kinase complex essential for NF-kappaB activation. *Cell* **93,** 1231–1240 (1998).
162. Rothwarf, D. M., Zandi, E., Natoli, G. & Karin, M. IKK-gamma is an essential regulatory subunit of the IkappaB kinase complex. *Nature* **395,** 297–300 (1998).
163. Lin, L., DeMartino, G. N. & Greene, W. C. Cotranslational Biogenesis of NF-κB p50 by the 26S Proteasome. *Cell* **92,** 819–828 (1998).
164. Senftleben, U. *et al.* Activation by IKKalpha of a second, evolutionary conserved, NF-kappa B signaling pathway. *Science* **293,** 1495–1499 (2001).
165. Claudio, E., Brown, K., Park, S., Wang, H. & Siebenlist, U. BAFF-induced NEMO-independent processing of NF-kappa B2 in maturing B cells. *Nat. Immunol.* **3,** 958–965 (2002).
166. Coope, H. J. *et al.* CD40 regulates the processing of NF-kappaB2 p100 to p52. *EMBO J.* **21,** 5375–5385 (2002).
167. Dejardin, E. *et al.* The Lymphotoxin-β Receptor Induces Different Patterns of Gene Expression via Two NF-κB Pathways. *Immunity* **17,** 525–535 (2002).
168. Novack, D. V. *et al.* The IkappaB function of NF-kappaB2 p100 controls stimulated osteoclastogenesis. *J. Exp. Med.* **198,** 771–781 (2003).
169. Fong, A. & Sun, S.-C. Genetic evidence for the essential role of beta-transducin repeat-containing protein in the inducible processing of NF-kappa B2/p100. *J. Biol. Chem.* **277,** 22111–22114 (2002).
170. Xiao, G., Fong, A. & Sun, S.-C. Induction of p100 processing by NF-kappaB-inducing kinase involves docking IkappaB kinase alpha (IKKalpha) to p100 and IKKalpha-mediated phosphorylation. *J. Biol. Chem.* **279,** 30099–30105 (2004).

171. Bours, V., Azarenko, V., Dejardin, E. & Siebenlist, U. Human RelB (I-Rel) functions as a kappa B site-dependent transactivating member of the family of Rel-related proteins. *Oncogene* **9,** 1699–1702 (1994).
172. DiDonato, J. A., Mercurio, F. & Karin, M. NF-κB and the link between inflammation and cancer. *Immunol. Rev.* **246,** 379–400 (2012).
173. Dajee, M. *et al.* NF-kappaB blockade and oncogenic Ras trigger invasive human epidermal neoplasia. *Nature* **421,** 639–643 (2003).
174. Fujioka, S. *et al.* Inhibition of constitutive NF-kappa B activity by I kappa B alpha M suppresses tumorigenesis. *Oncogene* **22,** 1365–1370 (2003).
175. Ling, J. *et al.* KrasG12D-induced IKK2/β/NF-κB activation by IL-1α and p62 feedforward loops is required for development of pancreatic ductal adenocarcinoma. *Cancer Cell* **21,** 105–120 (2012).
176. Luedde, T. *et al.* Deletion of NEMO/IKKgamma in liver parenchymal cells causes steatohepatitis and hepatocellular carcinoma. *Cancer Cell* **11,** 119–132 (2007).
177. Maeda, S., Kamata, H., Luo, J.-L., Leffert, H. & Karin, M. IKKbeta couples hepatocyte death to cytokine-driven compensatory proliferation that promotes chemical hepatocarcinogenesis. *Cell* **121,** 977–990 (2005).
178. Maier, H. J. *et al.* Requirement of NEMO/IKKγ for effective expansion of KRAS-induced precancerous lesions in the pancreas. *Oncogene* **32,** 2690–2695 (2013).
179. Maniati, E. *et al.* Crosstalk between the canonical NF-κB and Notch signaling pathways inhibits Pparγ expression and promotes pancreatic cancer progression in mice. *J. Clin. Invest.* **121,** 4685–4699 (2011).
180. Kondylis, V. *et al.* NEMO Prevents Steatohepatitis and Hepatocellular Carcinoma by Inhibiting RIPK1 Kinase Activity-Mediated Hepatocyte Apoptosis. *Cancer Cell* **28,** 582–598 (2015).
181. Chariot, A. The NF-kappaB-independent functions of IKK subunits in immunity and cancer. *Trends Cell Biol.* **19,** 404–413 (2009).
182. Lesina, M. *et al.* RelA regulates CXCL1/CXCR2-dependent oncogene-induced senescence in murine Kras-driven pancreatic carcinogenesis. *J. Clin. Invest.* **126,** 2919–2932 (2016).
183. Hamidi, T. *et al.* Nuclear protein 1 promotes pancreatic cancer development and protects cells from stress by inhibiting apoptosis. *J. Clin. Invest.* **122,** 2092–2103 (2012).
184. Hanson, J. L., Hawke, N. A., Kashatus, D. & Baldwin, A. S. The nuclear factor kappaB subunits RelA/p65 and c-Rel potentiate but are not required for Ras-induced cellular

transformation. *Cancer Res.* **64,** 7248–7255 (2004).

185. Finco, T. S. *et al.* Oncogenic Ha-Ras-induced signaling activates NF-kappaB transcriptional activity, which is required for cellular transformation. *J. Biol. Chem.* **272,** 24113–24116 (1997).
186. Meylan, E. *et al.* Requirement for NF-kappaB signalling in a mouse model of lung adenocarcinoma. *Nature* **462,** 104–107 (2009).
187. Bassères, D. S., Ebbs, A., Levantini, E. & Baldwin, A. S. Requirement of the NF-kappaB subunit p65/RelA for K-Ras-induced lung tumorigenesis. *Cancer Res.* **70,** 3537–3546 (2010).
188. Wang, W. *et al.* The nuclear factor-kappa B RelA transcription factor is constitutively activated in human pancreatic adenocarcinoma cells. *Clin. Cancer Res.* **5,** 119–127 (1999).
189. Daniluk, J. *et al.* An NF-κB pathway-mediated positive feedback loop amplifies Ras activity to pathological levels in mice. *J. Clin. Invest.* **122,** 1519–1528 (2012).
190. Vasudevan, K. M., Gurumurthy, S. & Rangnekar, V. M. Suppression of PTEN Expression by NF- B Prevents Apoptosis. *Mol. Cell. Biol.* **24,** 1007–1021 (2004).
191. Wilson, W. & Baldwin, A. S. Maintenance of constitutive IkappaB kinase activity by glycogen synthase kinase-3alpha/beta in pancreatic cancer. *Cancer Res.* **68,** 8156–8163 (2008).
192. Bang, D., Wilson, W., Ryan, M., Yeh, J. J. & Baldwin, A. S. GSK-3α promotes oncogenic KRAS function in pancreatic cancer via TAK1-TAB stabilization and regulation of noncanonical NF-κB. *Cancer Discov.* **3,** 690–703 (2013).
193. Wharry, C. E., Haines, K. M., Carroll, R. G. & May, M. J. Constitutive non-canonical NFkappaB signaling in pancreatic cancer cells. *Cancer Biol. Ther.* **8,** 1567–1576 (2009).
194. Kabacaoglu, D., Ruess, D. A., Ai, J. & Algül, H. NF-κB/Rel Transcription Factors in Pancreatic Cancer: Focusing on RelA, c-Rel, and RelB. *Cancers (Basel)* **11,** (2019).
195. Wong, T. C. & Lai, M. M. Avian reticuloendotheliosis virus contains a new class of oncogene of turkey origin. *Virology* **111,** 289–293 (1981).
196. Simek, S. & Rice, N. R. Detection and characterization of the protein encoded by the chicken c-rel protooncogene. *Oncogene Res.* **2,** 103–119 (1988).
197. Herzog, N. K., Bargmann, W. J. & Bose, H. R. Oncogene expression in reticuloendotheliosis virus-transformed lymphoid cell lines and avian tissues. *J. Virol.* **57,** 371–375 (1986).
198. Moore, B. E. & Bose, H. R. Transformation of avian lymphoid cells by

reticuloendotheliosis virus. *Mutat. Res.* **195,** 79–90 (1988).

199. Fan, Y., Rayet, B. & Gélinas, C. Divergent C-terminal transactivation domains of Rel/NF-kappa B proteins are critical determinants of their oncogenic potential in lymphocytes. *Oncogene* **23,** 1030–1042 (2004).
200. Romieu-Mourez, R. *et al.* Mouse mammary tumor virus c-rel transgenic mice develop mammary tumors. *Mol. Cell. Biol.* **23,** 5738–5754 (2003).
201. Belguise, K. & Sonenshein, G. E. PKCtheta promotes c-Rel-driven mammary tumorigenesis in mice and humans by repressing estrogen receptor alpha synthesis. *J. Clin. Invest.* **117,** 4009–4021 (2007).
202. Geismann, C. *et al.* c-Rel is a critical mediator of NF-κB-dependent TRAIL resistance of pancreatic cancer cells. *Cell Death Dis.* **5,** e1455 (2014).
203. Hunter, J. E. *et al.* Regulation of checkpoint kinase signalling and tumorigenesis by the NF-κB regulated gene, CLSPN. *BioRxiv* (2018). doi:10.1101/358291
204. Seguin, L. *et al.* An integrin β3-KRAS-RalB complex drives tumour stemness and resistance to EGFR inhibition. *Nat. Cell Biol.* **16,** 457–468 (2014).
205. Shuang, T., Wang, M., Zhou, Y. & Shi, C. Over-expression of nuclear NF-κB1 and c-Rel correlates with chemoresistance and prognosis of serous epithelial ovarian cancer. *Exp Mol Pathol* **100,** 139–144 (2016).
206. Shuang, T., Wang, M., Zhou, Y., Shi, C. & Wang, D. NF-κB1, c-Rel, and ELK1 inhibit miR-134 expression leading to TAB1 upregulation in paclitaxel-resistant human ovarian cancer. *Oncotarget* **8,** 24853–24868 (2017).
207. Burkitt, M. D. *et al.* NF-κB1, NF-κB2 and c-Rel differentially regulate susceptibility to colitis-associated adenoma development in C57BL/6 mice. *J. Pathol.* **236,** 326–336 (2015).
208. Fu, T. *et al.* c-Rel is a transcriptional repressor of EPHB2 in colorectal cancer. *J. Pathol.* **219,** 103–113 (2009).
209. Rovida, E. *et al.* The mitogen-activated protein kinase ERK5 regulates the development and growth of hepatocellular carcinoma. *Gut* **64,** 1454–1465 (2015).
210. Maity, P. C., Ray, T., Das, B. & Sil, A. K. IKKβ-I-κBε-c-Rel/p50: a new axis of NF-κB activation in lung epithelial cells. *Oncogenesis* **1,** e8 (2012).
211. Velmurugan, K. R., Varghese, R. T., Fonville, N. C. & Garner, H. R. High-depth, high-accuracy microsatellite genotyping enables precision lung cancer risk classification. *Oncogene* **36,** 6383–6390 (2017).
212. Gupta, S. *et al.* Constitutive activation and overexpression of NF-κB/c-Rel in conjunction

with p50 contribute to aggressive tongue tumorigenesis. *Oncotarget* **9,** 33011–33029 (2018).

213. King, K. E. *et al.* The p53 homologue DeltaNp63alpha interacts with the nuclear factor-kappaB pathway to modulate epithelial cell growth. *Cancer Res.* **68,** 5122–5131 (2008).
214. Liu, C.-J., Lin, S.-C., Chen, Y.-J., Chang, K.-M. & Chang, K.-W. Array-comparative genomic hybridization to detect genomewide changes in microdissected primary and metastatic oral squamous cell carcinomas. *Mol. Carcinog.* **45,** 721–731 (2006).
215. Lorenz, V. N., Schön, M. P. & Seitz, C. S. c-Rel downregulation affects cell cycle progression of human keratinocytes. *J. Invest. Dermatol.* **134,** 415–422 (2014).
216. Lu, H. *et al.* TNF-α promotes c-REL/ΔNp63α interaction and TAp73 dissociation from key genes that mediate growth arrest and apoptosis in head and neck cancer. *Cancer Res.* **71,** 6867–6877 (2011).
217. Singh, M. K. *et al.* Identification of canonical NFκB (C-NFκB) pathway in uveal melanoma and their relation with patient outcome. *Clin Exp Metastasis* **36,** 271–290 (2019).
218. Singh, M. K. *et al.* Constitutive expression of c-REL in uveal melanoma patients: correlation with clinicopathological parameters and patient outcome. *Clin Transl Oncol* **22,** 1193–1204 (2020).
219. Yang, X. *et al.* ΔNp63 versatilely regulates a Broad NF-κB gene program and promotes squamous epithelial proliferation, migration, and inflammation. *Cancer Res.* **71,** 3688–3700 (2011).
220. Barbie, D. A. *et al.* Systematic RNA interference reveals that oncogenic KRAS-driven cancers require TBK1. *Nature* **462,** 108–112 (2009).
221. Chien, Y. *et al.* RalB GTPase-mediated activation of the IkappaB family kinase TBK1 couples innate immune signaling to tumor cell survival. *Cell* **127,** 157–170 (2006).
222. Harris, J. *et al.* Nuclear accumulation of cRel following C-terminal phosphorylation by TBK1/IKK epsilon. *J. Immunol.* **177,** 2527–2535 (2006).
223. Gilmore, T. D. & Gerondakis, S. The c-Rel Transcription Factor in Development and Disease. *Genes Cancer* **2,** 695–711 (2011).
224. Muvaffak, A. *et al.* Evaluating TBK1 as a therapeutic target in cancers with activated IRF3. *Mol. Cancer Res.* **12,** 1055–1066 (2014).
225. Ou, Y.-H. *et al.* TBK1 directly engages Akt/PKB survival signaling to support oncogenic transformation. *Mol. Cell* **41,** 458–470 (2011).
226. Grinberg-Bleyer, Y. *et al.* NF-κB c-Rel Is Crucial for the Regulatory T Cell Immune

Checkpoint in Cancer. *Cell* **170,** 1096–1108.e13 (2017).

227. Li, T. *et al.* c-Rel is a myeloid checkpoint for cancer immunotherapy. *Nat. Cancer* **1,** 507–517 (2020).
228. Leslie, J. *et al.* c-Rel orchestrates energy-dependent epithelial and macrophage reprogramming in fibrosis. *Nat. Metab.* **2,** 1350–1367 (2020).
229. Beg, A. A., Sha, W. C., Bronson, R. T., Ghosh, S. & Baltimore, D. Embryonic lethality and liver degeneration in mice lacking the RelA component of NF-kappa B. *Nature* **376,** 167–170 (1995).
230. Köntgen, F. *et al.* Mice lacking the c-rel proto-oncogene exhibit defects in lymphocyte proliferation, humoral immunity, and interleukin-2 expression. *Genes Dev.* **9,** 1965–1977 (1995).
231. Yang, J. *et al.* Guidelines and definitions for research on epithelial-mesenchymal transition. *Nat. Rev. Mol. Cell Biol.* **21,** 341–352 (2020).
232. Zihni, C., Mills, C., Matter, K. & Balda, M. S. Tight junctions: from simple barriers to multifunctional molecular gates. *Nat. Rev. Mol. Cell Biol.* **17,** 564–580 (2016).
233. Harris, T. J. C. & Tepass, U. Adherens junctions: from molecules to morphogenesis. *Nat. Rev. Mol. Cell Biol.* **11,** 502–514 (2010).
234. Dubash, A. D. & Green, K. J. Desmosomes. *Curr. Biol.* **21,** R529-31 (2011).
235. Goodenough, D. A. & Paul, D. L. Gap junctions. *Cold Spring Harb. Perspect. Biol.* **1,** a002576 (2009).
236. Lamouille, S., Xu, J. & Derynck, R. Molecular mechanisms of epithelial-mesenchymal transition. *Nat. Rev. Mol. Cell Biol.* **15,** 178–196 (2014).
237. Kalluri, R. & Weinberg, R. A. The basics of epithelial-mesenchymal transition. *J. Clin. Invest.* **119,** 1420–1428 (2009).
238. Batlle, E. *et al.* The transcription factor snail is a repressor of E-cadherin gene expression in epithelial tumour cells. *Nat. Cell Biol.* **2,** 84–89 (2000).
239. Cano, A. *et al.* The transcription factor snail controls epithelial-mesenchymal transitions by repressing E-cadherin expression. *Nat. Cell Biol.* **2,** 76–83 (2000).
240. Savagner, P., Yamada, K. M. & Thiery, J. P. The zinc-finger protein slug causes desmosome dissociation, an initial and necessary step for growth factor-induced epithelial-mesenchymal transition. *J. Cell Biol.* **137,** 1403–1419 (1997).
241. Grooteclaes, M. L. & Frisch, S. M. Evidence for a function of CtBP in epithelial gene regulation and anoikis. *Oncogene* **19,** 3823–3828 (2000).
242. Comijn, J. *et al.* The two-handed E box binding zinc finger protein SIP1 downregulates

E-cadherin and induces invasion. *Mol. Cell* **7,** 1267–1278 (2001).

243. Yang, J. *et al.* Twist, a master regulator of morphogenesis, plays an essential role in tumor metastasis. *Cell* **117,** 927–939 (2004).
244. Shibue, T. & Weinberg, R. A. EMT, CSCs, and drug resistance: the mechanistic link and clinical implications. *Nat. Rev. Clin. Oncol.* **14,** 611–629 (2017).
245. Hapach, L. A., Mosier, J. A., Wang, W. & Reinhart-King, C. A. Engineered models to parse apart the metastatic cascade. *NPJ Precis. Oncol.* **3,** 20 (2019).
246. Rhim, A. D. *et al.* EMT and dissemination precede pancreatic tumor formation. *Cell* **148,** 349–361 (2012).
247. Fearon, E. R. Cancer: Context Is Key for E-cadherin in Invasion and Metastasis. *Curr. Biol.* **29,** R1140–R1142 (2019).
248. Padmanaban, V. *et al.* E-cadherin is required for metastasis in multiple models of breast cancer. *Nature* **573,** 439–444 (2019).
249. Fischer, K. R. *et al.* Epithelial-to-mesenchymal transition is not required for lung metastasis but contributes to chemoresistance. *Nature* **527,** 472–476 (2015).
250. Zheng, X. *et al.* Epithelial-to-mesenchymal transition is dispensable for metastasis but induces chemoresistance in pancreatic cancer. *Nature* **527,** 525–530 (2015).
251. Dongre, A. & Weinberg, R. A. New insights into the mechanisms of epithelial-mesenchymal transition and implications for cancer. *Nat. Rev. Mol. Cell Biol.* **20,** 69–84 (2019).
252. Hanahan, D. & Weinberg, R. A. Hallmarks of cancer: the next generation. *Cell* **144,** 646–674 (2011).
253. Greaves, M. Cancer stem cells as "units of selection". *Evol. Appl.* **6,** 102–108 (2013).
254. Visvader, J. E. & Lindeman, G. J. Cancer stem cells: current status and evolving complexities. *Cell Stem Cell* **10,** 717–728 (2012).
255. Hermann, P. C. & Sainz, B. Pancreatic cancer stem cells: A state or an entity? *Semin. Cancer Biol.* **53,** 223–231 (2018).
256. Mani, S. A. *et al.* The epithelial-mesenchymal transition generates cells with properties of stem cells. *Cell* **133,** 704–715 (2008).
257. Morel, A.-P. *et al.* Generation of breast cancer stem cells through epithelial-mesenchymal transition. *PLoS One* **3,** e2888 (2008).
258. Lambert, A. W. & Weinberg, R. A. Linking EMT programmes to normal and neoplastic epithelial stem cells. *Nat. Rev. Cancer* (2021). doi:10.1038/s41568-021-00332-6
259. Ikenaga, N. *et al.* Characterization of CD24 expression in intraductal papillary mucinous

neoplasms and ductal carcinoma of the pancreas. *Hum. Pathol.* **41,** 1466–1474 (2010).

260. Hong, S. P., Wen, J., Bang, S., Park, S. & Song, S. Y. CD44-positive cells are responsible for gemcitabine resistance in pancreatic cancer cells. *Int. J. Cancer* **125,** 2323–2331 (2009).
261. Maréchal, R. *et al.* High expression of CXCR4 may predict poor survival in resected pancreatic adenocarcinoma. *Br. J. Cancer* **100,** 1444–1451 (2009).
262. Deng, S. *et al.* Distinct expression levels and patterns of stem cell marker, aldehyde dehydrogenase isoform 1 (ALDH1), in human epithelial cancers. *PLoS One* **5,** e10277 (2010).
263. Ishiwata, T., Matsuda, Y. & Naito, Z. Nestin in gastrointestinal and other cancers: effects on cells and tumor angiogenesis. *World J. Gastroenterol.* **17,** 409–418 (2011).
264. Hermann, P. C. *et al.* Distinct populations of cancer stem cells determine tumor growth and metastatic activity in human pancreatic cancer. *Cell Stem Cell* **1,** 313–323 (2007).
265. Olempska, M. *et al.* Detection of tumor stem cell markers in pancreatic carcinoma cell lines. *HBPD INT* **6,** 92–97 (2007).
266. Huang, P. *et al.* Isolation and biological analysis of tumor stem cells from pancreatic adenocarcinoma. *World J. Gastroenterol.* **14,** 3903–3907 (2008).
267. Li, C. *et al.* Identification of pancreatic cancer stem cells. *Cancer Res.* **67,** 1030–1037 (2007).
268. Li, C. *et al.* c-Met is a marker of pancreatic cancer stem cells and therapeutic target. *Gastroenterology* **141,** 2218–2227.e5 (2011).
269. Ishiwata, T. *et al.* Pancreatic cancer stem cells: features and detection methods. *Pathol Oncol Res* **24,** 797–805 (2018).
270. Gou, S. *et al.* Establishment of clonal colony-forming assay for propagation of pancreatic cancer cells with stem cell properties. *Pancreas* **34,** 429–435 (2007).
271. Gaviraghi, M. *et al.* Pancreatic cancer spheres are more than just aggregates of stem marker-positive cells. *Biosci. Rep.* **31,** 45–55 (2011).
272. Ishiwata, T. *et al.* Electron microscopic analysis of different cell types in human pancreatic cancer spheres. *Oncol. Lett.* **15,** 2485–2490 (2018).
273. Maeda, S. *et al.* CD133 expression is correlated with lymph node metastasis and vascular endothelial growth factor-C expression in pancreatic cancer. *Br. J. Cancer* **98,** 1389–1397 (2008).
274. Immervoll, H., Hoem, D., Sakariassen, P. Ø., Steffensen, O. J. & Molven, A. Expression of the “stem cell marker” CD133 in pancreas and pancreatic ductal adenocarcinomas.

BMC Cancer **8,** 48 (2008).

275. Kure, S. *et al.* Expression of cancer stem cell markers in pancreatic intraepithelial neoplasias and pancreatic ductal adenocarcinomas. *Int. J. Oncol.* **41,** 1314–1324 (2012).
276. Kabacaoglu, D., Lesina, M. & Algül, H. *A pancreas specific* Ptf1a *-driven Cre mouse line causes paternally transmitted germline recombination*. (Genetics, 2020). at <http://biorxiv.org/lookup/doi/10.1101/2020.03.13.989178>
277. Heise, N. *et al.* Germinal center B cell maintenance and differentiation are controlled by distinct NF-κB transcription factor subunits. *J. Exp. Med.* **211,** 2103–2118 (2014).
278. Kober-Hasslacher, M. *et al.* c-Rel gain in B cells drives germinal center reactions and autoantibody production. *J. Clin. Invest.* **130,** 3270–3286 (2020).
279. Hu, Y. & Smyth, G. K. ELDA: extreme limiting dilution analysis for comparing depleted and enriched populations in stem cell and other assays. *J. Immunol. Methods* **347,** 70–78 (2009).
280. George, T. C. *et al.* Quantitative measurement of nuclear translocation events using similarity analysis of multispectral cellular images obtained in flow. *J. Immunol. Methods* **311,** 117–129 (2006).
281. Goldman, M. J. *et al.* Visualizing and interpreting cancer genomics data via the Xena platform. *Nat. Biotechnol.* **38,** 675–678 (2020).
282. Tang, Z. *et al.* GEPIA: a web server for cancer and normal gene expression profiling and interactive analyses. *Nucleic Acids Res.* **45,** W98–W102 (2017).
283. Rhodes, D. R. *et al.* ONCOMINE: a cancer microarray database and integrated data-mining platform. *Neoplasia* **6,** 1–6 (2004).
284. Logsdon, C. D. *et al.* Molecular profiling of pancreatic adenocarcinoma and chronic pancreatitis identifies multiple genes differentially regulated in pancreatic cancer. *Cancer Res.* **63,** 2649–2657 (2003).
285. Pei, H. *et al.* FKBP51 affects cancer cell response to chemotherapy by negatively regulating Akt. *Cancer Cell* **16,** 259–266 (2009).
286. Iacobuzio-Donahue, C. A. *et al.* Exploration of global gene expression patterns in pancreatic adenocarcinoma using cDNA microarrays. *Am. J. Pathol.* **162,** 1151–1162 (2003).
287. Grützmann, R. *et al.* Gene expression profiling of microdissected pancreatic ductal carcinomas using high-density DNA microarrays. *Neoplasia* **6,** 611–622 (2004).
288. Buchholz, M. *et al.* Transcriptome analysis of microdissected pancreatic intraepithelial neoplastic lesions. *Oncogene* **24,** 6626–6636 (2005).

289. Segara, D. *et al.* Expression of HOXB2, a retinoic acid signaling target in pancreatic cancer and pancreatic intraepithelial neoplasia. *Clin. Cancer Res.* **11,** 3587–3596 (2005).
290. Badea, L., Herlea, V., Dima, S. O., Dumitrascu, T. & Popescu, I. Combined gene expression analysis of whole-tissue and microdissected pancreatic ductal adenocarcinoma identifies genes specifically overexpressed in tumor epithelia. *Hepatogastroenterology* **55,** 2016–2027 (2008).
291. Ishikawa, M. *et al.* Experimental trial for diagnosis of pancreatic ductal carcinoma based on gene expression profiles of pancreatic ductal cells. *Cancer Sci.* **96,** 387–393 (2005).
292. Sachdev, S. & Hannink, M. Loss of IκBα-Mediated Control over Nuclear Import and DNA Binding Enables Oncogenic Activation of c-Rel. *Mol. Cell. Biol.* **18,** 5445–5456 (1998).
293. Starczynowski, D. T., Reynolds, J. G. & Gilmore, T. D. Deletion of either C-terminal transactivation subdomain enhances the in vitro transforming activity of human transcription factor REL in chicken spleen cells. *Oncogene* **22,** 6928–6936 (2003).
294. Vasaikar, S. V. *et al.* EMTome: a resource for pan-cancer analysis of epithelial-mesenchymal transition genes and signatures. *Br. J. Cancer* **124,** 259–269 (2021).
295. Aiello, N. M. *et al.* EMT subtype influences epithelial plasticity and mode of cell migration. *Dev. Cell* **45,** 681–695.e4 (2018).
296. Ischenko, I., Petrenko, O. & Hayman, M. J. Analysis of the tumor-initiating and metastatic capacity of PDX1-positive cells from the adult pancreas. *Proc. Natl. Acad. Sci. USA* **111,** 3466–3471 (2014).
297. Bosman, F. T., Carneiro, F., Hruban, R. H. & Theise, N. D. WHO classification of tumours of the digestive system. *WHO classification of tumours of the digestive system.* (2010).
298. Clark, C. J., Graham, R. P., Arun, J. S., Harmsen, W. S. & Reid-Lombardo, K. M. Clinical outcomes for anaplastic pancreatic cancer: a population-based study. *J. Am. Coll. Surg.* **215,** 627–634 (2012).
299. Komatsu, H. *et al.* Clinicopathological features and surgical outcomes of adenosquamous carcinoma of the pancreas: a retrospective analysis of patients with resectable stage tumors. *Surg Today* **45,** 297–304 (2015).
300. Oymaci, E., Yakan, S., Yildirim, M., Argon, A. & Namdaroglu, O. Anaplastic carcinoma of the pancreas: A rare clinical entity. *Cureus* **9,** e1782 (2017).
301. Si, H. *et al.* TNF-α modulates genome-wide redistribution of ΔNp63α/TAp73 and NF-κB cREL interactive binding on TP53 and AP-1 motifs to promote an oncogenic gene

program in squamous cancer. *Oncogene* **35,** 5781–5794 (2016).

302. Belguise, K. *et al.* Green tea polyphenols reverse cooperation between c-Rel and CK2 that induces the aryl hydrocarbon receptor, slug, and an invasive phenotype. *Cancer Res.* **67,** 11742–11750 (2007).
303. Lorenz, V. N., Schön, M. P. & Seitz, C. S. The c-Rel subunit of NF-κB is a crucial regulator of phenotype and motility of HaCaT keratinocytes. *Arch Dermatol Res* **307,** 523–530 (2015).
304. Liu, L. *et al.* Triptolide reverses hypoxia-induced epithelial-mesenchymal transition and stem-like features in pancreatic cancer by NF-κB downregulation. *Int. J. Cancer* **134,** 2489–2503 (2014).
305. Shin, S. R., Sánchez-Velar, N., Sherr, D. H. & Sonenshein, G. E. 7,12-dimethylbenz(a)anthracene treatment of a c-rel mouse mammary tumor cell line induces epithelial to mesenchymal transition via activation of nuclear factor-kappaB. *Cancer Res.* **66,** 2570–2575 (2006).
306. Ganesan, R., Mallets, E. & Gomez-Cambronero, J. The transcription factors Slug (SNAI2) and Snail (SNAI1) regulate phospholipase D (PLD) promoter in opposite ways towards cancer cell invasion. *Mol. Oncol.* **10,** 663–676 (2016).
307. Porter, R. L. *et al.* Epithelial to mesenchymal plasticity and differential response to therapies in pancreatic ductal adenocarcinoma. *Proc. Natl. Acad. Sci. USA* (2019). doi:10.1073/pnas.1914915116
308. Pinto, B., Henriques, A. C., Silva, P. M. A. & Bousbaa, H. Three-Dimensional Spheroids as In Vitro Preclinical Models for Cancer Research. *Pharmaceutics* **12,** (2020).
309. Desgrosellier, J. S. *et al.* An integrin alpha(v)beta(3)-c-Src oncogenic unit promotes anchorage-independence and tumor progression. *Nat. Med.* **15,** 1163–1169 (2009).
310. Ye, X. *et al.* Distinct EMT programs control normal mammary stem cells and tumour-initiating cells. *Nature* **525,** 256–260 (2015).
311. Phillips, S. *et al.* Cell-state transitions regulated by SLUG are critical for tissue regeneration and tumor initiation. *Stem Cell Rep.* **2,** 633–647 (2014).
312. Guo, W. *et al.* Slug and Sox9 cooperatively determine the mammary stem cell state. *Cell* **148,** 1015–1028 (2012).
313. Nassour, M. *et al.* Slug controls stem/progenitor cell growth dynamics during mammary gland morphogenesis. *PLoS One* **7,** e53498 (2012).
314. Chakrabarti, R. *et al.* ΔNp63 promotes stem cell activity in mammary gland development and basal-like breast cancer by enhancing Fzd7 expression and Wnt signalling. *Nat. Cell*

Biol. **16,** 1004–15, 1 (2014).

315. Muñoz, J. *et al.* The Lgr5 intestinal stem cell signature: robust expression of proposed quiescent "+4" cell markers. *EMBO J.* **31,** 3079–3091 (2012).
316. Horvay, K., Casagranda, F., Gany, A., Hime, G. R. & Abud, H. E. Wnt signaling regulates Snai1 expression and cellular localization in the mouse intestinal epithelial stem cell niche. *Stem Cells Dev.* **20,** 737–745 (2011).
317. Horvay, K. *et al.* Snai1 regulates cell lineage allocation and stem cell maintenance in the mouse intestinal epithelium. *EMBO J.* **34,** 1319–1335 (2015).
318. Krebs, A. M. *et al.* The EMT-activator Zeb1 is a key factor for cell plasticity and promotes metastasis in pancreatic cancer. *Nat. Cell Biol.* **19,** 518–529 (2017).
319. DA Cruz Paula, A. & Lopes, C. Implications of different cancer stem cell phenotypes in breast cancer. *Anticancer Res.* **37,** 2173–2183 (2017).
320. Nakshatri, H., Srour, E. F. & Badve, S. Breast cancer stem cells and intrinsic subtypes: controversies rage on. *Curr. Stem Cell Res. Ther.* **4,** 50–60 (2009).
321. Dirkse, A. *et al.* Stem cell-associated heterogeneity in Glioblastoma results from intrinsic tumor plasticity shaped by the microenvironment. *Nat. Commun.* **10,** 1787 (2019).

9 ABBREVIATIONS

PDAC	Pancreatic ductal adenocarcinoma
KRAS	Kirsten Rat Sarcoma 2 Viral Oncogene Homolog
CDKN2A	Cyclin Dependent Kinase Inhibitor 2A
TP53/Trp53	Tumor protein 53
SMAD4	SMAD Family Member 4
NF-κB	Nuclear Factor Kappa B
TGFβ	Transforming Growth Factor Beta
PanIN	Pancreatic intra-epithelial neoplasms
ADM	Acinar to ductal metaplasia
GATA6	GATA Binding Protein 6
QM-PDA	Quasi-mesenchymal pancreatic ductal adenocarcinoma
PDX	Patient derived xenograft
ADEX	Aberrantly differentiated endocrine exocrine subtype
TME	Tumor microenvironment
PI3K	Phosphatidylinositol-4,5-Bisphosphate 3-Kinase
GEMM	Genetically engineered mouse model
PSC	Pancreatic stellate cell
ECM	Extracellular matrix
CAF	Cancer associated fibroblast
TAM	Tumor associated macrophage
MDSC	Myledoid derived suppressor cell
CTL	Cytotoxic T lymphocyte
TAN	Tumor associated neutrophils
RelA	V-Rel Avian Reticuloendotheliosis Viral Oncogene Homolog A
RelB	V-Rel Avian Reticuloendotheliosis Viral Oncogene Homolog B
c-Rel	V-Rel Avian Reticuloendotheliosis Viral Oncogene Homolog C
IKK	Inhibitor of Nuclear Factor Kappa B Kinase
IKB	Inhibitor of Nuclear Factor Kappa B
TBK1	TANK Binding Kinase 1
EMT	Epithelial to mesenchymal transition
CTC	Circulating tumor cells
CSC	Cancer stem cell

TIC	Tumor initiating cell
TCGA	The Cancer Genome Atlas
IHC	Immunohistochemistry
TNFα	Tumor Necrosis Factor
eGFP	Enhanced green fluorescent protein
BrdU	Bromodeoxyuridine
Zeb1-2	Zinc Finger E-Box Binding Homeobox 1-2
Snai1-2	Snail Family Transcriptional Repressor 1-2
RT-qPCR	Real time quantitative PCR
RNAi	RNA interference
Sca1	Stem cells antigen-1
CXCR4	C-X-C Motif Chemokine Receptor 4
CD44	Hematopoietic Cell E- And L-Selectin Ligand
CD133	Prominin 1
ELDA	Extreme limiting dilution assay

10 ACKNOWLEDGEMENTS

Firstly, I would like to express my gratitude to Prof. Hana Algül for giving me this opportunity to work in his research group. Being a molecular biologist made me miss the chance to see when the hard work on the bench side gets translated into the bedside. Being privileged to be in Prof. Algül's research group, I experienced the excitement to work on scientific projects, which can actually matter in the patient life. Being both a medical doctor and scientist, Prof. Hana Algül taught me to see the connection between basic science and translational oncology. Additionally, I am very grateful to PD. Dr. Marina Lesina for her constant guidance during my studies relating to both professional and private matters. I would like to thank my thesis advisory committee members, Prof. Dr. med. Roland Schmid, Prof. Dr. Martin Klingenspor, and Prof. Dr. med. Florian Bassermann for their guidance with my studies. I am especially grateful to IMPRS-LS graduate office members Ingrid, Maxi, and Hans for their constant help during my studies. It has been my great pleasure to work with my dear colleagues and friends, including Kıvanç, Nina, Jiaoyu, Katrin, Dietrich, Nan, Alexandra, Marlena, Fränze, Larissa, Ezgi, Angelica, and Yuhui. I want to offer my sincere thanks to them since they all made the time in the laboratory not only fruitful but also fun. I want to thank Fränze, especially for her exceptional assistance and friendship during the last year of this study.

I am really grateful to my friends Eylem, Uğur, Haroon, Nico, Einari, Tuçem, Beytullah, Merve, Aylin, Cafer, Hilal, Ali, Olaf, Zinnur, Zeynep, Fatma, and Dora the Cat for their companionship. I can't imagine my six years in Munich without their constant support. I praise my dear friend Arzu, whom I discovered very late to be such a great person. Her friendship made me not only "stand still" but actually really enjoy the lock-down times of COVID-19.

There are no words to express my gratefulness, especially to Alex, Kıvanç, Hande, Dietrich, Jiaoyu, and Nan for being not only my friends but far beyond. As Dr. Neil deGrasse Tyson puts it, "Our imagination is nothing, compared with nature's awesome reality". Their support helped me dream, endure, laugh, love, prosper and always remember how "cool" science is. I dedicate this work to their constant companionship. I feel privileged to have them as my friend and be their friend.

Lastly and most importantly, I am deeply indebted to my mother Ayşe Kabacaoğlu, my father Enver Kabacaoğlu, and my sister Eda Kabacaoğlu Paakkanen. Their

unconditional love and support, no matter where and how I am, has given me the strength to celebrate life no matter what.